1987

Distortion-induced fatigue cracking at lateral gusset plate details /

David C. Wagner
Lehigh University

DISTORTION-INDUCED FATIGUE CRACKING

AT LATERAL GUSSET PLATE DETAILS

by

David C. Wagner

A Thesis

Presented to the Graduate Committee

of Lehigh University

in Candidacy for the Degree of

Master of Science

in

Civil Engineering

Lehigh University

Bethlehem, Pennsylvania

May 1987

CERTIFICATE OF APPROVAL

This thesis is accepted and approved in partial fulfillment of the requirements for the degree of Master of Science in Civil Engineering.

May 14, 1987
Date

John W. Fisher
Professor in Charge

Irwin J. Kugelman
Department Chairman

Acknowledgments

The analytical and experimental studies presented in this thesis were conducted at Fritz Engineering Laboratory, Lehigh University, Bethlehem, Pennsylvania. Dr. Irwin J. Kugelman is the Chairman of the Department of Civil Engineering.

The experiments conducted in this work are an integral part of the investigations of *"Distortion-Induced Fatigue Cracking in Steel Bridges."* The on-going research is sponsored through the National Cooperative Highway Research Program, as project 12-28(6).

Special thanks are due various support personnel in Fritz Engineering Laboratory. Dr. Roger G. Slutter, Director of Laboratory Operations, proved to be invaluable throughout the specimen preparation and testing phases. Messrs. Robert R. Dales, Charles F. Hittinger, Russel Longenbach, and Eugene Matlock provided services during the test set-up, instrumentation, and maintenance phases of the project. Mr. John M. Gera provided his skill as a draftsman and Mr. Richard N. Sopko supplied excellent photographic coverage.

The author wishes to express his sincere thanks to the following men for their contributions to his professional development: Dr. Ti Huang, for his dynamic interaction with the author at the undergraduate level, and for his encouragement to continue the education process through the pursuit of an advanced degree; Dr. Ben T. Yen, for constantly returning the author's attention to the practical application of structural mechanics, and for lending technical support and encouragement throughout the Graduate Program; and finally, Dr. John W. Fisher, the project's principal investigator and the author's advisor, for his dedication to the research of fatigue behavior. Dr. Fisher's

ability to detect fatigue limits has prolonged the lives of many in-service structures as well as many Research Assistants.

The author is indebted to his mother and father for much more than his physical being. Their support and guidance have had a profound effect on his personal and professional development. Mere words are not sufficient to express his gratitude, and fortunately, this gratitude need not be expressed in words.

Table of Contents

List of Figures

List of Tables

Abstract

In recent years, extensive fatigue cracking has developed in numerous lateral gusset plate details, on many steel bridges. Out-of-plane displacements generate secondary bending stresses within the unstiffened, horizontal web gaps. The forces causing the out-of-plane distortion are generally low. Since the usual structure idealizations do not provide a mechanism for estimating these forces, the resulting secondary stresses are not accounted for in the design process.

An experimental pilot study was initiated upon completion of a review of the field measurements associated with distortion-induced fatigue cracking. Two types of details were considered, and four of each type were tested. The variables included: the gap size, the magnitude of the distortion-induced stress range, and the degree of lateral physical deformation. A primary, in-plane bending stress range of 6 ksi (41.4 MPa) was maintained at the level of all gusset plate details. The study indicated that secondary stress ranges on the order of 24 ksi (165.6 MPa) could be induced by relative out-of-plane distortions of only thousandths of an inch, across the gaps of a flexible detail. However, the second type of detail investigated, included a positive attachment between the gusset and vertical connection plates. In such details, secondary stress ranges on the order of only 4 ksi (27.6 MPa) developed under comparable loadings. Furthermore, these details experienced only one-half of the relative distortions induced between the welded boundaries of the more flexible connections.

Secondary stresses may be correlated with specific degrees of distortion for a given detail and gap size. The effects of altering the connection's rigidity were also studied. Results indicated the bolted attachment's ability to reduce distortions by an order of magnitude, and stress ranges by a factor of two,

within cracked horizontal web gaps. Recommendations for future design considerations, as well as the retrofitting of existing details which have experienced such cracking, are also presented.

Chapter 1
INTRODUCTION

1.1 Problem Statement

1.1.1 General Overview

During the past fifteen years, extensive fatigue cracking has developed in a wide variety of steel bridges due to unanticipated out-of-plane distortions. These cracks often occurred after only a few years of service because of the high distortion-induced stress ranges which developed under normal traffic loadings. A summary of the conditions surrounding such cracking and a discussion of several specific cases is given by Fisher *[1]*.

Many details which are susceptible to displacement-induced fatigue cracking are included in current bridge designs. In general, any detail which includes or is adjacent to small, unstiffened segments of web plate, is a probable candidate for fatigue cracking. These web gaps result from past detailing and fabrication practices, as well as the design belief that it is poor practice to make a transverse weld across any portion of the tension flange. The resulting web gap is frequently bounded by longitudinal and/or transverse welds, and exhibits flexible behavior relative to its semi-rigid surroundings. It is within this length of web plate, that the majority of out-of-plane displacements are absorbed.

Field inspections and analytical investigations are providing information on the magnitude of stresses which are actually experienced by a number of common structures while in service. A comprehensive review of such field measurements is presented by Wagner *[2]*, and two of these cases are presented in greater detail in this study. A limited amount of laboratory testing has

focused on displacement-induced fatigue cracking. The only known study was reported in NCHRP Report 206 *[3]*. Testing was conducted on five full scale welded girders. Web cracking within the gaps at details was introduced by an externally applied load (displacement) with the girder flat, and under no in-plane loading. The adequacy of a retrofit procedure was then tested under in-plane bending stresses only, with no further distortion introduced. With the recent increase in the number of steel bridges which have developed cracks, further research on the causes of deformation-induced cracking has been sponsored. Additional studies involving methods of retrofitting damaged details are also underway.

1.1.2 Lateral Gusset Plate Detail

In order to distribute transverse wind loads, lateral bracing is often placed between adjacent girders on longer span structures. Earlier specifications required such bracing for spans over 125 ft. (38.1 m) long. However, current specifications *[4]* have increased the governing span length and provided additional design criteria. The attachment of bracing members is often made through gusset plates which are connected to the web plates. The lateral bracing system may be designed to interact with the main girders or to simply transfer the forces generated by wind. If the system is intended to interact with the main load carrying members, then the lateral bracing may be subjected to the same stress cycles as the main girder.

Regardless of interaction with main members, lateral gusset plate attachments result in a detail with low fatigue resistance. The welded connection accommodates the small out-of-plane displacements necessary to induce relatively high stress ranges in web gaps. These displacements, though

often on the order of only 0.004 in. (0.10 mm), are accommodated within the segment of web plate bounded by the transverse stiffener weld toe and the inside of the gusset plate edge. The out-of-plane deflections generate, in the unstiffened gaps, secondary bending stresses which are often sufficient to initiate cracking at weld toes. These secondary stresses are not calculated in normal rating procedures nor accounted for in the current design process. Thus, fatigue provisions have not been applied to this type of cracking.

The longitudinal web gap, present in most gusset plate connections, typically ranges from 0.25 in. to 4 in. (6.35 to 101.6 mm) in length. Details which include the smaller gaps risk the intersection of the transverse stiffener weld and the longitudinal gusset plate weld. Restraint due to large shrinkage strains along these welds, elevates local stresses within the smaller gap. Further problems may arise from lack of fusion or slag inclusions which may exist at such intersections. However, larger gaps are more flexible, and accommodate larger out-of-plane displacements with subsequently higher secondary stresses. The magnitude of distortion-induced fatigue cracking is directly related to the length of web plate over which the distortions must be absorbed.

With damage accumulating for each stress excursion above the detail's fatigue limit, a crack may initiate at the toe of a weld after only a brief period in service. The initial crack will grow perpendicular to the largest cyclic stresses. At longitudinal web gaps, the greatest restraint is provided by the boundaries at the ends of the web plate adjacent to the stiffener weld and the inner edge of the gusset plate. This restraint generates large secondary stresses parallel to the girder's main axis. Consequently, gusset plate web gaps must undergo the simultaneous effects of primary, in-plane bending stresses and

secondary, out-of-plane displacement-induced stresses. Thus, these horizontal gaps are very susceptible to fatigue crack growth and pose a serious threat to the servicability of the bridge.

1.2 Specific Case Studies

1.2.1 I-79 Bridge #2682, West Virginia

Cracking in the lateral gusset plate gaps developed in I-79 Bridge #2682 over Big Sandy Creek in West Virginia *[5]*. The twin roadway is supported by two main steel girders with four stringers resting on transverse floor beams. The continuous girders have three spans of 120ft.-130ft.-120ft. (36.6m-39.6m-36.6m). The lateral bracing is bolted to a gusset plate which is welded to the girder web, but not to the floor beam connection plate. The gusset plate detail is shown in Figure 1. The web gaps vary from 1/4 in. to 1 in. (6.4 to 25.4 mm) in length. The prevailing condition has resulted in the formation of vertical cracks along the outside (facia) transverse stiffener weld toes as shown in Figure 2.

Strain measurements of main girder flanges verified the composite behavior of the girder sections. A maximum in-plane bending stress range of 3 to 5 ksi (20.7 to 34.5 MPa) was recorded and is typical of stresses in other bridges of comparable span length. Strains recorded on the laterals indicated a maximum stress range of 2 to 3 ksi (13.8 to 20.7 MPa) in both members framing into a gusset plate. The equivalent maximum forces were 7.5 and 8.3 kips (33.4 and 37.0 Newtons). Figure 3 shows the time response of the two laterals as a truck crossed the bridge. The time-lag in the development of tensile stresses and the difference in magnitudes imply rotation of the lateral connection plate. This

rotation accompanies significant out-of-plane distortion of the web gap with high bending stresses. Additional strain-time records indicated that each primary stress cycle was associated with a truck passing over the region.

Strains were measured at the transverse connection plate weld toe within the gusset plate gap and along the toes of the outside (facia) stiffener. Evaluation of stresses indicated the outer stiffener weld toes to be the critical location for crack growth. Stress ranges of 8 to 12 ksi (55.2 to 82.7 MPa) were calculated at the weld toe on the outer surface of the web directly opposite the gusset plate gap. The stress range within the gap was found to be 3 ksi (20.7 MPa), but when extrapolated to the transverse weld the range was closer to 7 ksi (48.3 MPa). Maximum stresses of 9 to 15 ksi (62.1 to 103.4 MPa) were induced at the transverse weld in the gap.

The out-of-plane distortion produced by the forces transmitted through the bottom laterals, causes cyclic stresses well above the fatigue limit for the stiffener weld toe. The ADT volume observed by the West Virginia Department of Transportation was 5200 in 1984. The ADTT was found to be approximately 20% of the total number of vehicles per day. Therefore, about 1000 trucks have crossed the bridge for each day the structure has been in service. This suggests that over 5 million cycles of random variable stress have been applied to the lateral connection plate details. Hence, the fatigue cracking is indeed consistent with the observed cyclic stresses.

To arrest the growth of the vertical cracks at the weld toes, a retrofit was recommended. The cracks forming along the outer transverse stiffener weld, opposite the gusset plate, and within the gap at the gusset plate inner edge were to be halted by drilling holes in the web plate. The 2 in. (50.8 mm)

diameter holes were to be drilled on center, 2 in. (50.8 mm) above and below the gusset plate on each side of the transverse stiffener. The introduction of these holes was expected to dramatically reduce the magnitude of the stress field in the local region surrounding the crack tips. In addition, a positive attachment was installed between the gusset and transverse connection plates. It was believed that this attachment would reduce the out-of-plane deformation at the detail. This retrofit was completed at each gusset plate detail and further cracking has not developed.

1.2.2 Canoe Creek Bridge, Pennsylvania

Positive attachment may be made by framing the lateral bracing member directly to the transverse stiffener or connection plate. Rigid attachment tends to reduce the degree of out-of-plane displacement, but may increase the magnitude of loads in the components as well as the number of loading cycles. Cracking at such a connection was investigated on the Canoe Creek Bridge in Clarion County, Pennsylvania *[6]*.

Built in the 1960's, each bridge is a twin girder - floor beam type structure with five continuous spans and a simply supported multi-girder end span. The continuous portion of the structure consists of two 135 ft. (41.45 m) side spans and three center spans of 162 ft. (49.38 m). The two longitudinal plate girders vary in depth from 8 ft. (2.44 m) to 14 ft. (4.27 m), and include flanges which vary in cross-sectional area and web plates which change thickness over the length of the spans. The reinforced concrete deck is cast directly on the girder flanges and is further supported by stringers resting on transverse floor beams. No shear studs were used, but composite action under live loads takes place by friction in the longitudinal direction, and by positive restraint in

the transverse direction between the deck and the girders and stringers.

The laterals (ST7WF39) are connected to both the floor beam and the girder web through two gusset plates of 0.375 in. (9.5 mm) thickness. Inspection of the plate attachment, shown in Figure 4, revealed three types of fatigue crack indications. The first, shown in Figure 5, prevailed at the weld toe of the outer end of the gusset plate tabs. The second occurred in the small horizontal web gaps between the transverse connection plate and the gusset plate tabs. This mode of fatigue cracking is shown in Figure 6. The third type of crack indication was related to the horizontal web gap, but occurred on the outside surface of the girder web along the vertical stiffener as shown in Figure 7. These crack indications were observed on each side of the vertical stiffener at the level of the lateral gusset plates at most floor beam locations in both the negative and positive moment regions.

The existence of the second and third types of cracks was not expected. Referring again to Figure 4, the gusset plates are bolted to the bottom flange of the floor beam as well as the two horizontal connection plate tabs which are in turn welded to the girder web. The fabricated joint has a high degree of restraint, and no evidence of slip was detected at the bolts. The out-of-plane displacements necessary to induce secondary stresses above the detail's fatigue limit were not thought likely to develop within a connection of this type. Thus, even in the presence of positive attachment, local distortion has elevated the magnitude of the membrane stresses and contributed to the cyclic growth of fatigue cracks.

The response of the laterals was quite similar to that explained in the I-79 field study. The test results show that the out-of-plane bending is large at the

level of the gusset plate attachments. Gaging indicated that the stresses in the laterals were either of the same sign, indicating tension in both members, or of opposite signs and out-of-phase during the passage of test vehicles. The latter condition implies out-of-plane rotation of the lateral connection plate. This rotation reduces the stress range at one weld toe, but increases the range at another. The additional distortion of the plate rotation produces secondary stresses sufficient to propagate fatigue cracks.

The measured stress ranges in the bottom flanges were usually between 2.9 ksi (20 MPa) and 3.6 ksi (24.8 MPa). The magnitude of stress range near the weld terminations on the gusset plate tabs was 5 to 8 ksi (34.5 to 55.2 MPa). This magnitude resulted from the superposition of the in-plane bending stresses and the out-of-plane distortion-induced stresses. As a result, the stress range at the weld toe of the lateral gusset plate tab was almost twice as great as that experienced in the bottom flange, and often above the detail's fatigue limit.

Gages were mounted on the outer web surface, opposite the 1.5 in. (38.1 mm) web gap at the gusset plate level. Stresses of 8 to 16 ksi (55.2 to 110 MPa) were indicated. Stress ranges of up to 26 ksi (179 MPa) at the transverse connection plate weld toe were extrapolated from measured strain gradients. At these magnitudes of stress range and maximum stress, cracking would have been expected to occur quite early in the structure's service life.

The recommended retrofit for the lateral gusset plate attachments includes a means of arresting crack growth and accommodating for future out-of-plane displacements. The welded tabs were to be removed and the existing cracks repaired. Bolted angles would then be installed in place of the welded plates, thus increasing the detail's fatigue resistance to that of a Category B detail.

However, this new connection would not provide a retrofit for the vertical cracks along the transverse stiffener weld toes. Thus, these cracks must be handled independently. To arrest these cracks, it was necessary to install 2 in. (50.8 mm) diameter holes on each side of the stiffener and gusset plate as recommended by Fisher *[6]*. Within the retrofit procedures, the horizontal web gap was to be extended to a length of 4 in. (101.6 mm). This increase in gap length is expected to provide a more flexible region to accommodate distortion.

1.3 Research Objectives

The work in this project is directed toward the creation of a database to aid in the development of guidelines for the prevention and repair of distortion-induced fatigue cracking at lateral gusset plate details. Due to the lack of laboratory information on the types and behavior of fatigue cracks which form within, or adjacent to, these details, this work focuses primarily on experimental studies. With the information recently compiled on the stress magnitudes actually experienced by a number of bridge structures while in service *[2]*, the experimental studies simulated detail behavior under controlled conditions. These studies involved altering and examining the numerous variables associated with distortion-induced fatigue cracking.

Classification of a detail's severity is based on the prevailing variables which influence the degree of distortion-induced cracking, as well as the geometry and nature of the detail itself. A careful correlation of the following variables with those values and magnitudes reported in field studies permitted such a classification.

- The in-plane stress range generated at the level of the lateral gusset plate under a prescribed loading.

- The specific horizontal web gap geometry.
- The means of gusset plate attachment and degree of physical displacement.
    - The system by which the driving force is transmitted to the plate.
    - The actual magnitude of the resulting driving force.
- The magnitude of the secondary stress range induced within the web plate by lateral displacement.

Since the gusset plate is often coped to fit around the stiffener or connection plate, an unrestrained web gap may exist depending upon the means by which the gusset plate is connected to the transverse plate. Many existing structures have made use of gusset plates with no connection to the stiffener. However, most bridges include gusset plates that are attached to the transverse connection plate. Therefore, this research investigates the behavior of two lateral gusset plate connections:

1. A gusset plate welded to the girder web and bolted to the transverse connection plate (Detail B).
2. A gusset plate free of attachment to the transverse connection plate, but welded to the girder web (Detail C).

Thus, a detail including positive attachment was studied as well as a connection free of such lateral restraint. After a degree of fatigue crack development had been experienced, retrofit procedures were examined. These included:

- The introduction of drilled holes at the leading crack tips within the horizontal web gap.
- Further lateral restraint through the introduction of additional positive attachment between the gusset plate and the transverse plate.

This investigation provides valuable insight into the behavior of two lateral gusset plate attachments which have been found to be susceptible to distortion-induced fatigue cracking. A better understanding of secondary distortion should minimize the use of poor details in new structures. The experimental results indicate an accurate estimate of the fatigue life of various connection details and quantify the variables surrounding the conditions which foster distortion-induced fatigue cracks.

Furthermore, the experimental background should aid in the selection of a retrofit procedure for application to an existing structure. This will allow for the standardization of such procedures on the basis of the type of connection detail, the prevailing stress levels, and the magnitude of distortion encountered. A secondary result should be the identification of adequate repair procedures. A judgment could then be made on further crack growth and additional retrofit procedures to be taken. Many of the results of this work will become apparent in the design process. While no formal codes may be directly specified, the increased awareness of design engineers to the problems of distortion-induced fatigue, will increase the life and safety of our infrastructure, and minimize the cost of repair.

Chapter 2
TEST PROGRAM

2.1 Scope

For the purpose of developing a framework for the experimental portion of the project, initial efforts involved a review of field cases, and an analytical study of the proposed tests. Within the experimental phase of this work, two separate areas of study can be defined:

- The quantification of the fatigue resistance of lateral gusset plate connection details.
- The evaluation of retrofit procedures used to repair prevailing damage.

A testing program with four beam segments was used to analyze the behavior of two connections for the particular details shown in Figure 8. Each segment contained two test sites. Thus, a total of eight details were tested under prescribed loadings and controlled conditions. Table 1 shows the program's factorial arrangement. The arrangement's variables include the mode of positive attachment and the nominal length of unrestrained web plate. The nominal size of the web gap is defined as the distance between the transverse connection plate and the gusset plate's inner edge, without consideration of the weld lines. The actual size of the web gap is measured between the toes of the adjacent welds, and is considerably less than the nominal length noted.

The factorial includes four bolted positive attachment schemes, two with 1.5 in. (38.1 mm) nominal gaps, and two with 3 in. (76.2 mm) nominal web gaps. Four connections free of positive attachment are noted; two include 1 in. (25.4 mm) nominal gaps, and two include 3 in. (76.2 mm) nominal web gaps.

The nomenclature *"T5-6"* refers to *"Detail #6 of Test #5."*

All girder segments were exposed to secondary bending stresses in the vicinity of the detail. These stresses are generated through out-of-plane displacements. Vertical loads were applied through hydraulic jacks in order to produce a primary, in-plane bending stress of 6 ksi (41.4 MPa) at the gusset plate level. This magnitude of stress is quite common in bridge structures subjected to a normal load spectrum, and its selection is a result of the initial review of field studies. Under these operating conditions, the scope of this research covers two typical gusset plate connections, and focuses on the variables effecting distortion-induced fatigue cracking.

2.2 Specimen Description

2.2.1 Specimen Design

The specimens utilized in this portion of the experimental study were full scale, welded plate girder segments. This is due to the discrepancies found to exist between the results of small scale, laboratory fatigue tests and those of in-service field investigations. The segments containing the details are 10 ft. (3.048 m) long and are bolted between reuseable, 8 ft. (2.438 m) long end segments. The resulting simple span is approximately 25 ft. (7.62 m).

A typical test girder segment is illustrated in Figure 9. The flanges are 1 in. x 12 in. (25.4 mm x 304.8 mm) in cross section. The web plate is 0.375 in. (9.53 mm) thick and 40 in. (1016 mm) deep. Thus, the specimen has an overall depth of 42 in. (1066.8 mm). Standard AISC steel design specifications *[7]* were utilized to design a girder segment that best simulated those found in common bridge structures. The following considerations and limitations were

influential in specifying exact detail locations, bolt patterns, and weld sizes:

1. Span length of 25 ft. (7.62 m).

2. Loading capacity and stroke of the available hydraulic jacks.

3. Existing limitations posed by the laboratory's dynamic testing bay framework, and consequently, the longitudinal spacing of the hydraulic jacks.

4. Prescribed 6 ksi (41.4 MPa) primary, in-plane bending stress at the lateral gusset plate level.

5. Degree of anticipated lateral displacements and the magnitude of subsequent distortion-induced stresses.

6. Knowledge of the typical girder detail sizes and fabrication procedures utilized to produce and erect the bridge structures in service today.

7. Results of an extensive review of field measurements of distortion-induced fatigue cracking, as well as an investigation of the conditions surrounding the cracked detail.

8. Analytical results of a series of Finite Element models utilized throughout the parametric study phase of the research project.

9. Ease of fabrication and erection during the project's testing phase:

    - flexibility in specimen orientation
    - ease of installation and replacement during tests
    - safeguards for future changes in the testing procedures

10. Efficient use of symmetry throughout experimentation.

11. The major research objectives and the overall scope of the project.

The 0.375 in. (9.53 mm) thick concentrated load stiffeners run one-half of the specimen depth and are attached on each side of the web plate. The stiffeners are welded to both the web and the compression flange, and are spaced 5 ft. (1524 mm) apart. This spacing establishes a 5 ft. (1524 mm) length over which the moment remains constant under constant loading. The

outer extremes of the lateral gusset plates are positioned below these stiffeners. The gusset plates were located 6 in. (152.4 mm) above the top surface of the bottom flange. Analysis indicates that the out-of-plane displacements induced at one gusset plate will not effect the behavior of an adjacent plate.

The actual gusset plate web gaps are defined by the weld toe at the plate's inner edge and the transverse connection plate weld toe. The connection plates are 0.5 in. (12.7 mm) thick. The outer transverse plates are 5 in. (12.7 mm) wide. The inner connection plates vary in width from 5 in. (12.7 mm) to 6 in. (152.4 mm), depending on the lateral gusset plate detail and the size of the unstiffened web gap. The outer connection plates are perforated to accommodate the attachment of the secondary members through which out-of-plane displacements are imposed. All transverse connection plates are fillet-welded to the web plate and the compression flange, but are only tightly fit to the tension flange. If the connection plate were cut short of the tension flange, a transverse web gap would exist. Finite Element analyses indicated the development of high membrane stresses in such a transverse web gap. It is believed that crack growth at the lower end of the connection plate may effect the lateral flexibility at the gusset plate level and thus, alter the behavior of the actual details being tested. Should cracks still prevail, the transverse plate could be welded to the tension flange by laboratory technicians at any point in the testing procedure.

Weld sizes were dictated by component plate thicknesses and computed stress fields. The bolt patterns were specified on the basis of maximum shearing forces and desired moment capacities. All holes are 1.0 in. (25.4 mm) in diameter and hold 0.875 in. (22.23 mm) diameter, A325, high strength bolts.

The lateral gusset plate details are shown in Figure 8. All plates are 18 in. (457.2 mm) long, 14 in. (355.6 mm) wide and 0.5 in. (12.7 mm) thick. Detail B has a 6.5 in. (165.1 mm) deep cut from the web gap to clear the 6 in. (152.4 mm) wide stiffener. The gusset plate was fabricated to specifications for nominal web gap sizes of 1.5 in. (38.1 mm) and 3 in. (76.2 mm). Positive attachment is established by bolting a structural section (WT5X6) to both the lateral gusset plate and the transverse stiffener plate.

Detail C includes a 6 in. (152.4 mm) deep cut rounded to prevent contact with the 5 in. (127.0 mm) wide stiffener. The nominal gap sizes are 1.0 in. (25.4 mm) or 3.0 in. (76.2 mm), and no positive attachment exists between the gusset plate and the stiffener. All welds were sized on the basis of component thicknesses and standard design practices. Bolted attachments, including the lateral bracing members, were selected on the basis of Finite Element Analysis results. The criteria for the selection of the WT5X6 members included rigidity, cross-sectional area, and buckling capacity.

A test girder end segment is illustrated in Figure 10. The 42 in. (1066.8 mm) deep segment is reuseable and allows for an increase in the overall stiffness of the girder without increasing the jack force required to produce the prescribed bending stresses in the center segment. The top and bottom flanges are identical to those of the test segment. A pair of 24 in. x 6 in. x 1 in. (609.6 mm x 152.4 mm x 25.4 mm) plates were attached to both ends of these segments. These serve as false flanges for the attachment of 36 in. (914.4 mm) deep test segments; a phase of experimentation which is beyond the scope of this research. The "welded tab", detailed in Figure 11, enhances the girder's stiffness during the testing of the 42 in. (1066.8 mm) deep specimens.

The end segments have 0.375 in. (9.525 mm) thick webs and are fully compatible with the center segments. Furthermore, the end girders are symmetrical about the member's vertical centerline. This permits the segment to be revolved about this line of symmetry if the end attached to the center segment should be damaged during testing. Again, all holes were drilled to a 1.0 in. (25.4 mm) diameter to hold 0.875 in. (22.23 mm) diameter, A325 bolts.

The flange and web splice plates were designed simultaneously with the plate girder segments. All splice plates allow for a 0.125 in. (3.175 mm) deviation between the longitudinal dimensions of the girder segments. The test segment's compression flange is attached to that of the end girder's through four bolted splice plates. These plates are shown in Figure 12. The test section's tension flange is connected to that of the end segments through three bolted splice plates. Two of these are identical to those utilized in the compression flange attachment. The third is shown in Figure 13 and is bolted along the lower surface of the tension flange. All flange plates were designed to resist, and continuously transmit, the axial forces developed in the flanges through in-plane bending.

A web splice plate is illustrated in Figure 14. These plates include a simple bolt pattern designed to carry vertical shearing forces and resist the moments produced during loading. A pair of web splice plates are required to attach one end of the center test segment to an end girder segment. The 1.0 in. (25.4 mm) diameter holes hold 0.875 in. (22.23 mm) diameter A325 bolts.

All bolted connections were designed with careful consideration given to the transfer of stresses developed under the application of hydraulic loads. The bolted segments are expected to behave as a continuous plate girder. The

spliced connections are not within the constant moment region and do not effect the behavior of the lateral gusset plate details.

2.2.2 Specimen Fabrication

Upon completion of the project's design phase, a package including specimen component drawings and fabrication specifications was formulated. This package was then presented to four local fabricators along with a formal request for the submission of bids. The fabricator was to produce all plate girders, web and flange splice plates, and furnish complete field bolt fixtures. The contract was awarded to the *Lehigh Structural Steel Company* of Allentown, Pennsylvania.

The fabricator drafted a complete set of shop drawings for a design review. After approval was secured, the fabricator proceeded with a material order. All girder components were cut from A36 plate and all 1.0 in. (25.4 mm) holes were drilled as specified. The resultant mill scale was then removed from the web and flange plates with a power grinder and a wire brush. The web plate was then clamped to a fabrication bed and the flanges were positioned as noted. The components were manually tack-welded with Lincoln E7018 (low hydrogen base) electrodes.

The region surrounding the flange-to-web weld was then preheated to 100° Fahrenheit. This process involved the direct contact of an acytelene torch and the steel surface. The point of preheat contact was maintained at a constant 3.0 in. (76.2 mm) distance ahead of the welding arc. Alternatively, certain sections of the joint were preheated at the same rate from the opposite surface of the 1.0 in. (25.4 mm) thick flange plate. The plates were continuously welded at a rate of 12 to 14 inches per minute (304.8 mm to 355.6 mm per minute) with

a Submerged Arc-Welding Dart. Granular 780 flux and Lincoln L60 wire were used for the welds. The Dart has a 35 volt capacity and can maintain a 450 ampere current throughout the welding process. The 5/16 in. (7.94 mm) weld was completed in one pass. After cooling, the weld lines were vacuumed clean of excess flux, and chipped free of slag.

All stiffener plates were cut and cleaned of mill scale. Loading stiffeners were cut as noted, but transverse stiffener plates were milled for a tight fit to the tension flange. The criteria for the fit specified that 75% of the stiffener width bear within 0.010 in. (0.254 mm) of the flange surface. The remaining 25% could be no more than 1/32 in. (0.794 mm) from the surface. The exterior plates were then perforated as called for in the design. No joints connecting plates of less than 0.75 in. (19.05 mm) thickness were preheated. Lincoln E7018 electrodes were used to attach all loading stiffeners to the web and compression flange plates. The submerged arc process, with L60 wire and 780 flux, was then applied to the longer, transverse stiffener welds. The resultant weld profiles were of high quality. Furthermore, the weld legs were deposited at less than 45° to the web plate. This resulted in a smoother weld profile, and therefore a lower stress concentration at the weld toe.

Lateral gusset plates were cut, cleaned, and manually welded to the fabricated segments. The welds wrapped continuously around the entire perimeter of the gusset plates. Upon completion of weld deposition, the actual web gap lengths were measured as approximately 0.75 in. (19.05 mm) less than the prescribed nominal sizes. No holes were drilled in the gusset plates by the fabricator. This work was to be done by laboratory technicians at a later date. Thus, bracing properties and bolt patterns were not fixed at the time of girder

fabrication. All splice plates were cut, machined clean and smooth, and drilled as specified.

Upon inspection, five of the deep plate girders were found to exhibit severe web plate distortion. The free edges of the plate, at the ends of the segment, were warped due to the exposure to high temperatures during the welding process. In one case, the out-of-plane web distortion resulted in poor flange alignment. The fabricator applied further heat to the plates in order to induce a reverse curvature in the distorted fields. A second inspection showed the condition of the web plates to be acceptable. The fabricator then stored the plate girder segments in an enclosure until transportation to the laboratory was requested.

2.3 Experiment Design

2.3.1 Testing Layout

The girders are tested in pairs and are symmetrically oriented on the laboratory dynamic test bed as shown in Figure 15. The bay framework consists of W12X85 columns and pairs of W30X116 cross beams. Channels and miscellaneous wide flange sections are utilized to resist lateral displacements and increase the system's overall rigidity.

A typical test girder is illustrated in Figure 16. The center segment carries the two gusset plate details, and is bolted between the reuseable end segments. The continuous plate girder has a length of 26 ft. (7.925 m) and a simple span of 25 ft. (7.620 m). A pin support is simulated by the mechanism shown in Figure 17. The pinned system is bolted to a heavy pedestal which is anchored to the test bed's concrete floor. A roller support is simulated by the connection

shown in Figure 18.

Hydraulic jacks apply the loads designated as "*P*". The loads act through a bearing plate directly above the 21 in. (533.4 mm) long stiffeners. A heavy section is clamped between the adjacent tension flanges, below each of the lateral gusset plates. This strut prevents the tension flange from rotating or translating out of the plane of the web plate. This restraint is similar to that posed by an overlying concrete deck in a bridge's negative moment region.

2.3.2 Design and Fabrication of Secondaries

Out-of-plane displacements will be imposed at the gusset plate level through the restraint offered by an adjustable steel rod. The rod is fastened to the transverse connection plate, opposite the web gap, and pinned to an adjacent cross beam. The design of the rod's components relied on the previously listed considerations and limitations. However, the finite element analysis results were the major factor in the determination of the driving force required to induce the lateral displacements necessary to generate fatigue crack growth. Thus, a structural analysis program allowed for the rapid change of certain rod variables: cross-sectional area, overall length, and the angle of rod inclination.

The "driving force" member is illustrated in Figure 19. This secondary member is composed of four individual components:

1. A system of welded plates for the attachment of the pipe to the transverse connection plate

2. A 32.0 in. (812.8 mm) long steel pipe with a 2.5 in. (63.5 mm) nominal diameter

3. A 13.0 in. (330.2 mm) long steel pipe with a 3.0 in. (76.2 mm) nominal diameter

4. An *American Hoist Corp.* stock clevise grip for the attachment of the pipe to an adjacent cross beam

Within the scope of the project's research, a certain degree of distortion, produced through out-of-plane displacements, was anticipated. Analysis predicted the maximum load to be applied for the desired effect. This load was then considered to be the buckling load for the secondary member. On this basis, and for a rod length compatible with the testing layout, a controlling cross-sectional area was calculated with a factor of safety.

The 32.0 in. (812.8 mm) long component was rolled from ASA B36.10 steel, and supplied by the *Hajoca Corporation.* The outside diameter is 2.875 in. (73.03 mm) and the wall thickness is 0.552 in. (14.03 mm). The resulting metal cross-sectional area is 4.03 sq.in. (2600 sq.mm), and the component weighs 13.70 lb./ft. (20.4 g/mm). Because of the component's heavy wall, the section is referred to as *"double-extra strength pipe."* From one end, 9.0 in. (228.6 mm) of the rod's exterior was machined with 8 threads per in. (0.315 thread per mm).

In order to be able to adjust the rod angle, and consequently alter the degree of lateral distortion, a fitted sleeve was designed. This sleeve's interior was machined with 9.0 in. (228.6 mm) of 8 threads per in. (0.315/mm). Both pipe segments were machined round on a lathe prior to the cutting of threads. The 13.0 in (330.2 mm) long sleeve was also rolled from ASA B36.10 steel. The outside diameter is 3.5 in. (88.90 mm) and the wall thickness is 0.600 in. (15.24 mm). The metal cross-sectional area is 5.47 sq.in. (3529 sq.mm) and the component weighs 18.58 lb./ft. (27.67 g/mm).

The pinned connection to the test-bed cross beam is made through a stock grip. The grip was forged and drilled with a 1.875 in. (47.63 mm) diameter hole. The core-end was machined to a close fit with the inside diameter of the

sleeve. This connection allows for the vertical adjustment of the rod's end. During such an adjustment, the sleeve may be rotated on the grip's core to pull the narrow pipe taught and produce a continuous compression member.

The rod is bolted to the transverse connection plate. The attachment is made through a pair of plates which are welded perpendicular to a base plate. The base plate is fillet welded to the pipe segment as shown in Figure 19. The projecting plates are located in such a manner as to directly transfer the force developed in the pipe wall to the connection plate. The transverse connection plate has been enlarged at the point of contact by the attachment of a pair of 3.0 in. x 3.0 in. x 0.5 in. (76.2 mm x 76.2 mm x 12.7 mm) plates. These plates increase the stiffener bearing area to 1.5 sq.in. (967.7 sq.mm) at the point of force transfer. All attachment components were cut from A36 steel plate. All fillet welds were manually produced with E7018 electrodes.

The gusset plates were drilled for the attachment of WT5X6 lateral braces by Fritz Laboratory technicians. Figure 20 illustrates the bolt pattern for Detail B. The patterns for Details A and C are identical with the exception of the bolted positive attachment. The outer braces are bolted to each of the gusset plates as shown. All holes are 1.0 in. (25.4 mm) in diameter and hold 0.875 in. (22.23 mm) diameter A325 bolts. The pattern was selected on the basis of the finite element models developed, practical spacings, and ease of installation.

2.3.3 Loading

Throughout the experimentation phase, the details are tested on adjacent girders oriented symmetrically within a frame. Parallel girders are loaded through vertical, hydraulic jacks as shown in Figure 21. Two jacks, at a 5 ft. (1.524 m) spacing, are required for each girder. Thus, a total of four hydraulic jacks are utilized.

The hydraulic jacks induce vertical deflections within the plate girder's span. As the girder deflects, the secondary rods enter into compression and resist further vertical displacements. The rod's stiffness induces lateral displacements at the gusset plate level. Subsequently, these out-of-plane displacements generate secondary membrane stresses within the unrestrained web gaps. Therefore, by regulating the vertical loads, the lateral displacements can be governed. In the process, the driving force in the rods can be monitored. Through adjustment of the vertical loading and the rod angle, the magnitude of out-of-plane displacements and the associated web gap stresses can be directly controlled.

Four *Amsler* hydraulic jacks were supplied. Each has a 55,000 lb. (4,440 N) capacity. A typical *Amsler* jack is illustrated in Figure 22. Exterior springs pull the jack to a stationary position when the system is not under pressure. These springs are characterized by an elastic constant of 33.4 lb./in. (5.84 N/mm) and are accounted for in the selection of loads.

The four jacks are fixed to a base plate which is clamped to a deep cross beam. Each jack is connected to a single, common distribution cylinder by a series of sealed pipes. The distributor provides each jack with an identical volume of oil at a constant rate. Such a process balances the overall loading

system and provides a degree of continuity between the tests.

The distribution cylinder is connected to an *Amsler* Hydraulic Pulsator. The pulsator piston, whose displacement is basically a sinusoidal function of time, causes fluctuations in the oil pressure within the hydraulic jack. These fluctuations are subsequently transmitted to the specimen as alterations in load. Thus, the load variability maintains a sinusoidal profile. Such a profile is characteristic of a fatigue loading pattern.

The pulsator piston forces oil into the cylinder, thereby accumulating elastic potential energy within the jack. The ram, under the influence of the elasticity of the specimen, returns the oil to the pulsator. The factors effecting the true maximum load, and as a consequence, the upper limit of the vertical deflections, are complex. Pulsator and hydraulic jack strokes, dimensional, mass, and elastic characteristics of the specimen as well as the surrounding frame, and the elasticity of the connecting pipes and pulsator oil, are all considered to be influential in developing and sustaining a desired load.

The theoretical maximum stroke of each jack is 0.25 in. (6.35 mm). However, slip and flexibility inherent in the framework indicate a stroke of 0.22 in. (5.59 mm) as an attainable limit. An automatic load counter gives the number of load cycles. The system is provided with an electrical contact which interrupts the current to the pulsator motor upon specimen fracture, as defined by excessive vertical deflections.

The loading cycles were maintained at a constant amplitude and the frequency was set at 250 cycles per minute. The maximum load was set on the basis of the desired in-plane stress to be generated at the level of the gusset plate detail. This maximum could be altered as stresses decrease with the

increase in flexibility brought on by fatigue cracking. Finite element analysis indicated that maximum vertical deflections of 0.13 in. (3.30 mm) would be sufficient to generate high distortion-induced stresses within the detail's web gaps. This prediction allowed for a generous factor of safety in remaining below the available stroke of the jacks.

2.3.4 Instrumentation and Testing Procedure

Standard laboratory instrumentation was utilized to measure displacements and strains. Vertical deflections were measured with *Ames* dial gages; these are accurate to 0.001 in. (0.0254 mm). Surface strains at weld toes and plate edges were measured with electrical resistance micro-gages. Single and strip gages were applied. The single gages were *Type EA-06-250BG-120* and the strips were *Type EA-06-031MF-120* with a 0.080 in. (2.03 mm) centerline distance between adjacent gages. The resistance gages were wired to a *Cyber Data Acquisition System* for initial static tests. Strains were recorded for seven load increments to 55 kip. Web gap distortion was measured at each increment by calibrated "clip gages" wired to a *Vishay/Ellis-20 Digital Strain Indicator*. During dynamic testing, only certain gages were monitored through a manual switch-box and a *Peak Strain Indicator*. The tension flange strains and vertical deflections were used as the controlling factors. By comparison, the Dynamic Magnification Factor was calculated and applied to the strains measured during static testing.

The girder-detail relationships are outlined in Table 2. The details were assigned to specific girders on the basis of the number of detail types, the number of each type, and the degree of anticipated lateral distortion each might undergo. The details were matched with similar types between adjacent test girders. Figure 23 illustrates the layout of the six specimens. The tests were

completed on the girder pairs as indicated. Upon completion of the experimental phase for one pair of girders, another pair was placed within the test frame and the program commenced.

Chapter 3
FINITE ELEMENT ANALYSIS

3.1 Development of Finite Element Models

3.1.1 Overview

To aid in the project's design and experimentation phases, a series of finite element models was developed. Such an analysis permitted the researchers to rapidly obtain vital information pertaining to specimen behavior under a certain set of conditions. These conditions included: loading magnitude, geometrical aspects for the loading and restraint of the plate girder, specimen component section-properties, and secondary member characteristics. A database was generated for each set of parameters. The database was then attached to a finite element analysis program. The program utilized throughout the project was *"SAP IV: A Structural Analysis Program For Static And Dynamic Response Of Linear Systems" [8].* The analysis results were then applied to the design of the specimen and secondary members. Furthermore, these results were continuously referred to during the testing of each detail. Discrepancies were noted, and adjustments were made to the finite element models until the computer-simulated response was within reasonable bounds of the experimental observations.

3.1.2 Gusset Plate Detail Without Positive Attachment

An initial database was developed to model a lateral gusset plate detail without positive attachment to the transverse connection plate (Detail C). This model included a pair of 1.0 in. (25.4 mm) web gaps. The database makes use of 561 nodal points to define the boundaries of 107 truss elements, 23 beam elements, 185 plane stress elements, and 289 plate-bending elements. These elements were arranged in 18 individual families within the computer file.

Because of the specimen's symmetry, only one-half of the plate girder was modeled. A central region with a 41.0 in. (1041.4 mm) depth and a 13 ft. (3.96 m) length was discretized first. This depth extends from the center of the top flange to that of the bottom flange. The elements simulating the flanges were then superimposed on the plane. This overlay resulted in a 42.0 in. (1066.8 mm) deep section with an accurate distribution of stiffness. The loading stiffener and transverse connection plate elements were then superimposed on then web's mesh. Finally, a rectangular plate was discretized in the third dimension at the level of the gusset plate. This core model served as the first simulation of the physical specimen. A computer-generated plot of the finite element model is shown in Figure 24.

All flanges were modeled with truss elements. The girder depth is approximately 200 times greater than the anticipated maximum vertical deflections. Therefore, the flange plates do not have a major influence on the resistance of in-plane bending moments. Furthermore, the flanges are only 1.0 in. (25.4 mm) thick; the strain gradient is practically uniform through such a shallow depth. The flanges provide for the transfer of axial forces, hence, their behavior can be simulated with a continuous series of truss elements. The

elements' cross-sectional area was adjusted on the basis of the girder's global moments of inertia. This adjustment reflects the effect of the model's 41.0 in. (1041.4 mm) deep web plate. The element's are continuous over the model's length, and do not account for any gap between the girder's end or center segments. To restrain lateral motion of the tension flange during testing, a heavy structural section was clamped between adjacent girders. The model simulates this restraint through the "locking" of out-of-plane translational and rotational degrees of freedom. The nodes which bound the lower line of truss elements are only given in-plane D.O.F.

From the left edge of the model, to a length of 118.0 in. (2997 mm) along the girder's longitudinal axis, 99 plane stress elements form the web plate. These elements are large at a considerable distance from the gusset plate detail. However, at this point triangular plane stress elements provide a transition to smaller scale elements. The elements are noticeably finer in the vicinity of the detail. The last column of plane stress elements is 8.0 in. (203.2 mm) from the outer edge of the gusset plate. Plane stress behavior implies a lack of lateral deflections and subsequent out-of-plane bending moments. The magnitude of the out-of-plane displacements at the gusset plate web gaps is expected to be on the order of 0.02 in. (0.51 mm). Previous research indicates that these displacements decrease rapidly and are usually insignificant within several inches of the weld toe *[9]*. Thus, prohibiting lateral deflections within the region defined by plane stress elements does not have a detrimental effect on the local analysis results. Stresses generated in this section of the model are accurate, and provided an excellent means of verifying bending moment computations.

The model's remaining 38 in. (965.2 mm) length is formulated with 289

plate-bending elements. These elements develop transverse moments as a result of lateral distortion. The out-of-plane behavior of each region of elements is refined by the addition of smaller plates. Therefore, the mesh is reduced to an ordered collection of 1.0 in. x 1.0 in. (25.4 mm x 25.4 mm) elements in the local region surrounding the web gaps and connection plate. This discretization captures the strain gradient within large web gaps from which displaced shapes may then be plotted. The elements' dimensions are within an aspect ratio of 4:1 and are expected to predict lateral deflections and secondary bending moments within reasonable error. These elements are arranged in three families within the database. The importance of this arrangement is manifested in the order of the tabulated results, which aids in the attachment of a series of post-processor programs. All elements' material and section characteristics were specified as follows:

- Modulus of Elasticity = 29,500 ksi (203,450 MPa)
- Poisson's Ratio = 0.30
- Bulk Modulus of Rigidity = 11,346 ksi (78,250 MPa)
- Plate Thickness = 0.375 in. (9.525 mm)

Each node is given all six degrees of freedom, except the column which defines the girder's vertical centerline. Due to symmetry, the girder's centerline can only undergo vertical deflections. These nodes can not rotate or undergo longitudinal translation. They may, however, experience lateral motion under the influence of plate element distortion. The appropriate D.O.F. have been assigned.

The concentrated load stiffener and transverse connection plate are modeled with 6 and 17 beam elements respectively. Each element has the properties of a pair of stiffener plates separated by a thin web plate. The elements are

superimposed on the mesh and the associated nodes are given the D.O.F. necessary to simulate actual behavior. The beam elements enhance the local stiffness of the plate-bending elements and provide the rigidity needed to transfer stresses in the transverse direction. The length of these linear elements was governed by the previously established web discretization.

The gusset plate was modeled with a total of 86 plane stress elements. The girder is loaded vertically and secondaries are attached in the plane of the gusset plate. There is no loading transverse to the gusset plate surface; behavior should remain entirely in-plane. Since the cracks develop in the specimen's web plate, the gusset plate is considered to be a means through which lateral distortion is introduced. The plate's largest area is comprised of 58 elements. The remaining section of the plate, that within the vicinity of the transverse connection plate, is formulated with a finer mesh. This discretization is fully compatible with that of the local web region and is organized in four families in the database. The families are sequentially deleted from the file as the elements are "stripped" from the inside of the plate. This "stripping" process adjusts the size of the unrestrained web gap without the introduction of additional nodes or element types. The database is then copied to additional files until all desired web gap sizes have been analyzed. The discretization allowed for a change in the nominal web gap length from 1.0 in. (25.4 mm) to 3.0 in. (127.0 mm) by 1.0 in. (25.4 mm) increments. However, no weld lines could be modeled. The elements were given properties identical to those of the plane stress elements utilized in the web discretization, with the exception of the plate thickness being 0.5 in. (12.7 mm). Each nodal point within the gusset plate boundaries was given all six D.O.F. and no attachment was made between

these elements and those of the transverse connection plate.

A boundary element was attached under the left end of the model's lower flange to simulate the actual "roller" support. The chosen element provides linear elastic resistance to nodal displacements. The boundary element is essentially a spring with a prescribed axial stiffness of 1.0E+10 kip/in. (1.75E+12 N/mm). Basically, a stiffness of this magnitude, when associated with the test's maximum loading, implies vertical rigidity at the support. This allows for the computation of the support reaction, which serves as an excellent means of verifying model results.

Secondary members, specifically the "driving" rod and the lateral braces, are simulated with truss elements. The overall testing layout is symmetrical about a centerline between the pair of girders. This centerline divides the girders and allows for the modeling of only one-half of each bracing length. The braces will undergo the same vertical deflections that are introduced to the plate girder. However, symmetry will not permit the end node of each brace to rotate or translate in any direction except the vertical. Accordingly, the corresponding D.O.F. have been eliminated from the outer element's node for each lateral brace. The brace's cross-sectional area was altered until acceptable behavior resulted. Three truss elements are used to form each brace. Two of these elements overlap the plane stress elements of the gusset plate. Several nodes are common to both the truss and plane stress elements, thereby simulating a bolt line. The actual braces transmit restraining forces in the plane of the gusset plate. Similarly, the truss elements will behave as axial, two-force members. They provide the constraint necessary to induce curvature within the web's plate-bending elements.

The rod is assumed to behave as a simple compression member. The actual rod is pinned to both the transverse connection plate and the surrounding test frame. The boundaries are set and the length is adjustable to compensate for angular alterations. Therefore, the element's nodal D.O.F. reflect these conditions. Member length, as well as angular orientation, was varied by changing the nodal coordinates. Cross-sectional area was also a variable in the database. This analysis resulted in the selection of a section area on the basis of the force developed in the rod and the lateral displacement introduced in the web gap region.

The model was loaded with a single, negative, vertical force over the node at the top of the stiffener's beam elements. The negative value reflects the orientation of the system's global axes. The load magnitude was initially altered to verify that the results were elastic. Once this criterion was established, any convenient load could be specified, and a proportional factor applied to the results for an incremental shift in load. Initial "pilot" computer analyses were made to verify the model's behavior. Primary bending moments, maximum vertical deflections, support reactions, and displacements under the loaded stiffener, were all extracted from the finite element analysis results. Comparison of these values with those calculated by popular theories indicated that the model was accurately simulating the girder's anticipated behavior under any given set of conditions.

3.1.3 Gusset Plate Detail With Positive Attachment

This model is a simple extension of the initial database. The bolted attachment of the gusset plate and the transverse connection plate made use of a structural section identical to those serving as lateral braces. The section provides additional lateral resistance to the opposing force developed in the rod. Consequently, the segment is assumed to behave as an axial compression member.

The member is modeled with four truss elements whose properties are identical to those described for the lateral braces. The inner element shares a common end node with the transverse connection plate. This element's other defining node is at the inner boundary of the gusset plate. The remaining three elements overlap the gusset plate's plane stress elements and share nodes along the member's longitudinal axis. Therefore, a single line of elements has been fixed to both the gusset plate and the connection plate.

The database was copied from the initial study, and the same parameters were varied. All geometrical and loading conditions were constant between the two models. The characteristics of the braces and the rod are identical to those of the base model. Therefore, a degree of consistency has been preserved throughout the analyses, and a comparison of the two model's results implies the effect of a bolted positive attachment.

3.2 Parametric Study

3.2.1 Analytical Variables

As previously noted, several parameters were varied until the analysis results indicated acceptable behavior. These parameters included the length and cross-sectional properties of the secondary elements. Values were set prior to the final design, and the parametric study commenced. The analytical variables in the study were:

- The length of the unrestrained web plate referred to as the "web gap"
- The angular orientation of the secondary compression member referred to as the "driving rod"

The web gap length was varied from 1.0 in. (25.4 mm) to 3.0 in. (76.2 mm) by 1.0 in. (25.4 mm) increments. A Finite Element model was developed for each of the three web gap sizes. Furthermore, a set of models was required for each of the two details studied; the case of positive attachment and that without such a connection. Therefore, six separate models were analyzed.

The driving rod angle was varied from 0.00° to 30.00° by 5.00° increments. This angle is referenced to the horizontal, thereby placing the rod in compression throughout the testing process. Therefore, seven specific values of rod angle were investigated for each web gap size. In all, 42 final Finite Element analyses were provided by the *SAP IV* computer program.

Pertinent results of each of the 42 analyses were extracted, tabulated, and plotted through the attachment of post-processor programs. The following sections will discuss the results for the case of a 3.0 in. (76.2 mm) web gap and a rod angle of 20.00°. The finite element model behavior will be compared for

the 3.0 in. (76.2 mm) web gap as the rod angle is varied from 0.00° to 30.00°. Finally, a tabulation of the key results for each web gap size and each of the two details is presented.

3.2.2 Typical Results: Without Positive Attachment

The Finite Element analysis results for Detail C are presented for the case of a 3.0 in. (76.2 mm) web gap and a rod angle of 20°. The model was loaded to the jack's capacity of 55 kip (245 kN). The out-of-plane displaced shape along the gusset plate is plotted in Figure 25. Note the plot's overall symmetry and the short distance to each side of the plate in which the out-of-plane displacements rapidly decrease. The lateral translation of the plate's outer edges is 0.001 in. (0.025 mm). However, the rigidity of the braces restrains the deflection to 0.0005 in. (0.013 mm) at their point of attachment. The inner edges of the gusset plate translate 0.0012 in. (0.030 mm), while the driving rod forces the stiffener to undergo a lateral displacement of 0.0082 in. (0.208 mm). Thus, the difference in the deflections of the web gap boundaries defines a relative distortion of 0.007 in. (0.178 mm) within the unrestrained web plate.

The bending moments developed through the in-plane loading and the out-of-plane distortion were calculated in the analysis. The resulting stress distributions along the gusset plate are shown in Figure 26. The variation in primary membrane stress is due to the increased rigidity of the web plate in the vicinity of the gusset plate and connection plate attachments. This stress is approximately 6.0 ksi (41.4 MPa) and is developed through the in-plane loading. The secondary membrane stresses along the gusset are induced by lateral distortion. The plate's outer edges are exposed to virtually no secondary stresses while the inner edges undergo distortion-induced stresses of -9.0 to -10.0 ksi

(-62.0 to -69.0 MPa) on one side of the web plate. Secondary stresses of 14.0 ksi (96.5 MPa) developed at the connection plate weld toes. Thus, distortion-induced stresses range from 9.0 ksi (62.0 MPa) of compression to 14.0 ksi (96.5 MPa) of tension on one side of the web plate. These magnitudes are 2 to 3 times greater than the primary, in-plane membrane stresses.

The combined stress distribution is illustrated in Figure 27. This plot is a superposition of both primary and secondary stresses associated with in-plane loading and lateral distortion respectively. The figure predicts stresses of 5.2 ksi (35.9 MPa) at the gusset's outer edge and -9.8 ksi (-67.6 MPa) at the inner edges. The transverse weld toes are exposed to a combined membrane stress of 18.7 ksi (129 MPa). These values clearly indicate double-curvature of the web plate. Furthermore, this condition is produced by the distribution of distortion-induced stresses. It is these secondary stresses which have determined the form of the overall longitudinal stress distribution.

3.2.3 Typical Results: With Positive Attachment

The Finite Element analysis results of Detail B are presented for the case of a 3.0 in. (76.2 mm) web gap and a rod angle of 20 degrees. The load was 55 kip (245 kN) and post-processors were used to tabulate and plot the stresses.

The out-of-plane displaced shape along the gusset plate is plotted in Figure 28. Again, the form is symmetrical and indicates the negligible lateral deflections at a short distance from the gusset plate detail. The lateral displacement of the plate's outer edges is 0.003 in. (0.076 mm). The inner edges, those serving as the outer boundaries of the web gaps, displaced 0.0025 in. (0.064 mm). However, one point along each of the weld lines between the inner and outer edges, is shown to have experienced a deflection of only 0.0022 in. (0.056 mm).

These points are in the vicinity of the lateral brace attachments. The driving force, developed in the rod, introduces an out-of-plane displacement of 0.0058 in. (0.147 mm) at the transverse connection plate weld toe. Therefore, a relative distortion of 0.0033 in. (0.084 mm) has been induced within the unrestrained web plate.

The distributions associated with the primary, in-plane bending stresses and the secondary, displacement-induced stresses are shown in Figure 29. The sudden variation in the primary membrane stress occurs at the points of lateral brace attachment. This reduction is due to the restraint offered by these rigid components. The nominal primary stress is 5.8 ksi (40.0 MPa) at the level of the gusset plate. The distribution of distortion-induced stresses clearly reveals the development of double-curvature within the web gap. The plate's outer edges are exposed to stresses of less than 1.0 ksi (6.9 MPa), while the inner edges undergo secondary stresses of -4.5 to -5.0 ksi (-31.0 to -34.5 MPa) on one side of the web plate. Distortion-induced stresses of 6.4 ksi (44.1 MPa) developed at the transverse connection plate weld toes. These values are comparable in magnitude to the prevailing primary membrane stresses.

The combined stress distribution is illustrated in Figure 30. The plot predicts stresses of 5.75 ksi (39.6 MPa) and less than 1.0 ksi (6.9 MPa) at the gusset plate's outer and inner edges respectively. The transverse connection plate weld toes are exposed to a combined longitudinal stress of 11.0 ksi (75.8 MPa). As in the analysis results of Detail C, the secondary stress distribution has determined the form of the overall longitudinal stress distribution. The differences between the cases of Details B and C will be discussed with an overall comparison of the F.E. results in a latter section.

3.3 Application of Finite Element Analyses to Experimental Procedures

3.3.1 Characteristic Curves: Without Positive Attachment

For each of Detail C's three web gap sizes, results similar to those shown in the previous sections were developed at each of the seven rod angles. Then, for each of the detail's web gap sizes, a series of resultant parameters were plotted with respect to the associated rod angles. These curves display the Finite Element analysis-predicted impact of the rod angle on the variables related to distortion-induced fatigue cracking. The curves were then utilized to set the geometrical conditions during the experimentation tasks. All results shown in this section are for a 3.0 in. (76.2 mm) web gap and a load of 55 kip (245 kN).

The variation in the primary membrane stress developed at the outer edge of the gusset plate is plotted in Figure 31. This stress, produced solely by the in-plane loading, is shown to decrease significantly as the rod angle is increased. The stress is 8.3 ksi (57.2 MPa) when the driving rod is horizontal, and decreases to 3.8 ksi (26.2 MPa) when the rod is 30° below the horizontal. This is to be expected since the primary membrane stresses are produced by the vertical deflections of the girder. As the rod angle increases, the vertical component of the force in the rod also increases. This component resists the vertical load of the hydraulic jacks and consequently reduces the magnitude of the vertical deflections.

Figure 32 illustrates the effect of the rod angle on the total longitudinal stresses developed at three sites. The plotted stress is a superposition of primary, membrane and secondary, distortion-induced stresses. The locations

noted are the transverse connection plate weld toe, the weld termination at the gusset plate's outer edge, and the weld termination at the plate's inner edge. At any given rod angle, the difference between the top and bottom curves represents the extent of the stress gradient across the 3.0 in. (76.2 mm) web gap. The greatest difference is 22.7 ksi (156.4 MPa) and occurs at a rod angle of 20 degrees. The stress at the connection plate weld toe increases with corresponding increases in the rod angle through 15°. But, this stress levels off between 15° and 20° and then decreases slightly as the angle is increased to 30°.

The stress at the web gap's outer boundary (the gusset plate's inner edge) is 8.3 ksi (57.2 MPa) when the rod is horizontal. But the same point undergoes compressive stresses when the rod angle is increased beyond 10°. The gap's outer boundary is exposed to a stress of -5.4 ksi (-37.4 MPa) at a rod angle of 30°. The total membrane stress at the outer edge is also 8.3 ksi (57.2 MPa) when the rod is horizontal. Actually, the longitudinal stresses are identical at each point along the gusset plate-to-web plate weld line when the rod is level. This indicates that the horizontal rod does not induce secondary stresses. When this curve is compared to that in Figure 31, the effect of the rod angle on the secondary distortion-induced stresses is apparent.

Figure 33 displays the effect of the rod angle on the magnitude of the compressive force developed in the driving rod. Ideally, the rod is unloaded when horizontal. The force-angle relationship is almost linear to 49 kip (218 kN) at an angle of 15°. Beyond this point, the curve increases gradually and levels off at 56 kip (249 kN) when the angle is 25° to 30°. The force plotted is the axial force developed along the wall of the rod at each subsequent rod angle.

The vertical component of this force is greatest at 30° when it approaches 28 kip (124.6 kN).

The effect of the rod angle on the out-of-plane displacement of the transverse weld toes is shown in Figure 34. Again, the lateral distortion is shown to be zero when the rod is horizontal. The out-of-plane displacement increases almost linearly to 0.0074 in. (0.188 mm) at an angle of 15°. The curve then rounds off and peaks at a displacement of 0.0083 in. (0.211 mm) and an angle between 20° and 25°. The lateral displacements decrease beyond an angle of 25°. At this point, the incremental increases in the driving force are primarily manifested in the force's vertical component. Thus, the greatest out-of-plane displacement is expected to develop at a rod angle of 25° to 30°.

A plot of the rod's axial force vs. the out-of-plane displacement is reproduced in Figure 35. The plot is virtually linear through a force of 54.9 kip (244 kN) at a displacement of 0.008 in. (0.20 mm). At this point, the plot curves back on itself as the increases in axial force are manifested in the vertical component. Note that the increases in out-of-plane displacement are accompanied by subsequent increases in the rod angle to 25°. The rod force has already been shown to decrease beyond this angle.

These curves only represent the behavior of Detail C with a 3.0 in. (76.2 mm) web gap. However, they were investigated in order to recognize the inherent relationship between certain test variables. With the knowledge of the "trade-off" between these parameters, the testing conditions were prescribed. The selection was based on the desired degree of lateral distortion and the associated stresses.

3.3.2 Characteristic Curves: With Positive Attachment

The analysis procedure described in the previous section was also applied to the three web gap sizes associated with Detail B. The results shown in this section are for a 3.0 in. (76.2 mm) web gap and a loading of 55 kip (245 kN).

The effect of the rod angle on the primary membrane stress at the gusset's outer edge is shown in Figure 36. The stress is 8.3 ksi (57.2 MPa) when the rod is horizontal, and decreases to 3.7 ksi (25.5 MPa) at an angle of 30°. This curve is quite similar to that developed under the same conditions for Detail C. The form and general behavior result from the same reasoning as discussed in the previous section.

Figure 37 illustrates the effect of the rod angle on the welded sites noted. The upper curve predicts a stress of 8.0 ksi (55.2 MPa) at the transverse weld toe in the web gap when the rod is horizontal. This stress increases to 11.5 ksi (79.8 MPa) at an angle of 15°. Beyond this angle, the total longitudinal stresses decrease. This is due to the decrease in the magnitude of the girder's vertical deflection and the reduction in the degree of lateral distortion.

The stress developed at the web gap's outer boundary (the gusset plate's inner edge) is 8.3 ksi (57.2 MPa) when the rod is horizontal. But, the same site undergoes compressive stresses when the rod angle is increased beyond 20°. The boundary is exposed to a stress of -1.0 ksi (6.9 MPa) at a rod angle of 30°. At any given angle, the difference between the top and bottom curves represents the severity of the stress gradient across the 3.0 in. (76.2 mm) web gap. The greatest difference is 10.9 ksi (75.25 MPa) and occurs at a rod angle of 20°.

The total membrane stress at the gusset's outer edge is also shown to

decrease from 8.3 ksi (57.2 MPa) to 4.2 ksi (28.9 MPa) over an angular variation of zero to 30°. Comparison of this curve to that in Figure 36, indicates the effect of the rod angle on the distortion-induced stresses. A horizontal rod has very little impact on the stress distribution. But, a slight angular orientation of the rod introduces secondary stresses and decreases the magnitude of the girder's vertical deflections.

Figure 38 illustrates the effect of the rod angle on the magnitude of the driving force in the rod. The form is similar to that shown and discussed for Detail C. The plot predicts a maximum force of 58 kip (258 kN) at a rod angle between 20° and 30°.

Figure 39 show's the out-of-plane displacement of the gap's transverse weld toe as the angle is varied. The lateral displacement increases linearly to 0.0054 in. (0.137 mm) at an angle of 15°. The plot peaks at a lateral deflection of 0.0058 in. (0.148 mm) and a rod angle of 20°. The out-of-plane displacements decrease beyond this point due to the greater inclination of the driving rod.

A plot showing the relationship between the driving force and the subsequent out-of-plane displacement is found in Figure 40. The plot is virtually linear through a force of 57 kip (254 kN) at a maximum displacement of 0.0058 in. (0.147 mm). The curve then doubles back on itself as the rod force is increasingly directed vertically. As the rod angle increases, the horizontal force component decreases, and the degree of lateral distortion is reduced.

These curves predict the effect of the rod angle on specific variables in the overall analysis. This relation was influential in establishing an optimum testing procedure. Furthermore, the relation was useful in defining the conditions which

surround specific degrees of distortion-induced stresses.

3.3.3 Production of Test Curves

An initial phase of the Finite Element Analysis involved the verification of the model's elastic behavior. The same model was progressively loaded with 10 kip (44.5 kN), 25 kip (111 kN), and 55 kip (245 kN). The results were extracted, tabulated, and compared. The comparison indicated an increase in the displacements and stresses which was consistently proportional to the ratio of the applied loads. Thus, a scale factor could be calculated for each increment of load. This factor relates the predicted specimen behavior at a given load, to the behavior predicted at 55 kip (245 kN).

The factors were applied to each of the five characteristic curves developed for each detail to produce a set of *"Test Curves."* The curves were utilized in setting the experiment's geometrical conditions which govern the degree of lateral distortion. Typical test curves are shown in Figure 41 for Detail C with 3.0 in. (76.2 mm) web gaps. The plots represent the F.E.-predicted stresses at three sites for loads of 10 kip (44.5 kN), 20 kip (89 kN), 30 kip (133.5 kN), 40 kip (178 kN), and 55 kip (245 kN). A load can be prescribed if a specific rod angle and stress level are desired. This allowed the stress levels to be adjusted without disassembling the test setup. Results at loading magnitudes not shown can easily be interpolated from the test curves. A set of similar curves was developed for each characteristic curve, at each web gap size, for each detail.

3.3.4 Conclusions Drawn from the Finite Element Analyses

The previous sections have presented the case of a 3.0 in. (76.2 mm) web gap in Details B and C. These examples were useful in explaining the test procedure and predicting laboratory behavior. However, the major advantages of the analyses are the conclusions which may be drawn from a comparison of a broad range of cases. After reviewing the characteristic curves for each case, the worst condition was identified as occurring during the maximum load of 55 kip (245 kN) and at a rod angle of 15°. This is the condition which most frequently prevailed at the peak of the plots relating local stress to the associated rod angle.

Twelve common parameters were selected from the analysis results for each web gap size in each detail. These parameters are compared in Table 3 for a 55 kip (245 kN) load and a 15° rod angle. Detail C analysis results are shown in the first three numerical columns under the title *"No Positive Attachment."* Detail B (containing positive attachment) analysis results are shown in the remaining three columns.

The average primary stress remains relatively constant for each detail at the three web gap sizes. The consistency of this parameter is related to the narrow range of vertical deflections to which the girder is confined. These deflections produce the bending moment distribution. This distribution is the main factor in the development of primary membrane stresses at any level in the girder's depth. The subtle increase in this stress within larger gaps is most likely due to the decrease in connection rigidity. The rigidity is reduced as the length of the gusset plate-to-web weld line is reduced. This reduction occurs as the web gaps are lengthened.

The maximum vertical deflection has been predicted as 0.133 in. (3.38 mm) downward for each of the three web gap sizes of Detail C. The same deflection is shown to be 0.130 in. (3.30 mm) downward for the girder carrying Detail B. The difference in the values may be assumed to be due to the contribution of the positive attachment to the girder's stiffness in the vicinity of the detail.

The maximum, absolute lateral deflection increases from 0.0064 in. (0.163 mm) to 0.0076 in. (0.193 mm) for Detail C as the web gap increases in length from 1.0 in. (25.4 mm) to 3.0 in. (76.2 mm). The out-of-plane displacement for Detail B ranges from 0.0051 in. (0.130 mm) to 0.0054 in. (0.137 mm) as the gap size approaches 3.0 in. (76.2 mm). The increase in the magnitude of absolute deflections reflects the enhanced flexibility of the unrestrained web plate as the gap expands. Larger web gaps accommodate larger out-of-plane displacements. However, the lower values for the detail including positive attachment consistently indicate the connection's contribution to lateral restraint.

The difference in the lateral displacements of a web gap's boundaries is defined as the gap's relative distortion. This distortion increases from 0.0027 in. (0.069 mm) to 0.0064 in. (0.163 mm) for Detail C as the web gap approaches 3.0 in. (76.2 mm). The relative distortion ranges from 0.0013 in. (0.033 mm) to 0.0030 in. (0.076 mm) for the detail which includes bolted positive attachment. Similar to the absolute, lateral displacement, the distortion grows with the gap size due to enhanced plate flexibility. However, the degree of distortion in the largest web gap of Detail B is the almost identical to that of the smallest gap in Detail C. The bolted positive attachment reduced the relative distortion by a factor of two for each web gap size investigated.

The compressive force in each of the two lateral braces decreases as the web gap is lengthened. This is the case for both details. But, the brace force is consistently much larger for the girder system that includes Detail B. Furthermore, the progressive decrease in the brace forces of Detail B is not as large as that shown for Detail C. Thus, the positive attachment aids in the transfer of the rod force through the transverse connection plate and into the lateral braces.

The force developed in the rod is shown to decrease slightly for each detail with a corresponding increase in web gap size. Again, this is due to the enhanced flexibility of the larger gaps and the subsequent loss of resistance to lateral motion. The force is larger in the positive attachment case due to the inherent rigidity of the connection.

The compressive force in the positive attachment is shown to gradually increase as the gap size increases. This behavior is due to the larger gap's flexibility and the associated larger out-of-plane displacements. The displacements are shown to increase slightly. Therefore, the positive attachment member undergoes a greater axial thrust induced by lateral distortion.

The maximum secondary stress is shown to slightly decrease with larger web gaps for each detail. This distortion-induced stress is still considered to be high, at levels of 13.0 to 16.0 ksi (89.6 to 110.3 MPa). But, the positive attachment has reduced this range by a factor of two at the worst condition. The larger gaps are more flexible and do not provide the same degree of restraint that is found in a narrow gap. The gap's boundary conditions are assumed to remain constant. Therefore, the increased length of the unrestrained web plate accommodates greater distortion without elevating the secondary

moments.

The total longitudinal stress at the transverse connection plate weld toe (the web gap's inner boundary) behaves similarly to the secondary stress pattern. This has been shown to prevail due to the primary stress' uniform profile and the extent of the distortion-induced stresses. This stress has been predicted to reach 20.5 ksi (141.3 MPa) within a 1.0 in. (76.2 mm) gap in Detail C. However, the stress at the same point is shown to be 13.0 ksi (89.6 MPa) for the same gap size with positive attachment. The total stress is only slightly reduced by an increase in the size of the web gap.

The total longitudinal stress at the gusset plate's inner edge (the gap's outer boundary) is shown to be tensile for the narrow gap but, compressive for the 3.0 in. (76.2 mm) web gap. Again, the larger gap accommodates a larger out-of-plane displacement and subsequently undergoes a greater degree of relative distortion between its boundaries. The negative stress reflects the presence of double-curvature within the gap. The stresses decrease in the same fashion for Detail B, but are less due to the connection's lateral rigidity. The positive attachment apparently prevents the development of double-curvature through a gap size of 3.0 in. (76.2 mm).

The total stress at the plate's outer edge also decreases with an increase in gap size. Although, the reduction is quite small. The stress is also relatively constant between Details B and C. This is due to the rapid decrease in the magnitude of out-of-plane displacements at greater distances from the web gap. The distortion-induced stresses were shown to be considerably lower at the plate's outer edge.

The total longitudinal stress at a point 1.0 in. (25.4 mm) along the weld

line from the web gap has also been tabulated. The resulting values are compressive. This indicates that while double-curvature may not have developed within the boundaries of the web gap, it does often develop over a slightly greater length. The condition has produced a stress of -7.9 ksi (-54.5 MPa) just outside of a 1.0 in. (25.4 mm) web gap. The positive attachment scheme has significantly reduced this stress, but still only seems to have prevented double-curvature in the case of a 3.0 in. (76.2 mm) web gap.

The following conclusions result from these comparisons:

1. Larger web gaps accommodate larger absolute, out-of-plane displacements in both details, and progressively increase the force developed in positive attachment while decreasing that developed in lateral braces.

2. The gap size has no effect on the girder's vertical deflection. The detail which includes positive attachment will slightly decrease such deflections due to the enhanced local stiffness.

3. The primary membrane stress at the gusset plate level is effected to the same extent as the girder's vertical deflections.

4. Larger web gaps accommodate greater degrees of relative distortion without elevating the secondary bending moments at the gap boundaries (all other conditions remaining constant).

5. The unrestrained plate within web gaps may experience only tensile or compressive stresses on one side of the plate (single-curvature). However, double-curvature of the web plate will occur within a short distance beyond the gap.

6. Positive attachment provides a means for the lateral transfer of forces transmitted through the gusset plate. This capability increases the axial thrust in the lateral braces.

7. Positive attachment reduces the magnitude of out-of-plane displacements experienced by the girder's web plate. This same attachment decreases the gap's relative distortion, and reduces the subsequent secondary stresses along the detail.

8. The secondary, distortion-induced stress levels dominate the resultant total stresses. The primary membrane stress is virtually constant.

Therefore, the secondary stress distribution determines the form of the overall distribution:

- single vs. double-curvature
- extent and magnitude of stress gradient

9. The stress at the gusset plate's outer edge is effected by lateral displacements to a lesser degree than the regions within the web gap. Although distortion-induced stresses are still present, this point is on the outer reaches of the lateral displacement field.

These conclusions were drawn from the F.E. analysis only. The results of the experimental tasks may support or alter these conclusions. The accuracy of the F.E. results is dependent upon the size of the elements used in the model's discretization. Therefore, the results only reflect the precision of the models. However, the behavioral trends provide considerable insight into the benefits of larger web gaps and more rigid detail attachments. Note that the results are only for the *"uncracked"* condition. Stresses and displacements are expected to change with the onset and propagation of fatigue cracks. The following sections present the physical laboratory test results and compare these results to the modeled behavior.

Chapter 4
EXPERIMENTAL RESULTS: INTERMEDIATE DISTORTION

4.1 Detail Without Positive Attachment

Two details without positive attachment to the vertical connection plate underwent intermediate degrees of out-of-plane distortion during testing. A web gap distortion stress range of 15 to 25 ksi (103.5 to 172.5 MPa) is defined as an intermediate range. This corresponds to the level of cracking that would be expected after only a few years of service. Details *T5-9* and *T5-10* include gaps of 0.2 in. (5.08 mm) and 0.3 in. (7.62 mm) lengths between weld toes.

4.1.1 Measured Stresses

Sixty strain gages were utilized for each pair of test girders. Web gap stress gradients were mapped for a series of consecutive loadings during static testing. Single gages at the outer edges of the gusset plates were also monitored. Detail C (*T5-10*) is shown in Figure 42. The detail is not connected to the transverse connection plate. A plot of the typical stress gradients across a pair of 0.2 in. (5.08 mm) gaps is shown in Figure 43. The loads for the upper and lower gradients were 55 kips (245 kN) and 4.1 kips (18.3 kN) respectively, and the rod angle was 14.6°. Note that similar points, oriented symmetrically with respect to the transverse connection plate, do not undergo identical stresses. This is due to the rotation of the vertical connection plate. Such a rotation increases the stress at one vertical weld toe while reducing the magnitude at the opposite site. However, the difference between two corresponding gage readings was constant for each load applied. Therefore, the stress ranges developed at

weld toes within the adjacent web gaps were identical during testing. The range is also indicated in the plot.

A tension flange stress range of 9.0 ksi (62.1 MPa) corresponded to a nominal, primary stress range of 6.0 ksi (41.4 MPa) at the gusset plate level. Upon establishing this controlling factor, web gap stress ranges were monitored. The vertical connection plate weld toe experienced a stress range of 26 ksi (179.4 MPa) in a 0.2 in. (5.08 mm) web gap, and a range of 23 ksi (158.7 MPa) in a 0.3 in. (7.62 mm) web gap under identical loading conditions. The measured gradients extrapolated to ranges of over 17 ksi (117.3 MPa) and 12 ksi (82.8 MPa) at the toe of the gusset's inner edge weld for these same gaps. These values were all tensile and were measured on the gusset's side of the girder's web plate. This indicates the development of single-curvature within the narrow, horizontal web gaps.

The weld terminations at the outer edges of the gusset plates were found to undergo a consistent stress range of 9.4 ksi (64.9 MPa) on the gusset's side of the web plate. The same point on the opposite side of the web plate experienced a stress range of 2.5 ksi (17.3 MPa). These ranges result from a primary range of 5.95 ksi (41.1 MPa) and a secondary gradient through the web thickness. The deformation-induced stress ranges were 3.45 ksi (23.8 MPa) of tension or compression on the web plate's opposite surfaces.

The displacement-induced stress ranges were the direct result of the range of force developed in the driving rods. This range was found to be approximately 38 kips (168 kN). The rods were on an angle of 14.6° and developed sufficient force to elevate gap stresses to 2-4 times that of the primary stress range at the gusset plate's level.

4.1.2 Measured Distortion

At any point along the gusset plate level, the elevation of the stress range above the nominal 6.0 ksi (41.4 MPa) was caused by out-of-plane displacements. Secondary stresses were generated by a relative distortion of 0.0013 in. (0.033 mm) prior to the onset of fatigue cracking in a 0.3 in. (7.62 mm) gap. The relative distortion could not be measured in the narrow confines of the 0.2 in. (5.08 mm) gap.

Relative distortion is defined as the difference between the out-of-plane displacements of a web gap's welded boundaries. Such distortion was measured for a 0.3 in. (7.62 mm) gap in Detail *T5-9* as a crack developed and propagated. Table 4 provides a listing of the recorded distortion. A relative distortion of only 0.0013 in. (0.033 mm) developed initially, and was associated with a stress range of 23 ksi (158.7 MPa) at the vertical weld toe. The distortion remained almost constant until a 1.40 in. (35.5 mm) crack was detected on the web's surface. At that time, the relative distortion increased over six fold with the enhanced flexibility of the local gap boundaries.

As the crack grew in length the relative out-of-plane displacements continued to increase. After a 1.0 in. (25.4 mm) diameter retrofit hole was introduced at the crack tips, the distortion almost doubled due to the reduction in the web plate's lateral stiffness. The measured distortion reached a maximum of 0.0317 in. (0.81 mm) at a crack length of 4.60 in. (116.8 mm) before a positive attachment retrofit was installed. With the introduction of a bolted attachment similar to that utilized in Detail B, the relative distortion within the horizontal web gap was reduced by a factor of 17. The attachment simply connected the lateral gusset and vertical connection plates. The stress ranges at

the gap boundaries could not be measured after the crack had grown to such lengths due to the retrofit procedures followed. As further noted in Table 4, the relative distortion increased slightly during the first million cycles beyond the final retrofit. This may be attributed to initial slippage in the bolted attachment. Beyond 6.5 million cycles, the distortion remained within a range of 0.0022 to 0.0026 in. (0.056 to 0.066 mm).

4.1.3 Comparison of Predicted and Measured Results

Several measurements were selected for comparison with the results of the finite element model. Stress ranges at weld toes were extrapolated from measured gradients and scaled from the model's 1.0 to 3.0 in. (25.4 to 76.2 mm) gap analyses. Table 5 shows the comparison for Detail C. The model provided stress ranges in the local gap region within 8% of those measured. The relative distortions vary by only 15% between measured and computed. However, at the gusset's outer edge, where the displacement field was found to have a significant effect on the stress ranges, the computed value fell 18% below that measured. The range of force developed in the driving rod differed by 9%, with the F.E. analysis indicating a greater axial stiffness in the member. This enhanced stiffness is inherent in F.E. analyses and is also evident in the lower value of the global, vertical deflection predicted by the model. Furthermore, a portion of the difference may also be attributed to the experimental frame's elastic nature.

4.1.4 Fatigue Behavior and Retrofit

The plate girders were cycled through a constant amplitude stress range until fatigue cracks developed. The cracks initially appeared on the web plate surface at the connection plate weld toe. Figure 44 shows a 3.0 in. (76.2 mm) crack in the horizontal gap. The cracks were detected in the four horizontal gaps at lengths between 1.0 and 1.3 in. (25.4 and 33.0 mm). Table 6 provides an account between the crack propagation behavior of a Detail *T5-10*, 0.2 in. (5.08 mm) web gap. A 1.30 in. (33.0 mm) long crack appeared after 1,280,000 cycles at a stress range of 26.3 ksi (181.5 MPa). At that length, the crack still remained within the out-of-plane displacement field. The distortion-induced stresses increased the growth rate while the crack tips were still in the local region surrounding the web gaps. However, the rate is expected to be higher at the lower tip than at the upper due to the higher primary membrane stress as the crack advances toward the tension flange. Once the crack grows beyond the influence of the out-of-plane displacement field, the length is then sufficient to promote accelerated growth at lower stress ranges. The nominal stress range at the level of the bottom crack tip is tabulated in column three. As the crack grows further from the neutral axis, this stress range increases. This increase, coupled with the progressive extensions in crack length, elevated the growth to 1.5×10^{-6} in./cycle (3.81×10^{-5} mm/cycle) through a crack length of over 4.0 in. (101.6 mm). A degree of secondary out-of-plane displacement-induced stress still existed at the level of the bottom crack tip.

Further measurements indicated an acceleration in the growth rate to 3.0×10^{-6} in./cycle (7.62×10^{-5} mm/cycle) through a crack length of 6.30 in. (160.0 mm). This length includes the diameters of several holes introduced

during the application of two retrofits. However, at this length considerable out-of-plane displacements were evident. The vertical connection plate weld on the web plate's outer surface, opposite the horizontal gap, cracked through the throat of the weld. Lateral translation of the two crack surfaces was obvious upon inspection. Thus, the plate's flexibility permitted the elevation of secondary stresses beyond the initial out-of-plane displacement field. This field expanded as the fatigue crack extended towards the tension flange.

Column two of Table 6 presents the extrapolated stress range at the vertical connection plate weld toe slightly above the horizontal web gap. The gap gages were monitored as the upper crack tip advanced from within the gap, toward the gages. The tabulation indicates the effect of the crack tip presence on the prevailing stress range. The flexibility of the unrestrained web plate increases with crack growth. With the enhanced flexibility, the gap's curvature is increased and the stress range in front of the leading tip is elevated. The crack eventually broke the seal between the gage and the web plate.

An initial retrofit was introduced at Detail *T5-10* after 2,900,000 cycles. A 0.75 in. (19.1 mm) diameter hole was drilled at the tips of each crack as shown in Figure 45. This was intended to remove the crack tips, reduce the magnitude of the prevailing stress field along the weld toes, and provide additional flexibility along the connection plate. When dynamic loading commenced, the effect of the added flexibility was monitored. The driving rod force range dropped to 36.2 kips (161.3 kN) from 38.8 kips (172.8 kN) under the same loading conditions applied before retrofitting. Furthermore, the stress range at the outer edges of the gusset plate fell to 8.3 ksi (57.3 MPa) from the 9.4 ksi (64.9 MPa) which was measured earlier. Thus, the reduction in lateral

restraint, brought on by the initial retrofit, decreased the stress ranges experienced along the gusset plate as well as within the horizontal web gap.

Table 7 presents the effect of the progressive retrofits on these variables. The stress range at the outer edge of the gusset plate was reduced by drilling holes along the vertical connection plate weld toe. However, the stress range at the same location was elevated with the installation of the bolted positive attachment. Since the range measured at the outer weld termination changed at different phases of the test, an effective stress range was calculated. A *Miner's* effective stress range of 8.1 ksi (55.9 MPa) was associated with this particular detail's outer weld termination.

The force range developed in the driving rod was effected in the same manner. Thus, greater lateral restraint elevated the stresses at considerable distances from the gap while increasing the external driving force. These results are further supported by those of Table 4. The drilled holes increased the relative distortion and subsequently relaxed the stresses beyond the gap and decreased the resistance to the thrust of the driving rod. Furthermore, the bolted retrofit drastically reduced the relative distortion and provided a more rigid connection for the transfer of lateral deformations.

The magnitude of the stress range below a given retrofit hole was also investigated. The results are shown in Table 8. As the crack grew in length and further retrofit holes were drilled, the prevailing stress range just below the hole increased. These stresses were often three times greater than the primary, in-plane range at the level of the lower crack tip. Therefore, the introduction of such holes was found to accelerate the crack growth rate. Finally, with the simultaneous introduction of a 1.25 in. (31.75 mm) diameter hole and a bolted

attachment, the stress range was reduced by a factor of two.

The stress range at the gusset plate's horizontal weld termination within the gap also changed with crack growth and the introduction of retrofits. The range drastically decreased with further extensions of the vertical cracks. However, the stress range increased with the installation of the bolted positive attachment. A *Miner's* effective stress range of 7.1 ksi (49 MPa) was calculated based on the measurements made throughout the test period.

The datapoints for initial cracking along the vertical connection plate weld toes are compared to the AASHTO Fatigue Design Category C curve and test data in Figure 46. The cracks, at detection, fall at the upper bound for the Category C test data. No cracks were detected at the gusset plates' horizontal weld terminations. Effective stress ranges were calculated for the inner and outer termination at each detail. These values are compared to the AASHTO Category E curve and test data at the test's completion in Figure 47.

Table 9 presents the retrofit history for cracking along the vertical connection plate welds of Details *T5-9* and *T5-10*. T5-9L refers to the left gap of Detail *T5-9*. The crack length, and the type of retrofit introduced are noted. Bolted attachment of the lateral gusset and vertical connection plates was introduced at both details after 5,300,000 cycles. No further crack growth was witnessed at any drilled hole site through 10,000,000 cycles. Thus, the final retrofit underwent 4.7 million cycles before the test ended. The number of cycles to which specific retrofits were exposed is also tabulated. From this information, a degree of reliability and effectiveness may be assumed.

4.2 Detail With Positive Attachment

Two details including bolted positive attachment of the lateral gusset and vertical connection plates were tested under similar loading conditions. One such detail and laterals are shown in Figure 48. Details *T5-6* and *T5-7* have 2.2 in. (55.9 mm) gaps.

4.2.1 Measured Stresses

Web gap stress gradients were plotted for consecutive static loadings identical to those of Detail C. Detail B (*T5-6*) is shown in Figure (49. Typical stress gradients across a pair of 2.2 in. (55.9 mm) web gaps are shown in Figure 50. The corresponding jack loads for the upper and lower gradients were 55 kips (245 kN) and 4.1 kips (18.3 kN) respectively. The rods were also angled at 14.6°. Again, due to the rotation of the vertical connection plate, similar points do not necessarily undergo identical stresses.

The connection plate weld toe experienced a stress range of approximately 11.5 ksi (79.3 MPa) in the 2.2 in. (55.9 mm) web gaps. The measured gradients extrapolated to ranges of 4.3 to 5.0 ksi (29.7 to 34.5 MPa) at the toe of the gusset plate's inner edge weld. These tensile values were measured on the gusset's side of the web plate, indicating the development of single-curvature within these larger gaps.

The weld terminations at the gusset's outer edges experienced a stress range of 9.9 to 10.1 ksi (68.3 to 69.7 MPa). These magnitudes developed on the gusset side of the web. The corresponding points on the outside surface of the web plate underwent stress ranges of only 2.4 ksi (16.6 MPa) and 2.2 ksi (15.2 MPa) respectively. These ranges are based on a primary range of 6.15 ksi (42.4 MPa). Therefore, a secondary gradient of 3.95 ksi (27.3 MPa) exists through

the web thickness.

Force ranges of 38.0 to 39.4 kips (168.0 to 174.0 kN) developed in the driving rods. These ranges were sufficient to elevate gap stresses to 2 times the primary stress range at the gusset plate's level.

4.2.2 Measured Distortion

The relative distortion was measured in one gap on each of the sites tested. Tables 10 and 11 present the results for details *T5-6* and *T5-7* respectively. Differences between the measured stress ranges and the primary, in-plane bending stress range of 6 ksi (41.4 MPa) were brought on by out-of-plane displacements. As implied, secondary stresses of 5 to 6 ksi (34.5 to 41.4 MPa) were generated by distortions on the order of 0.003 in. (0.076 mm).

The two details, opposite each other, did not experience identical distortions. This was expected when driving force ranges of 38.0 kip (169 N) and 41.4 kip (184 N) were measured at the opposite sites. Although no fatigue cracks were detected during the testing, the relative distortion generally increased with time. This trend may be attributed to slip in the bolted joint. Therefore, the cyclic loading progressively increased the detail's flexibility.

4.2.3 Comparison of Predicted and Measured Results

Selected measured results are compared to Finite Element predictions in Table 12. The model provided stress ranges at the vertical connection plate weld within 13% of those measured. Relative distortions vary by 19% between measured and computed. However, at the gusset plate's outer edge, where lateral translations were greater than expected, the computations fell 27% below that measured. The range of force developed in the driving rods differed by 9%

with the F.E. analyses predicting a much stiffer member. The results are highly dependent upon the means by which the positive attachment is simulated.

4.2.4 Fatigue Behavior and Retrofit

The details were cycled through a constant amplitude stress range for 10,000,000 cycles (the duration of the test period). No fatigue cracks were detected at any site. Therefore, no retrofit measures were required. The datapoints associated with the completion of the test are compared to the AASHTO Fatigue Design Category C test data in Figure 51. These correspond to the uncracked condition and again fall at the upper bound of the 95% confidence limit for Category C details. The datapoints associated with the horizontal weld terminations are compared to the AASHTO Category E test data in Figure 52. The points bound the plotted scatter.

Chapter 5
EXPERIMENTAL RESULTS : HIGH DISTORTION

5.1 Detail Without Positive Attachment

A high degree of relative deformation is associated with a web gap distortion stress range above 25 ksi (172.5 MPa). Two Detail C-type connections were exposed to high degrees of out-of-plane distortion during testing. This level corresponds to the condition where cracking initiates within a very short period of time after the bridge is placed into service. Detail *T5-11* includes gaps of 2.4 in. (61.0 mm) and 2.6 in. (66.0 mm) length. Detail *T5-12* includes gaps of 2.3 in. (58.4 mm) and 2.6 in. (66.0 mm) length.

5.1.1 Measured Stresses

A plot of the measured stress gradients across the pair of Detail *T5-12* gaps is shown in Figure 53. The loads for the upper and lower gradients were 55 kips (245 kN) and 8.2 kips (36.5 kN) respectively, and the rod angle was 20.5°. A tension flange stress range of 9.0 ksi (62.1 MPa) was maintained in order to guarantee the development of a 6.0 ksi (41.4 MPa) primary bending stress at the gusset plate level.

Stress ranges of 30 to 31.5 ksi (207 to 217 MPa) developed along the vertical connection plate weld toe within the horizontal gaps. The measured gradients extrapolated to compressive stress ranges of 4.0 to 6.0 ksi (27.6 to 41.4 MPa) at the toe of the gusset's inner edge weld for these gaps. The slight difference in the magnitudes of the corresponding stress ranges is due to rotation of the vertical connection plate. The difference in the sign of the stress ranges

at the gap's boundaries indicates the development of double-curvature within these sections of unrestrained web plate.

The weld terminations at the outer edges of the gusset plates experienced a consistent stress range of 9.0 ksi (62.1 MPa). The corresponding point on the outside surface of the web plate underwent a range of 4.0 ksi (27.6 MPa). These values are based on a primary range of 6.5 ksi (44.9 MPa) and are evidence of the development of a secondary gradient through the web thickness. Therefore, a distortion-induced stress range of 2.5 ksi (17.25 MPa) was generated at the outer weld terminations.

The lateral displacements and subsequent stresses were induced by the force range within the external rods. The rods associated with these details transferred a force range of 44.3 to 46.1 kips (197 to 205 kN). The driving rods thus elevated the gap stresses to 5 times the nominal bending stress at the gusset plate level.

5.1.2 Measured Distortion

The relative distortion between two adjacent welded boundaries was measured for each of the four gaps. Table 13 provides a listing of these measurements for the 2.6 in. (66 mm) gap of Detail *T5-11*. An initial distortion of 0.0061 in. (0.15 mm) was associated with a stress range on the order of 30 ksi (207 MPa) at the vertical connection plate weld toe. The distortion was elevated by a factor of 3 with the development of a 1.05 in. (26.7 mm) surface crack.

As the crack propagated, the out-of-plane deformation increased. With the rapid growth of a larger crack in an adjacent web gap of the same detail, the distortion was elevated to 0.0225 in. (0.57 mm). The relative distortion reached

a maximum of 0.0259 in. (0.66 mm) at a crack length of 2.20 in. (55.9 mm). At 3,300,000 cycles, two 1.25 in. (31.75 mm) diameter holes were drilled along the vertical connection plate welds. The bottom hole removed the lower crack tip. However, due to space limitations, the upper hole was drilled above the leading crack tip. Bolted positive attachment of the gusset and vertical connection plates was also made at this time. The positive attachment was installed to reduce the large out-of-plane displacements. The resultant crack length was 3.40 in. (86.4 mm). With the introduction of the retrofit, the relative distortion was reduced by a factor of 11. As noted, the distortion then remained virtually constant with minor deviations attributed to bolt slippage.

Table 14 presents similar measurements for the 2.6 in. (66 mm) gap of Detail *T5-12*. An initial distortion of 0.0063 in. (0.16 mm) was also associated with a 30 ksi (207 MPa) stress range at the vertical weld toe. Upon detection of a 0.80 in. (20.3 mm) long fatigue crack, the relative distortion was measured as 0.018 in. (0.46 mm); 2.9 times higher than that generated in the uncracked plate. Deformation behavior was quite similar to that of Detail *T5-11*. Distortion increased to a maximum value of 0.0257 in. (0.65 mm) at a crack length of 2.35 in. (59.7 mm). Retrofit holes were drilled with the simultaneous installation of a bolted positive attachment. The measured distortion was subsequently reduced by a factor of 13. The final crack length was 3.10 in. (78.7 mm). While distortion initially increased, the measured values eventually stabilized for the remaining 6.5 million cycles.

5.1.3 Comparison of Predicted and Measured Results

Stress ranges at weld toes were extrapolated from plotted gradients and scaled from the F.E. model analyses. The results are compared in Table 15. The model provided stress ranges along the vertical connection plate weld toe within 13% of those measured. However, the double-curvature was more severe than accounted for by F.E., and the model predicted compressive stresses of one-half the magnitude of those measured. Relative distortions vary by only 8% between measured and computed. The stress range at the gusset's outer edge was computed within 20% of that experienced. The force range developed in the external driving rod differed by 10%, with F.E. analyses indicating a greater axial stiffness in the member.

5.1.4 Fatigue Behavior and Retrofit

The cracks initially appeared on the web plate surface within the horizontal gaps along the vertical connection plate weld toe. Figure 54 shows a 2.35 in. (59.7 mm) long crack at the weld toe within Detail *T5-12*. The cracks were detected in the four gusset plate gaps at lengths between 0.60 and 1.05 in. (15.2 and 26.7 mm) within 50,000 cycles of each other. Table 16 provides an account of the crack propagation behavior within the 2.6 in. (66 mm) web gap of Detail *T5-12*. A 0.80 in. (20.3 mm) long crack appeared after 1,100,000 cycles at a stress range of 30 ksi (207 MPa).

At that length, the out-of-plane displacement field still surrounded the crack. Consequently, distortion-induced stresses elevated the growth rate. The lower crack tip was also driven by the higher primary stress range as extensions neared the tension flange. The nominal stress range at the bottom crack tip is listed in column three. As shown, the growth rate increased from 5.0×10^{-7}

in./cycle (1.27 X 10^{-5} mm/cycle) to 1.0 X 10^{-6} in./cycle (2.54 X 10^{-5} mm/cycle) during testing. These rates are associated with an extension in the crack length from 0.80 in. (20.3 mm) to 2.35 in. (59.7 mm) over the course of 2,200,000 cycles. The higher primary stress range was not the only element responsible for the increased rates, as distortion-induced stresses were still significant within the local region surrounding the gaps at smaller crack lengths.

Column two of Table 16 presents the extrapolated stress range at the vertical connection plate weld toe within the horizontal web gap. Progressive increases in the stresses measured were the result of two factors. First, the crack tip was advancing toward the gages as the strains were recorded. The significance of the crack tip accuity is evident. In addition, the flexibility of the unrestrained web plate increases with crack growth. The crack eventually separated the gage from the web plate surface.

Extensive cracking developed in the 2.4 in. (61 mm) gap of Detail *T5-11*. The initial 0.85 in. (21.6 mm) long crack developed in the horizontal gusset gap. The same crack rapidly grew along the vertical weld and through the transverse web gap as shown in Figure 55. This lower, 0.30 in. (7.62 mm) gap, is bounded by the vertical connection plate and the longitudinal web-to-flange fillet weld. The crack reached the longitudinal weld and penetrated the web's entire thickness. Figure 56 shows the 6.80 in. (172.7 mm) long crack as it appeared on the web plate's opposite surface prior to retrofitting.

Retrofits were introduced in each of the Detail C connections at 3,300,000 cycles. 1.25 in. (31.75 mm) diameter holes were drilled along the vertical welds, and bolted attachments were installed. Several of the holes were drilled in front of the crack tips because of the tight confines of the experimental set-up. The

retrofit, as applied to Detail *T5-11*, is shown in Figure 57.

Table 17 presents the effects of crack length on the prevailing stress range at the gusset's outer edge. The force range in the driving rod, and the stress range measured at the upper crack tip are also tabulated. A stress range of 31.5 ksi (217.4 MPa) was extrapolated to the vertical connection plate weld toe within the gap prior to cracking. Upon initial detection of a surface crack, and at intermittent crack lengths, a gage was installed on the web surface at the crack's upper edge. The measured stresses were found to increase with crack length to a maximum of 43.7 ksi (301.5 MPa) at a crack length of 1.95 in. (49.5 mm). With the installation of the positive attachment retrofit, the stress range in front of the crack was reduced by a factor of 3.

The force range developed in the external driving rods decreased with crack propagation. Yet, the force range increased with the increase in lateral stiffness associated with the positive attachment retrofit. The stress range at the outer edges of the gusset plate also decreased with progressive crack extensions. However, the stress range at the same location was raised with the installation of the bolted retrofit. Thus, increased flexibility within the horizontal gap relaxed stresses along the entire gusset plate, and reduced the resistance to the thrust of the external rod. In contrast, the bolted attachment restored lateral rigidity to the detail and reduced relative distortions.

Since the horizontal gusset plate's weld terminations underwent varying stress ranges, effective stress ranges were calculated from measurements taken throughout the test. A *Miner's* effective stress range of 8.0 ksi (55.2 MPa) was associated with the outer weld terminations of Detail *T5-12*. With the development of double-curvature across the web gap, the gusset's inner weld

termination underwent only compressive stress ranges. Therefore, cracking did not occur at the web gap's outer boundary within either detail.

The datapoints for initial cracking along the vertical connection plate weld toes are compared to the AASHTO Fatigue Design Category C curve and test data in Figure 58. The cracks, at detection, fall at the upper bound of the scatter shown. Upon inspection, it was noted that the vertical welds were deposited at a shallow angle with the web plate. The same welds were also undercut at the toe in contact with the vertical plate. Thus, the vertical fillet welds were unequal leg fillet welds. The stress concentrations at the web-to-connection plate weld toes were considerably lower than observed with equal leg fillet welds *[10]*.

No fatigue cracks were detected at the horizontal weld terminations. The tensile effective stress ranges at the outer terminations are compared to the AASHTO Category E test data in Figure 59. These points correspond to the test's completion and fall above the test data's scatter. The data associated with the inner terminations are not plotted since the stress ranges were compressive.

Table 18 presents the retrofit history for cracking along the vertical welds of Details *T5-11* and *T5-12*. Retrofit holes were drilled and bolted attachment of the lateral gusset and vertical connection plates was made at 3,300,000 cycles. The cracks did not extend beyond the retrofit holes at any sites through 10,000,000 cycles. Thus, the final retrofit underwent 6.7 million cycles before the test ended.

5.2 Detail with Positive Attachment

Two Detail B-type connections were tested under conditions of high distortion. Detail *T5-3* includes 0.80 in. (20.3 mm) web gaps, and Detail *T5-4* includes gaps of 0.85 in. (21.6 mm) and 0.90 in. (22.9 mm) length. A typical Detail B attachment and web gap are shown in Figure 60.

5.2.1 Measured Stresses

The stress gradients developed in the 0.90 in. (22.9 mm) web gap of Detail *T5-4* are shown in Figure 61. The corresponding loads for the upper and lower gradients were 55 kips (245 kN) and 8.2 kips (36.5 kN). The connection plate weld toe underwent a stress range of approximately 15 ksi (103.5 MPa). The measurements extrapolated to a range of 2.5 ksi (17.3 MPa) at the gap's outer boundary. The tensile values were measured on the gusset's side of the web plate, and indicate the development of single-curvature within the gap.

The weld termination at the gusset's outer edges experienced stress ranges identical to those measured at the Detail C connections. Force ranges of 42.9 to 45.1 kips (191 to 201 kN) were transfered from the driving rods. These ranges were sufficient to raise the gap stresses to 2.5 times the primary range at that level.

5.2.2 Measured Distortion

The relative distortion was measured in one gap within each detail. Table 19 presents the results for a typical gap. Deviations from the in-plane bending stress range of 6 ksi (41.4 MPa) were generated through out-of-plane displacements. As implied, secondary stress ranges of 8 to 9 ksi (55.2 to 62.1 MPa) were associated with distortions of 0.0013 in. (0.033 mm).

Although no fatigue cracks were detected during the testing, the relative distortion generally increased with the number of cycles to which the detail was exposed. Thus, the cyclic loading enhanced the connection's flexibility over time. The variations in the measured stress ranges within the gap were due to intermittent system "shut-downs". Upon "start-up", the force range developed in an external rod often deviated by 3 to 5%. However, the distortion was not notably affected. And the trend was still one of progressively increased flexibility under virtually constant loading.

5.2.3 Comparison of Predicted and Measured Results

Selected measured results are compared to Finite Element predictions in Table 20. The model provided ranges at the vertical connection plate welds within 14% of those measured. Relative distortions varied by 15% between measured and computed. Stress ranges at the gusset's inner edge were predicted to within 16%, and outer edge stresses differed by 17%. The range of force developed in the external rods varied by 13% at most, with F.E. predicting a stiffer axial member.

5.2.4 Fatigue Behavior and Retrofit

The details were tested through 10,000,000 cycles. At no time were fatigue cracks apparent upon visual inspection. Therefore, no measures to retrofit were required. The datapoints associated with the completion of the test are compared to the AASHTO Fatigue Design Category C curve and test data in Figure 62. The line shown, represents the 95% confidence limit. The points are for the uncracked condition and fall at the upper bound of the scatter associated with the Category C test data.

The datapoints associated with the horizontal weld terminations are compared to the AASHTO Category E curve and test data in Figure 63. No cracks were detected and these points correspond to the test's completion.

Chapter 6
CONCLUSIONS

6.1 General Fatigue Behavior

A summary of the relative distortions initially induced within uncracked Detail C web gaps is provided in Table 21. The stress ranges, extrapolated to vertical connection plate weld toes from measured gradients, are also tabulated. The smaller gap was exposed to an intermediate degree of distortion as defined by the magnitude of the prevailing stress range; between 15 and 25 ksi (103.5 and 172.5 MPa). The larger gaps, by definition, underwent high degrees of distortion.

The 2.3 in. to 2.6 in. (58.4 mm to 66.0 mm) gaps experienced relative distortions 5 times greater than the 0.3 in. (7.6 mm) gap while undergoing stress ranges only 1.5 times greater. Therefore, the larger gaps accommodated greater degrees of relative distortion without proportionally elevating the secondary bending stresses. While still in the uncracked condition, the larger gaps experienced a consistent 0.006 in. (0.15 mm) distortion. This repetition indicates the negligible effect of minor variations in gap size above a certain length under constant loading conditions.

A similar summary for uncracked Detail B web gaps is shown in Table 22. The stress ranges, by definition, are associated with lesser degrees of distortion than generated within the Detail C gaps. Simultaneous testing of both types of details prohibited the development of higher degrees of distortion within Detail B'gaps while that within Detail C was easily attained.

The 2.2 in. (55.9 mm) web gaps experienced relative distortions 2.5 times

greater than those induced within the 0.8 in. to 0.9 in. (20.3 mm to 22.9 mm) gaps. Furthermore, even with the higher degree of physical deformation, extrapolated stress ranges were actually less than those of the narrower gaps. The consistency of the measured distortions for a given gap length is a result of symmetry and fabrication quality and uniformity.

The data, at detection of cracks at the vertical weld toes in the case of Detail C, and at the test's completion in the case of Detail B, is compared to the AASHTO Fatigue Design Category C test data in Figure 64. The cracks at detection fall at the upper bound of Category C test data for varied degrees of distortion and several gap lengths. 95% of the test data are above the line shown, and the results of these experiments adequately comply with prior results. The data for Detail B runs out above the constant amplitude fatigue limit for Category C. These points also fall at the upper bound of the scatter for AASHTO Category C details at lower stress ranges. Thus, both types of details indicate a higher than average fatigue resistance compared to the Category C lower bound resistance. The resistance was in part higher than expected due to the vertical connection plate's weld profile. Quality welds were deposited at shallow angles with the web plates. Thus, the stress concentration at the weld toes were considerably less than expected.

Strain measurements at all gusset plate outer edges indicated the development of a secondary bending gradient through the web's thickness. The nominal, in-plane bending stress of 6 ksi (41.4 MPa) was maintained. However, the driving forces produced an overall lateral translation of the gusset plates. Such translations were sufficient to elevate the secondary stress ranges at the outer weld terminations. Therefore, the out-of-plane displacement field had a

significant effect on the stress ranges along the entire gusset plate attachment.

The data for the horizontal weld terminations is compared to the AASHTO Fatigue Design Category E test data in Figure 65. No cracks were detected at the terminations, and all results generally conform to the bounds of the known scatter. The points are plotted on the basis of calculated *Miner's* effective stress ranges.

Initial relative distortions remained virtually constant until the onset of fatigue cracking. Table 23 presents a listing of measured distortions before and after the detection of fatigue cracks within the Detail C gaps. The crack length upon first detection is also tabulated. The 0.3 in. (7.62 mm) gap of Detail *T5-9* experienced a 7 fold increase in the relative distortion across its welded boundaries with the onset of cracking. Yet, the 2.3 to 2.6 in. (58.4 to 66 mm) gaps underwent an increase in distortion of only 2 to 3 times that measured prior to the detection of cracks. Therefore, the larger web gaps did not experience as great a loss of lateral rigidity as the smaller gaps. The welded boundaries of the narrow gaps provide enhanced restraint within the local region. The larger gaps are more flexible prior to the development of fatigue cracks. Thus, their affinity for further increases in flexibility is not as significant as was found in the smaller web gaps.

As the cracks grew beyond the initial length noted, the relative deformations progressively increased. At short lengths, the stresses associated with the out-of-plane displacements are the driving force for crack extension. However, it was believed that once the crack grew beyond the influence of the displacement field, the existing crack length alone would be sufficient to promote accelerated growth at lower stress ranges. This has been found to be true in the

case of both vertical and horizontal web gaps. However, in the case of the horizontal web gaps, primary and secondary stresses are directly combined to accelerate fatigue crack growth. The major difference has been the change in not only the magnitude of, but the dimensions of the displacement field with progressive crack extensions. As the vertical cracks grew, the enhanced local flexibility increased the magnitude and the vertical dimension of the field. The consistently higher stress ranges measured below successive retrofit holes are evidence of the alteration of the field's form. A simultaneous contraction of the field width also occurred. This decrease in horizontal field size was indicated by a reduction in the secondary stresses developed at the gusset plate's outer edges as the cracks grew vertically. Thus, greater crack length, as well as the influences of an ever-extending out-of-plane displacement field, contributed to the fatigue crack growth acceleration.

The following conclusions summarize the general fatigue behavior of Details B and C:

1. With regard to each detail type alone, and under constant loading conditions, larger web gaps were able to undergo greater degrees of relative distortion without proportionally elevating the secondary stress ranges.

2. For horizontal gusset plate web gaps of comparable size and under identical loading conditions:

   - Detail B (bolted positive attachment) gaps initially experienced one-half of the relative distortion induced between the welded boundaries of Detail C (no positive attachment) gaps.

   - Detail B gaps underwent one-third of the magnitude of subsequent secondary stress ranges induced within the Detail C gaps.

3. Detail C (no positive attachment) connections may be classified as having a web gap fatigue resistance comparable to AASHTO

Category C details.

4. Detail B (positive attachment) connections may be classified as having a web gap fatigue resistance comparable to AASHTO Category C details.

5. The extreme inner and outer edges of both Detail B and Detail C horizontal gusset plates may be classified as AASHTO Category E (long attachment) details.

6. The quality of the weld profile has a significant effect on a detail's fatigue resistance. Welds deposited at a shallow angle to the web plate elevate Category C detail fatigue resistance. Wrapping the welds continuously around the gusset plate perimeter elevates Category E detail fatigue resistance.

7. Prior to the onset of fatigue cracking in either detail, local web gap distortion is sufficient to induce a secondary bending gradient through the web thickness along the entire horizontal gusset plate.

8. With the development of fatigue cracks, the relative distortion across Detail C gaps increases 5 to 6 times over that measured prior to cracking.

9. Under an essentially constant driving force range, relative distortions increase with progressive crack extensions.

10. With the growth of fatigue cracks, the secondary stresses are redistributed and the out-of-plane displacement field changes magnitude and dimension. The field grows in the direction of crack extension and contracts in the transverse dimension.

11. The out-of-plane displacement field adjusts to elevate secondary stresses at advancing fatigue crack tips.

6.2 Retrofit Behavior

After the length of fatigue cracks approached 3.0 in. (76.2 mm), an initial retrofit consisting of drilled holes at the crack tips was introduced. As shown in the experimental results under intermediate degrees of distortion for Detail C gaps, this type of retrofit was not effective in preventing further crack propagation. At best, the holes served as a temporary means of arresting crack

growth at the vertical weld toes. Furthermore, the increased lateral flexibility brought on with such a removal, consistently elevated the curvature of the unrestrained web plate. As a result, the displacement-induced stress field grew along with the vertical cracks.

The loss of resistance to lateral deformation decreased the magnitude of the driving force in the external rods. In addition, the stress ranges at the gussets' outer edges decreased as a consequence of the reduction in overall plate translation. However, the enhanced flexibility drastically increased the relative distortions and subsequently elevated the secondary stresses at successive retrofits. With further increases in flexibility and the larger resultant crack length, the growth rate accelerated. Only a narrow range of hole diameters were installed. Larger diameter holes would further elevate the gap's flexibility, but may not increase the secondary stresses.

The largest holes were 1.25 in. (31.75 mm) in diameter and were drilled with the simultaneous installation of a bolted positive attachment. This final hole removed the crack tip, blunted the crack's leading edges, and again altered the prevailing displacement field. The bolted positive attachment was instrumental in reducing relative distortions and subsequent secondary stress ranges. The attachment restored lateral restraint to deformations and resisted the thrust of the driving forces. Thus, the external rods developed a slightly higher axial force after the bolted retrofit was installed. The secondary stresses at the gusset's outer edges were also raised as a consequence of the reduction in overall plate translation. The following conclusions summarize the behavior of the retrofits applied to the Detail C connections and gaps:

1. Drilling holes at the ends of vertical fatigue cracks propagating from

horizontal web gaps:

- increases web plate flexibility within the local gap region.
- reduces the gusset plate's overall translation, thereby decreasing secondary stress ranges along the horizontal welds.
- increases the relative distortion within the web gap itself.
- extends the out-of-plane displacement field in the direction of further crack propagation.
- may elevate the secondary stress range below the retrofit, thereby increasing the likelihood of further growth.

2. Bolting a positive attachment between the horizontal gusset and vertical connection plates:

- restored a degree of stiffness to the web gap region, thereby resisting lateral deformations.
- increased the gusset plate's overall translation and elevated secondary stresses at the gusset's outer weld terminations.
- reduced the relative distortion across the web gaps by at least one order of magnitude.
- reduced the stress range in front of the crack's leading edges by a factor of two.

6.3 Recommendations for Design and Retrofit

An objective of this pilot study was to assess the fatigue resistance characteristics of specific lateral connection details. With such an assessment, potential guidelines for the prevention of displacement-induced fatigue cracking at horizontal gusset plate details could be developed. It became apparent during the course of the investigation that the only certain recommendations that may be made, that will prevent this type of cracking, are:

1. the enlargement of the horizontal web gap.

2. a positive attachment between the horizontal gusset and vertical connection plates.

Considering the multitude of variables involved in any study regarding the fatigue of connections, only qualitative judgements may be made. Present standards /1/ call for gusset plate cope distances of 4 to 6 times the web thickness, or 2 in. (50.8 mm), whichever is larger. The results of this study indicate minimum "actual" web gap sizes of 2.5 in. (63.5 mm) to be sufficient. With the typical scale of welds associated with such connections, the nominal gap size, (equivalent to the cope distance) should measure at least 3.25 in. (84.6 mm). A gap of this size will minimize the adverse effects of weld shrinkage and subsequent restraint. While the magnitude of out-of-plane displacements is obviously a function of gap length, among other variables, distortions have been shown to remain comparatively constant for gaps above a certain length (assuming the loads do not increase).

To assure the structure of a longer service life free of distortion-induced cracks, positive attachment of the gusset and transverse plates should be specified. The attachment may take many forms, however, the bolted scheme was shown to reduce gap distortions and subsequent secondary stresses. Similar attachment schemes should find wide application as retrofits for details in existing bridge structures which are plagued by distortion-induced cracks. The ease of installation and the excellent benefits make the rigid connection retrofit an attractive alternative to increasing the detail's flexibility.

A gusset plate detail's fatigue resistance may be elevated with the deposition of quality welds. Profiles which make use of shallow angles to the web plate reduce the stress concentration at the weld toe. Furthermore, welds which run uninterrupted around the entire gusset-to-web joint have been shown

to provide details with a higher fatigue resistance.

Thus, the study's results support the following recommendations:

1. The nominal length of lateral gusset plate web gaps should be 8 to 10 times the web thickness of the attached plate girder.

2. Bolted positive attachment of the horizontal gusset and transverse connection plates should be included in all lateral connections.

3. The same mode of attachment should be broadly applied as a retrofit for existing gusset gaps exposed to various degrees of distortion.

4. Welds should be wrapped continuously around the entire perimeter of the gusset-to-web plate joint.

Tables

Nominal Web Gap Length (in.)	Detail Type	
	Bolted Attachment (B)	No Attachment (C)
1.0		T5-9 T5-10
1.5	T5-3 T5-4	
3.0	T5-6 T5-7	T5-11 T5-12

Table 1: Factorial Arrangement

Nominal Web Gap Length (in.)	Detail Type	
	Bolted Attachment (B)	No Attachment (C)
1.0		17 & 18
1.5	15 & 16	
3.0	17 & 18	15 & 16

Table 2: Girder - Detail Relationship

Lateral Gusset Plate Details

	Detail C (No Positive Attachment)			Detail B (Positive Attachment)		
Ave. Primary Stress (ksi)	5.8	5.8	6.0	5.5	5.7	5.8
Gap Size (in.)	1.0	2.0	3.0	1.0	2.0	3.0
Max. Vertical Disp. (in.)	-0.133	0.133	0.134	0.130	0.130	0.130
Max. Lateral Disp. (in.)	0.0064	0.0069	0.0076	0.0051	0.0053	0.0054
Relative Distortion (in.)	0.0027	0.0051	0.0064	0.0013	0.0024	0.0030
Force in Braces (kip)	5.9	3.9	1.6	10.3	9.6	9.1
Force in Rod (kip)	-50.8	50.1	-49.3	52.4	52.2	52.0
Force in Pos. Attach. (kip)				15.3	16.9	17.2
Max. Secondary Stress (ksi)	16.0	14.9	13.0	7.9	8.5	8.0
Stress at Trans. Weld Toe (ksi)	20.5	19.7	18.7	13.0	14.0	11.5
Stress at Pl. Inner Edge (ksi)	7.0	3.2	-3.0	5.8	1.0	1.1
Stress at Pl. Outer Edge (ksi)	7.0	6.6	6.1	7.0	6.9	6.8
Stress 1.0 in. Beyond Gap (ksi)	-7.9	6.1	-3.6	-1.7	0.75	0.36

Table 3: Comparison of Finite Element Results; Θ -15°, P 55 kip.

Cycles	Crack Length (in.)	Relative Distortion (in.)	Remarks
10,000	undetectable	0.0013	---
100,000	undetectable	0.0015	---
1,280,000	1.40	0.0097	---
2,100,000	1.70	0.0144	---
3,800,000	3.30	0.0260	Retrofitted with a 1.0 in. diameter hole at each crack tip
4,100,000	4.10	0.0266	---
5,000,000	4.10	0.0281	---
5,300,000	4.60	0.0317	Bolted attachment made between the gusset & connection plates
5,600,000	4.60	0.0019	---
6,000,000	4.60	0.0020	---
6,500,000	4.60	0.0025	---
7,000,000	4.60	0.0026	---
7,500,000	4.60	0.0023	---
8,500,000	4.60	0.0025	---
10,000,000	4.60	0.0022	test ended

Table 4: Relative Distortion Recorded in Detail T5-9

	Measured	Finite Element	Measured	Finite Element
Detail	T5-9		T5-10	
Gap Size (in.)	0.3		0.2	
Maximum Vertical Displacement (in.)	0.138	0.133	0.138	0.133
Web Gap Relative Distortion (in.)	0.0013	0.0011	*	0.0008
S_r at Conn. Pl. Weld Toe (ksi)	23.3	21.6	26.3	24.6
S_r at Gusset Inner Edge (ksi)	12.1	11.3	17.5	16.4
S_r at Gusset Outer Edge (ksi)	9.4	7.7	9.4	7.8
Driving Force Range in Rod (kip)	38.1	41.4	38.8	41.4

* Relative Distortion could not be physically measured in 0.2 in. gaps

Table 5: Comparison of Measured and F.E. Results for Detail C

Number of Cycles	Extrapolated Weld Toe S_r (ksi)	Lower Crack Tip Nominal S_r (ksi)	Crack Length (in)	Growth Rate (in/cycle)
100,000	26.3	---	---	
1,000,000	26.3	---	---	
1,280,000	26.2	6.21	1.30	
1,420,000	27.0	6.26	1.40	7.1×10^{-7}
1,600,000	27.9	6.30	1.50	5.6×10^{-7}
1,800,000	30.4	6.36	1.65	7.5×10^{-7}
1,920,000	34.2	6.41	1.75	8.3×10^{-7}
2,000,000	33.5	6.45	1.85	1.2×10^{-6}
2,100,000	**	6.49	1.95	1.0×10^{-6}
2,300,000	--	6.60	2.20	1.2×10^{-6}
2,500,000	--	6.73	2.50	1.5×10^{-6}
2,700,000	--	6.86	2.80	1.5×10^{-6}
2,900,000	--	6.99	3.10	1.5×10^{-6}
Detail retrofitted with 0.75 in. diameter holes at the crack tips				
3,100,000	--	7.42	4.10	
3,300,000	--	7.55	4.40	1.5×10^{-6}
3,500,000	--	7.72	4.80	2.0×10^{-6}
3,800,000	--	7.94	5.30	2.5×10^{-6}
Detail retrofitted with a 1.25 in. diameter hole at the lower crack tip				
4,700,000	--	8.03	5.50	
4,800,000	--	8.14	5.75	2.5×10^{-6}
4,900,000	--	8.25	6.00	2.5×10^{-6}
5,000,000	--	8.38	6.30	3.0×10^{-6}

Detail retrofitted with a 1.0 in. diameter hole at the upper crack tip

** gage rendered inoperative by crack propogation

Table 6: Crack Propogation Behavior of Detail T5-10

Retrofit	S_r at Gusset Plate Outer Edges (ksi)	Driving Rod force (kips)
0.75 in. dia. holes	9.40	38.8
1.25 in. dia. holes	8.31	38.2
1.00 in. dia. holes	7.10	33.3
1.25 in. dia. holes and bolted positive attachment	8.10	38.0

Table 7: Retrofit Effects at Detail T5-10

Crack Length (in.)	Retrofit Hole Diameter (in.)	Stress Below Retrofit Hole (ksi)
3.80	0.75	18.6
5.50	1.25	23.1
7.20	1.00	25.7
8.80	1.25#	12.4

Bolted positive attachment made between the lateral gusset and vertical connection plates.

Table 8: Stress Range at Detail T5-10 Retrofits

Detail	T5-9L	T5-9R	T5-10L	T5-10R
Gap Size (in.)	0.3	0.2	0.2	0.2
Extrapolated S_r	23.3	23.3	26.3	26.3
Cycles to Crack	1,280,000	1,280,000	1,280,000	1,280,000
First Crack Length (in.)	1.40	1.00	1.30	1.00
Cycles at First Retro.	3,800,000	3,800,000	2,900,000	2,900,000
Length at First Retro.	3.30	2.90	3.10	2.30
Holes Drilled (dia. in.)	1.0	1.0	0.75	0.75
Length After Retro. (in.)	4.10	4.40	3.80	3.00
Cycles at Reinitiation	5,100,000	4,200,000	3,100,000	5,100,000
Cycles at Second Retro.	5,300,000	5,000,000	3,800,000	5,300,000
Length at Second Retro.	4.60	5.80	5.30	3.70
Holes Drilled (dia. in.)	**	1.25	1.25	**
Length After Retro. (in.)		6.00	5.50	
Cycles at Reinitiation		5,100,000	4,700,000	
Cycles at Third Retro.		5,300,000	5,000,000	
Length at Third Retro.		6.40	6.30	
Holes Drilled (dia. in.)		**	1.00	
Length After Retro. (in.)			7.20	
Cycles at Reinitiation			5,100,000	
Cycles at Fourth Retro.			5,300,000	
Length at Fourth Retro.			8.60	
Holes Drilled (dia. in.)			1.25**	
Length after Retro. (in.)			8.80	

** Bolted positive attachment was made between the lateral gusset and vertical connection plates. No further growth was apparent through 10,000,000 cycles at which point the test ended.

Table 9: Retrofit History of Details T5-9 and T5-10

Cycles	Crack Length (in.)	Relative Distortion (in.)	S_r at Vertical Connection Plate Weld Toe (ksi)
10,000	undetectable	0.0029	11.8
100,000	"	0.0028	11.8
1,280,000	"	0.0028	11.7
2,000,000	"	0.0029	11.7
3,000,000	"	0.0029	11.5
4,000,000	"	0.0028	11.5
5,000,000	"	0.0031	11.6
7,000,000	"	0.0029	11.6
9,000,000	"	0.0035	11.9
10,000,000	"	0.0033	11.7

Table 10: Relative Distortion Measured in Detail T5-6

Cycles	Crack Length (in.)	Relative Distortion (in.)	S_r at Vertical Connection Plate Weld Toe (ksi)
10,000	undetectable	0.0031	11.5
100,000	"	0.0031	11.6
1,280,000	"	0.0031	11.6
2,000,000	"	0.0034	11.7
3,000,000	"	0.0030	11.6
4,000,000	"	0.0033	11.6
5,000,000	"	0.0033	11.7
7,000,000	"	0.0036	11.7
9,000,000	"	0.0038	11.5
10,000,000	"	0.0037	11.6

Table 11: Relative Distortion Measured in Detail T5-7

Detail	Measured T5-6	Finite Element T5-6	Measured T5-7	Finite Element T5-7
Gap Size (in.)	2.2		2.2	
Maximum Vertical Displacement (in.)	0.138	0.130	0.138	0.130
Web Gap Relative Distortion (in.)	0.0029	0.0025	0.0031	0.0025
S_r at Conn. Pl. Weld Toe (ksi)	11.8	13.0	11.5	13.0
S_r at Gusset Inner Edge (ksi)	5.4	6.2	5.0	6.2
S_r at Gusset Outer Edge (ksi)	9.9	7.3	10.1	7.3
Driving Force Range in Rod (kip)	38.0	41.4	39.4	43.1

Table 12: Comparison of Measured and F.E. Results for Detail B

Cycles	Crack Length (in.)	Relative Distortion (in.)	Remarks
10,000	undetectable	0.0061	---
100,000	undetectable	0.0063	---
1,000,000	undetectable	0.0065	---
1,150,000	1.05	0.0194	surface crack
1,500,000	1.25	0.0207	---
1,750,000	1.35	0.0216	---
2,000,000	1.50	0.0225	extensive cracking in adjacent gap
2,500,000	1.75	0.0228	---
3,000,000	2.05	0.0246	crack is now appearing as through thickness
3,300,000	2.20	0.0259	
1.25 in. diameter retrofit holes were drilled and bolted positive attachment made between the gusset and vertical connection plates.			
3,300,000	3.40	0.0023	upper crack tip has not grown to the retrofit hole yet
3,500,000	3.40	0.0024	
3,800,000	3.40	0.0024	
4,200,000	3.40	0.0025	---
5,000,000	3.40	0.0026	---
6,000,000	3.40	0.0026	---
6,600,000	3.40	0.0026	---
7,100,000	3.40	0.0027	---
8,200,000	3.40	0.0031	---
9,000,000	3.40	0.0026	---
10,000,000	3.40	0.0027	test ended

Table 13: Relative Distortion Measured in T5-11

Cycles	Crack Length (in.)	Relative Distortion (in.)	Remarks
10,000	undetectable	0.0063	---
100,000	undetectable	0.0063	---
1,000,000	undetectable	0.0065	---
1,100,000	0.80	0.0180	surface crack
1,500,000	1.00	0.0189	---
1,750,000	1.15	0.0200	---
2,000,000	1.30	0.0220	---
2,500,000	1.60	0.0228	---
3,000,000	2.05	0.0241	additional cracks appearing on the surface
3,300,000	2.35	0.0257	

1.25 in. diameter retrofit holes drilled and bolted positive attachment made between the gusset and vertical connection plates.

3,300,000	3.10	0.0020	upper crack tip has not grown to retofit hole yet
3,500,000	3.10	0.0028	
3,800,000	3.10	0.0028	---
4,200,000	3.10	0.0026	---
5,000,000	3.10	0.0026	---
6,000,000	3.10	0.0027	---
7,100,000	3.10	0.0027	---
8,000,000	3.10	0.0025	---
8,600,000	3.10	0.0026	---
9,200,000	3.10	0.0028	---
10,000,000	3.10	0.0026	test ended

Table 14: Relative Distortion Measured in T5-12

Detail	Measured	Finite Element	Measured	Finite Element
	T5-11		T5-12	
Gap Size (in.)	2.4		2.6	
Maximum Vertical Displacement (in.)	0.150	0.134	0.150	0.134
Web Gap Relative Distortion (in.)	0.0061	0.0056	0.0063	0.0059
S_r at Conn. Pl. Weld Toe (ksi)	28.3	25.9	31.5	27.3
S_r at Gusset Inner Edge (ksi)	-4.9	-3.1	-6.0	-3.2
S_r at Gusset Outer Edge (ksi)	9.0	7.1	9.1	7.2
Driving Force Range in Rod (kip)	44.3	48.6	46.1	48.6

Table 15: Comparison of Measured and F.E. Results for Detail C

Number of Cycles	Extrapolated Weld Toe S_r (ksi)	Lower Crack Tip Nominal S_r (ksi)	Crack Length (in.)	Growth Rate (in/cycle)
100,000	30.0	---	---	
1,000,000	30.8	---	---	
1,100,000	32.3	6.4	0.80	
				5.0×10^{-7}
1,500,000	32.8	6.7	1.00	
				6.0×10^{-7}
1,750,000	32.8	6.9	1.15	
				6.0×10^{-7}
2,000,000	33.6	7.2	1.30	
				7.2×10^{-7}
2,500,000	34.4	7.4	1.65	
				8.0×10^{-7}
3,000,000	34.6	7.7	2.05	
				1.0×10^{-6}
3,300,000	34.8	7.9	2.35	
1.25 in. diameter retrofit holes drilled and bolted positive attachment made between the gusset and vertical connection plates.				
3,300,000	**	8.1	3.10	
3,500,000	**	8.1	3.10	

No further crack growth was experienced through 10,000,000 cycles, at which time the test was ended.

** the strain gages were destroyed with the installation of the retrofit to this detail

Table 16: Crack Propogation Behavior of Detail T5-12

Crack Length (in.)	S_r at Crack Tip (ksi)	Force Range (kips)	S_r at Outer Edges (ksi)	Remarks
undetected	31.5 in gap	46.1	9.1	---
0.60	33.0	45.9	9.0	surface crack
0.70	--	45.9	9.0	---
0.95	--	45.5	8.8	---
1.30	39.0	44.1	8.5	---
1.65	--	43.7	8.0	through thickness
1.95	43.7	43.0	7.6	retrofit *
2.90	14.3	45.7	8.5	

* drilled holes and positive attachment installed as retrofit

Table 17: Crack Length Effects at Detail T5-12

Detail	T5-11L	T5-11R	T5-12L	T5-12R
Gap Size (in.)	2.6	2.4	2.6	2.3
Extrapolated S_r	not gaged	28.3	30.0	31.5
Cycles to Crack	1,150,000	1,150,000	1,100,000	1,100,000
First Crack Length (in.)	1.05	0.85	0.80	0.60
Cycles at Retrofit	3,300,000	3,300,000	3,300,000	3,300,000
Length at Retrofit	2.20	6.80	2.35	1.95
Holes Drilled (dia. in.)	1.25	1.25	1.25	1.25
Length After Retro. (in.)	3.40	9.40	3.10	2.90

** Bolted positive attachment was made between the lateral gusset and vertical connection plates. No further growth was apparent through 10,000,000 cycles at which point the test ended.

Table 18: Retrofit History of Details T5-11 and T5-12

Cycles	Crack Length (in.)	Relative Distortion (in.)	S_r at Vertical Connection Plate Weld Toe (ksi)
4,000	undetectable	0.0013	15.0
50,000	"	0.0013	14.8
100,000	"	0.0013	14.7
250,000	"	0.0014	14.8
1,000,000	"	0.0014	14.4
1,500,000	"	0.0014	14.5
2,500,000	"	0.0015	14.9
3,000,000	"	0.0015	14.8
4,000,000	"	0.0017	15.1
6,000,000	"	0.0017	14.8
7,000,000	"	0.0018	14.7
8,000,000	"	0.0018	14.7
9,000,000	"	0.0019	14.8
10,000,000	"	0.0018	14.5

Table 19: Relative Distortion Measured in Detail T5-3

Detail	Measured	Finite Element	Measured	Finite Element
	T5-3		T5-4	
Gap Size (in.)	0.8		0.9	
Maximum Vertical Displacement (in.)	0.150	0.130	0.150	0.130
Web Gap Relative Distortion (in.)	0.0013	0.0011	0.0013	0.0011
S_r at Conn. Pl. Weld Toe (ksi)	15.0	12.9	15.0	13.0
S_r at Gusset Inner Edge (ksi)	2.8	2.9	2.5	2.9
S_r at Gusset Outer Edge (ksi)	9.0	7.6	9.0	7.5
Driving Force Range in Rod (kip)	42.9	48.6	45.1	48.6

Table 20: Comparison of Measured and F.E. Results for Detail B

Gap Length (in.)	Stress Range (ksi)	Relative Distortion (in.)
0.3	23.3	0.0013
2.3	31.5	0.0063
2.4	28.3	0.0061
2.6	30.0	0.0063
2.6	not gaged	0.0060

Table 21: Initial Distortion in Uncracked Detail C Connections

Gap Length (in.)	Stress Range (ksi)	Relative Distortion (in.)
0.80	15.0	0.0013
0.80	not gaged	0.0012
0.85	not gaged	0.0013
0.90	15.0	0.0013
2.20	11.8	0.0029
2.20	not gaged	0.0032
2.20	11.5	0.0031
2.20	11.7	0.0031

Table 22: Initial Distortion in Detail B Connections

Detail	Uncracked Condition Rel. Distortion (in.)	First Detected Crack Length (in.)	Cracked Condition Rel. Distortion (in.)
T5-9L	0.0013	1.40	0.0097
T5-11L	0.0060	1.05	0.0194
T5-11R	0.0081	0.85	0.0171
T5-12L	0.0063	0.80	0.0180
T5-12R	0.0063	0.60	0.0121

Table 23: Cracked and Uncracked Distortions in Detail C

Figures

Figure 1: I-79 Bridge #2682 Lateral Gusset Plate Detail

Figure 2: Cracking at Transverse Weld Toe Opposite Horizontal Web Gap

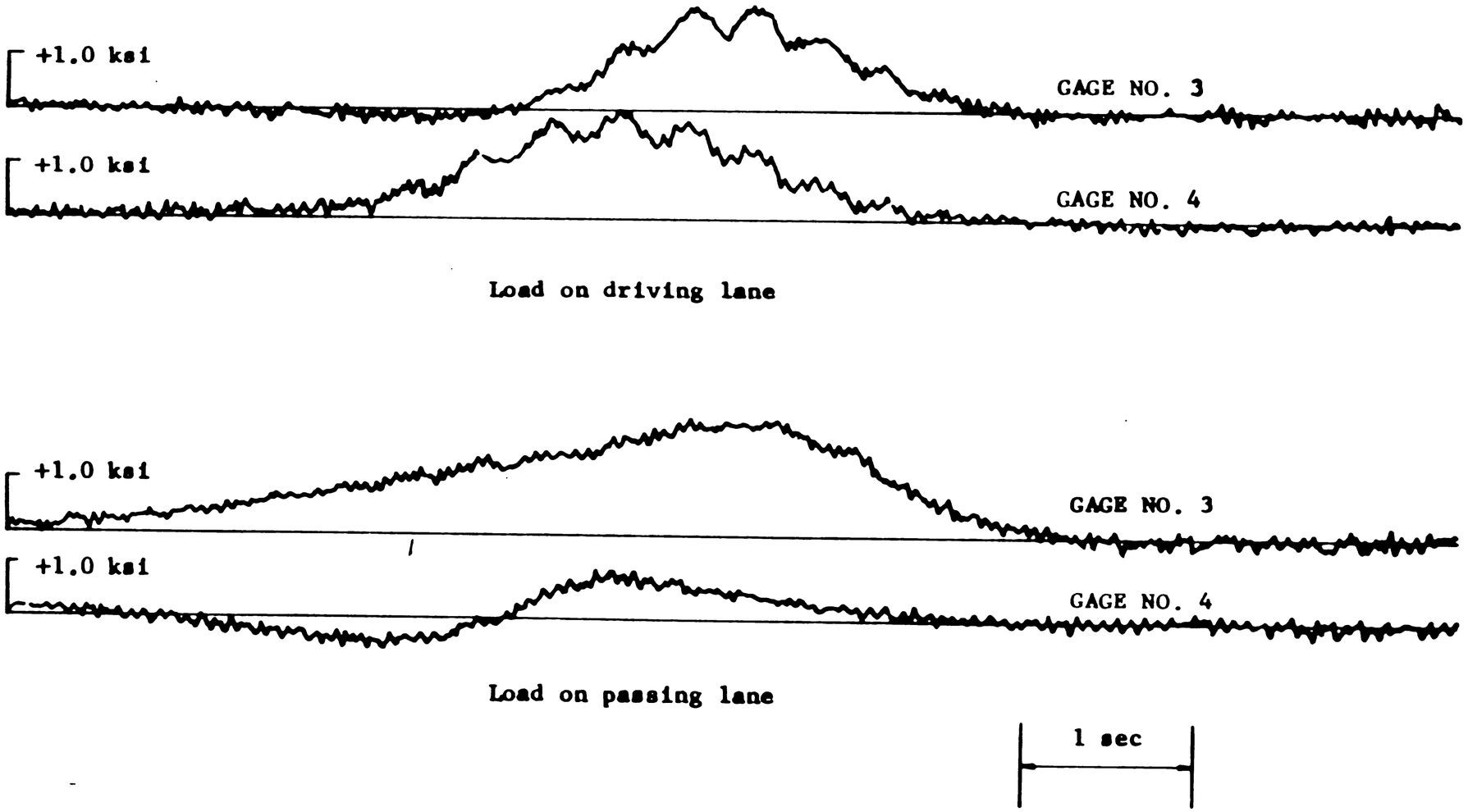

Figure 3: Time Response of Two Lateral Braces

Figure 4: Canoe Creek Bridge Lateral Gusset Plate Detail

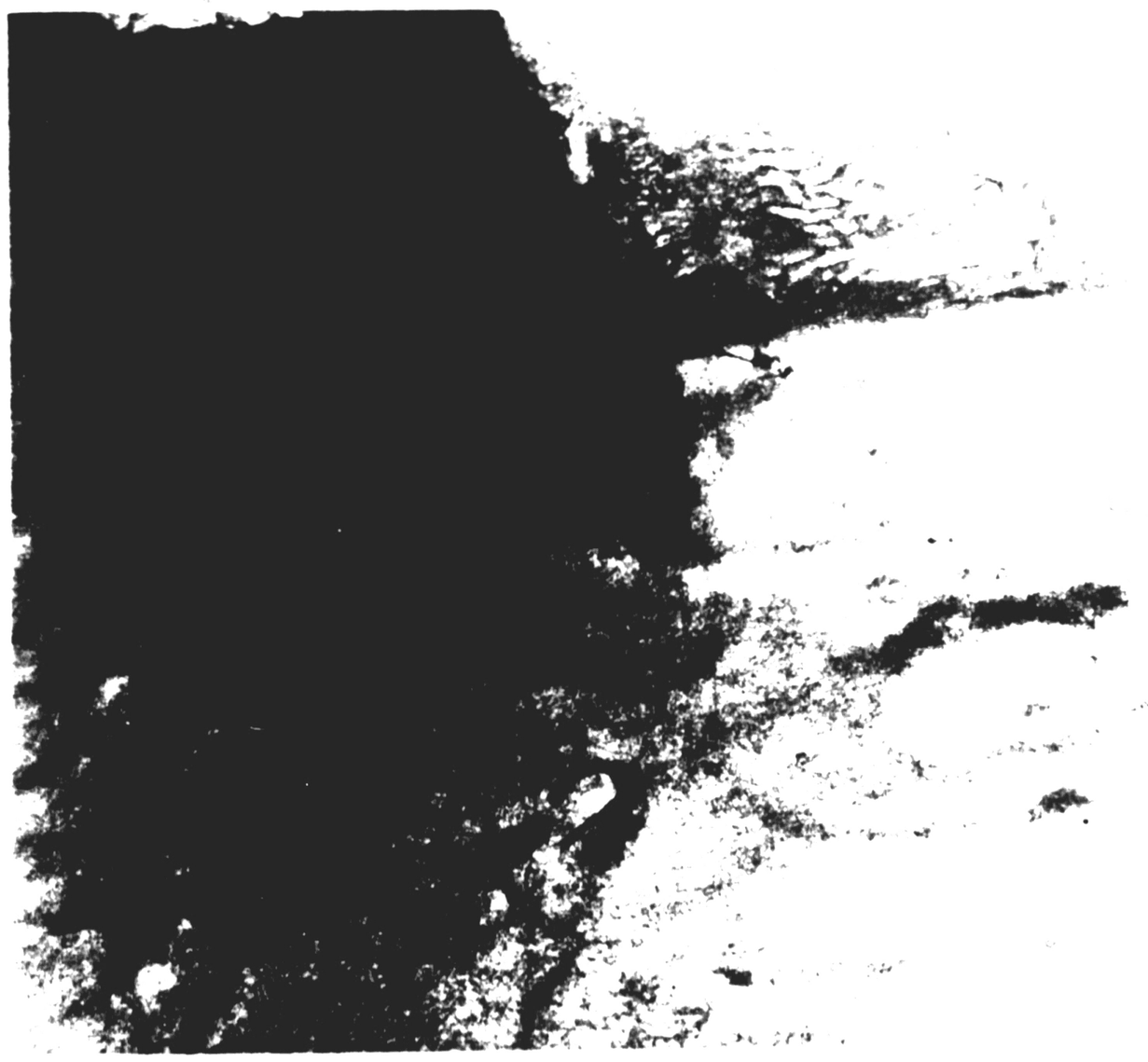

Figure 5: Cracking at the Outer Ends of the Gusset Plate Tabs

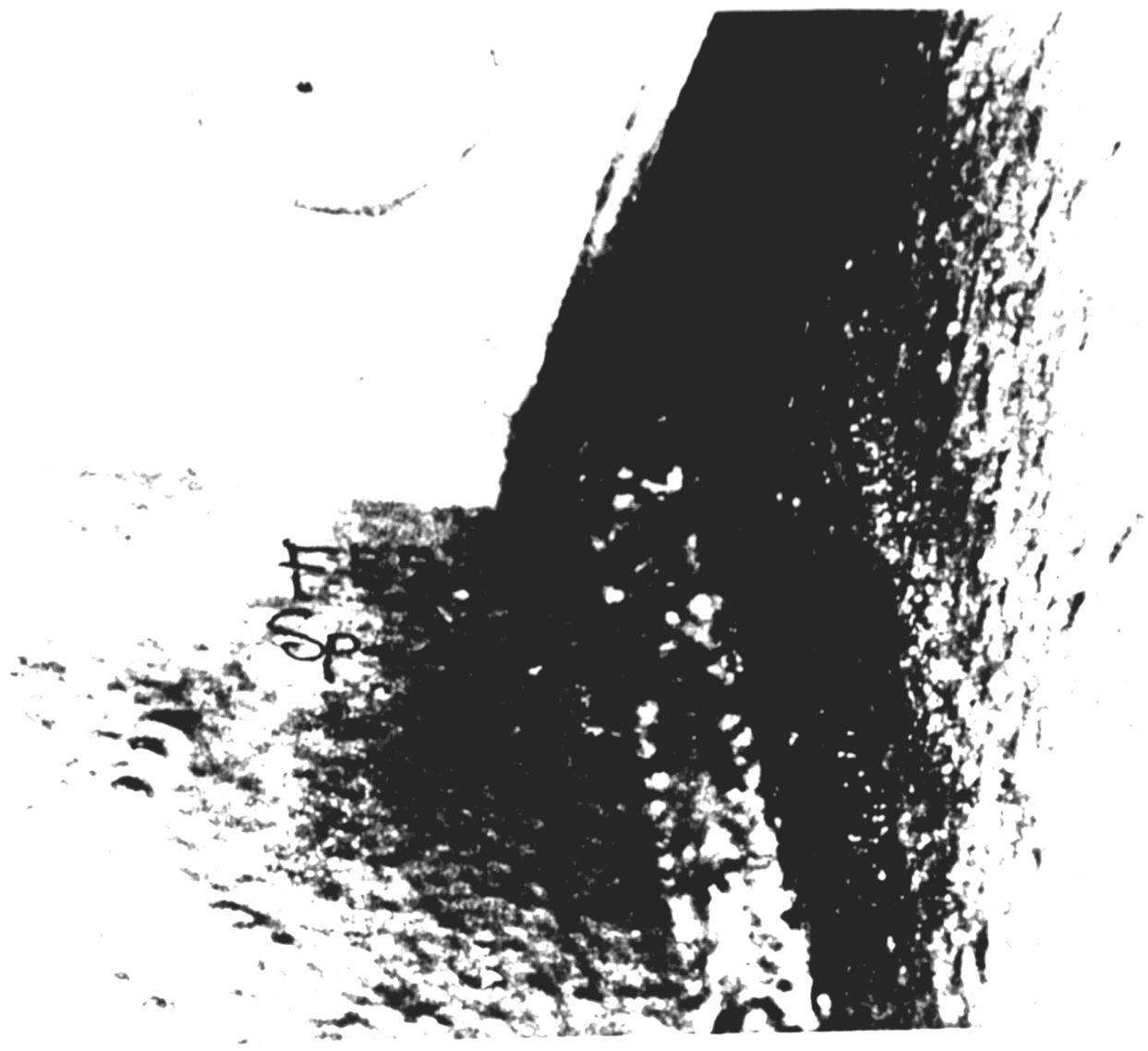

Figure 6: Cracking within the Horizontal Web Gaps

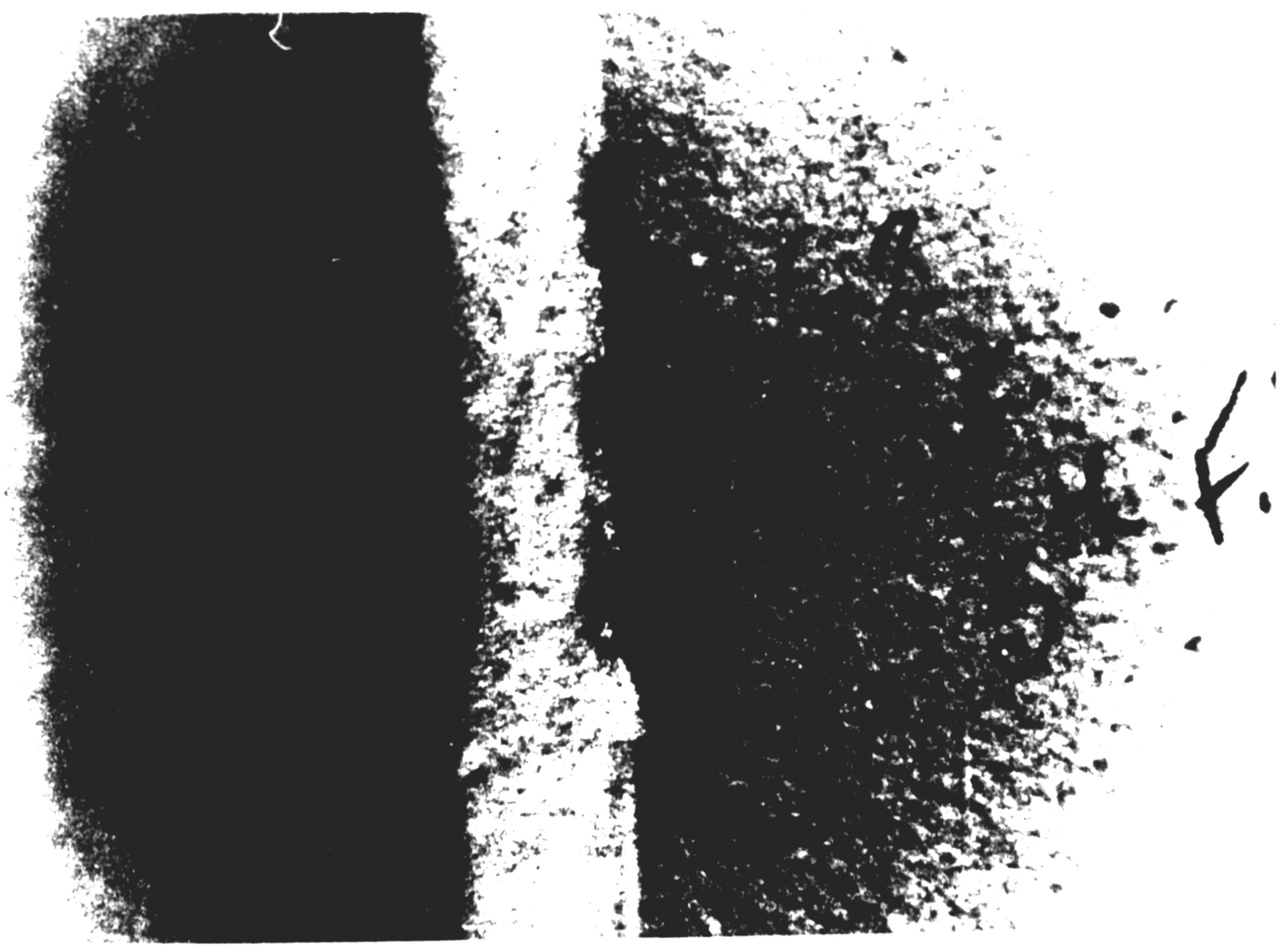

Figure 7: Cracking Along Transverse Weld Toes Opposite Gusset Plate Gaps

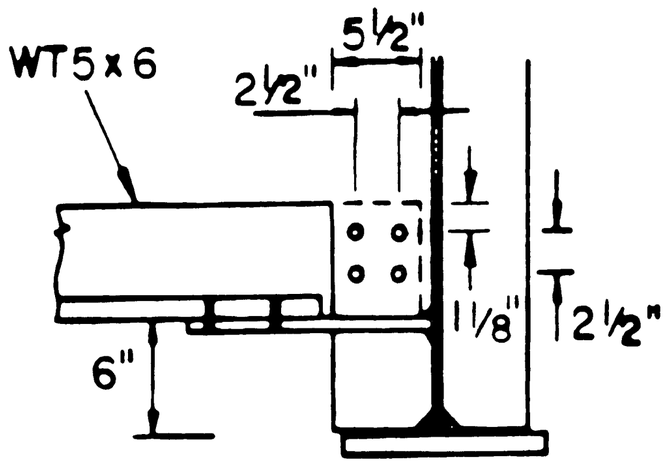

Detail B

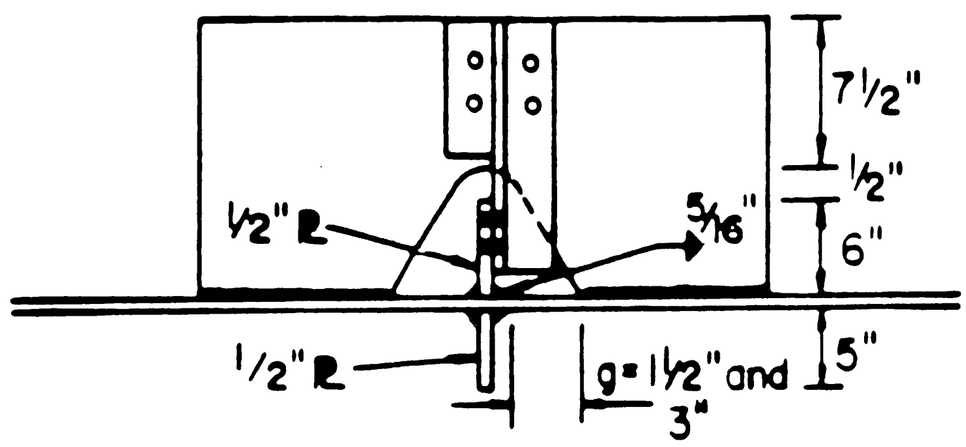

- All Holes To Be 1" dia. For 7/8" dia. Bolts
- All Gusset R. To Be 1/2" Thick
- All Gusset To Web Welds To Be 5/16"
- All 1/2" R. Welds To Be 5/16"

Detail C

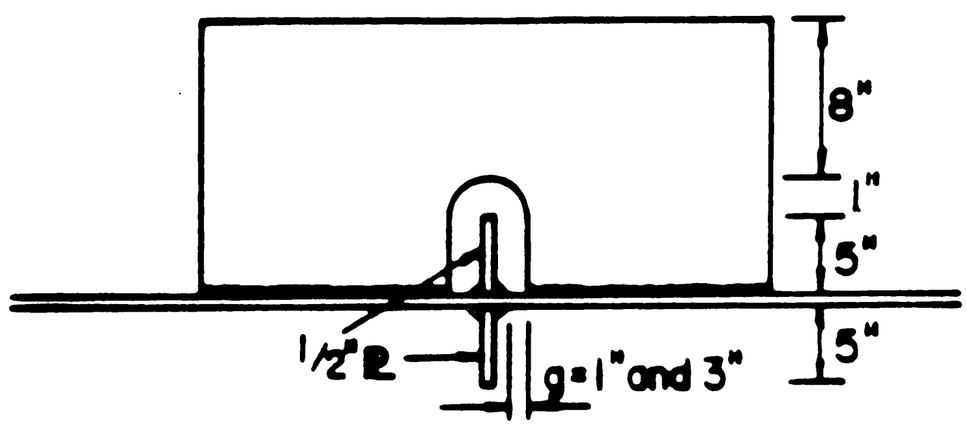

Figure 8: Lateral Gusset Plate Connection Details

- All 3/8" Thick Stiffeners To Get 3/16" Fillet Welds
- All 1/2" Thick Connection PL To Get 5/16" Fillet Welds
- All Holes To 1" dia. For 7/8" dia. A325 Bolts
- All Connection PL Are Tight Fit To Tension Flange
- Outer Connection PL To Be 40" x 5" x 1/2"
- Inner Connection PL To Be 40" x 5" x 1/2"
- Or 40" x 6" x 1/2" Based On Detail Type
- Outer PL To Be Perforated As Shown

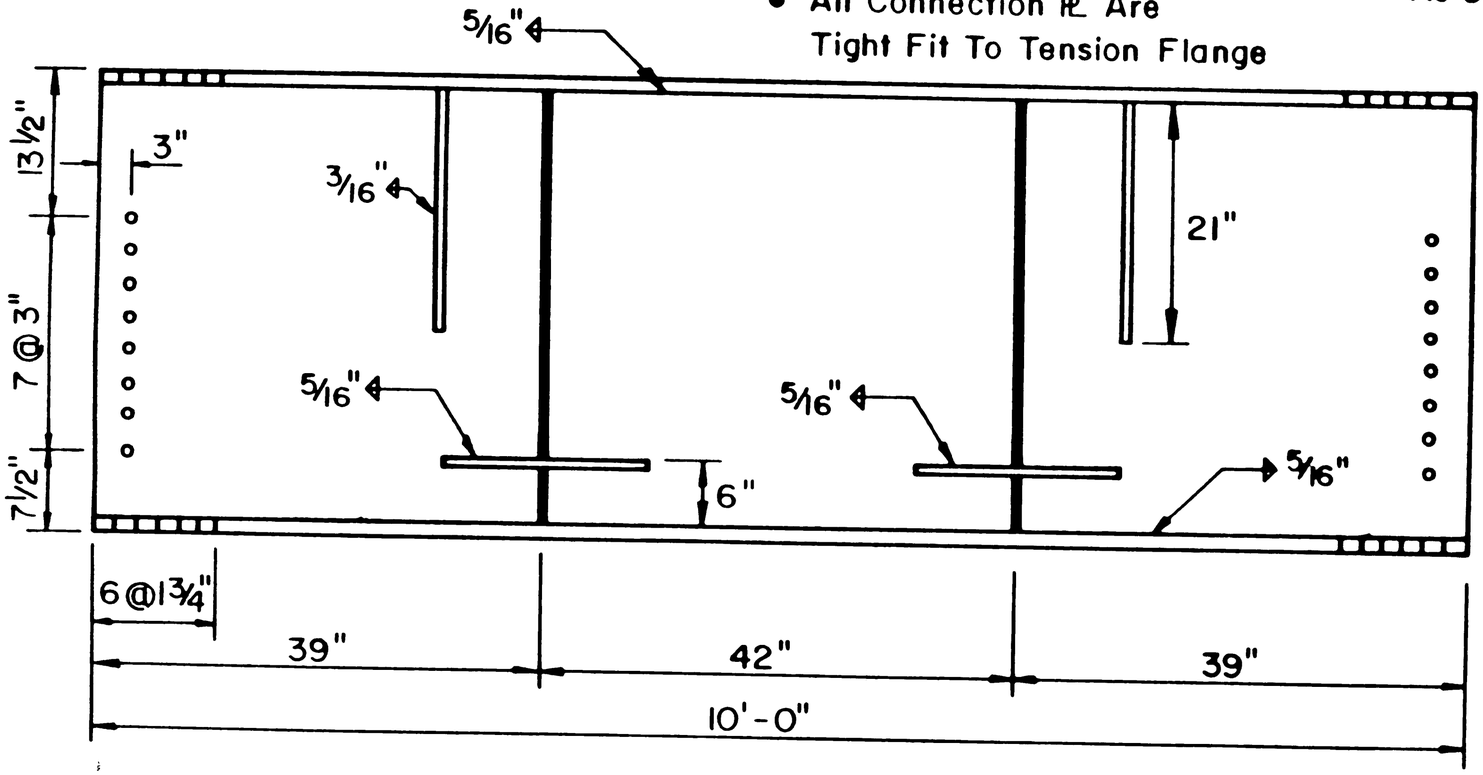

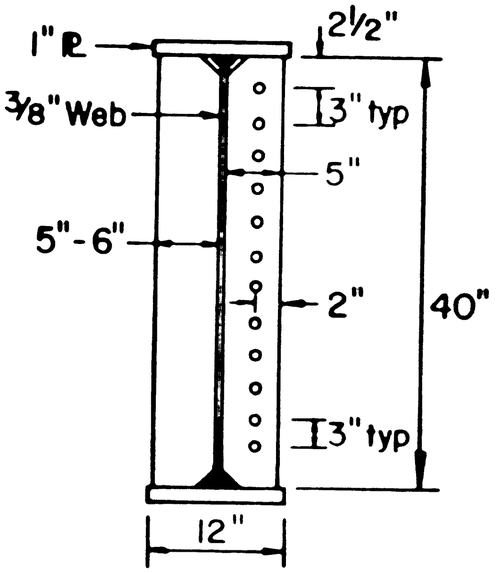

Figure 9: Test Girder Center Segment with Gusset Plate Details

- All Holes Are 1" dia.
  For 7/8" dia. A325 Bolts
- Hole Patterns In Flanges
  Are To Match Those Of
  The Splice Plates

Both Ends To Be Identical

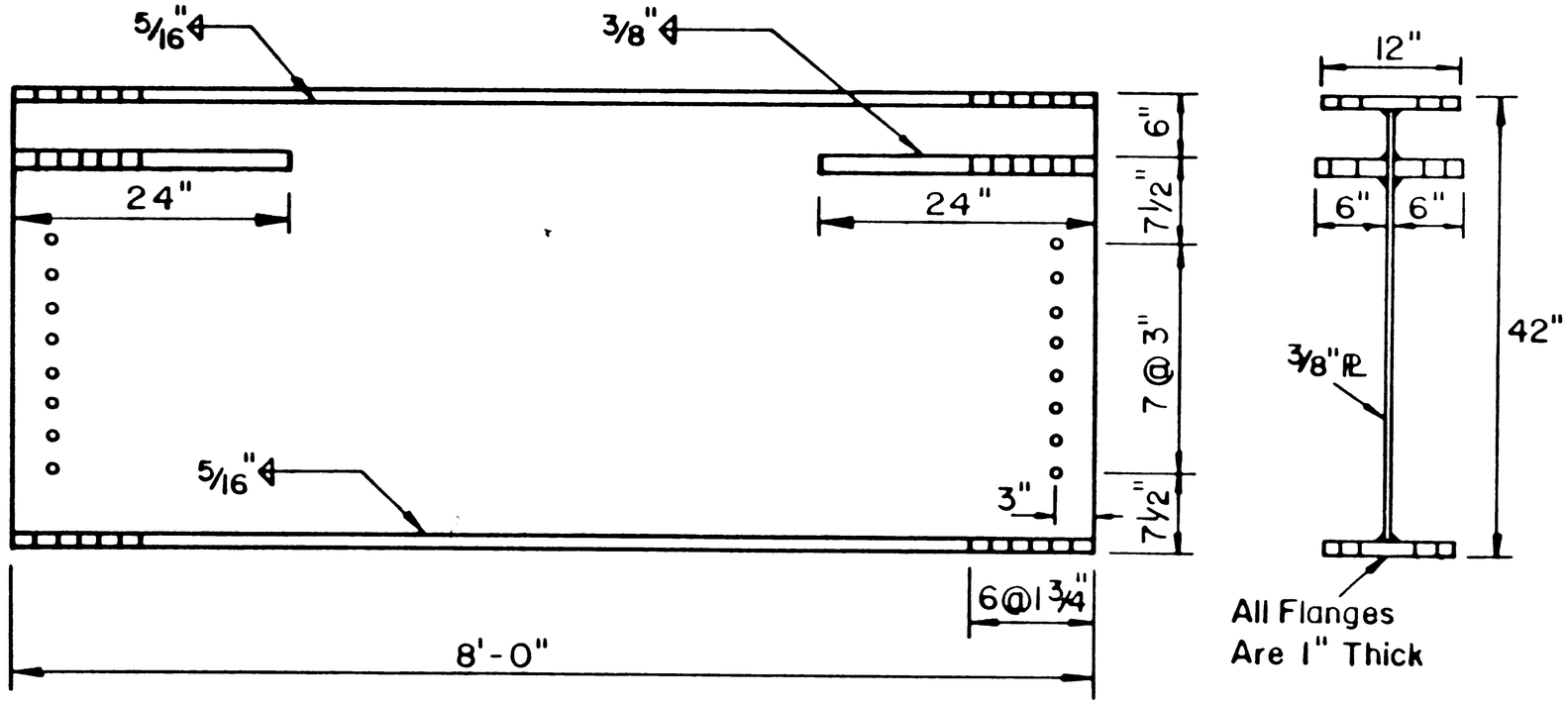

Figure 10: Test Girder End Segment

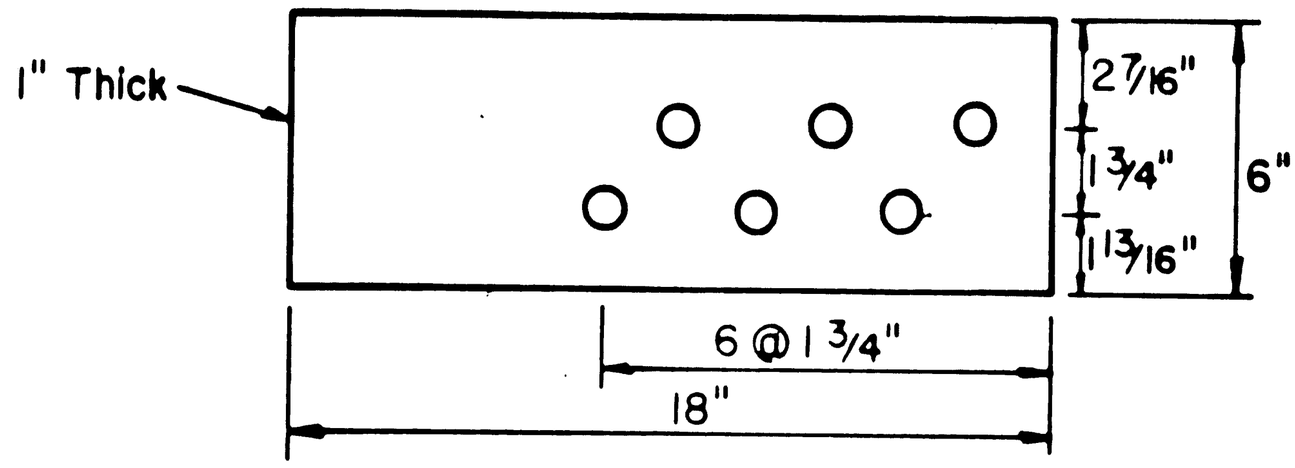

Identical Pattern and Hole Size as
Shown on the Above Splice Pl's.

Figure 11: Welded Web Tab

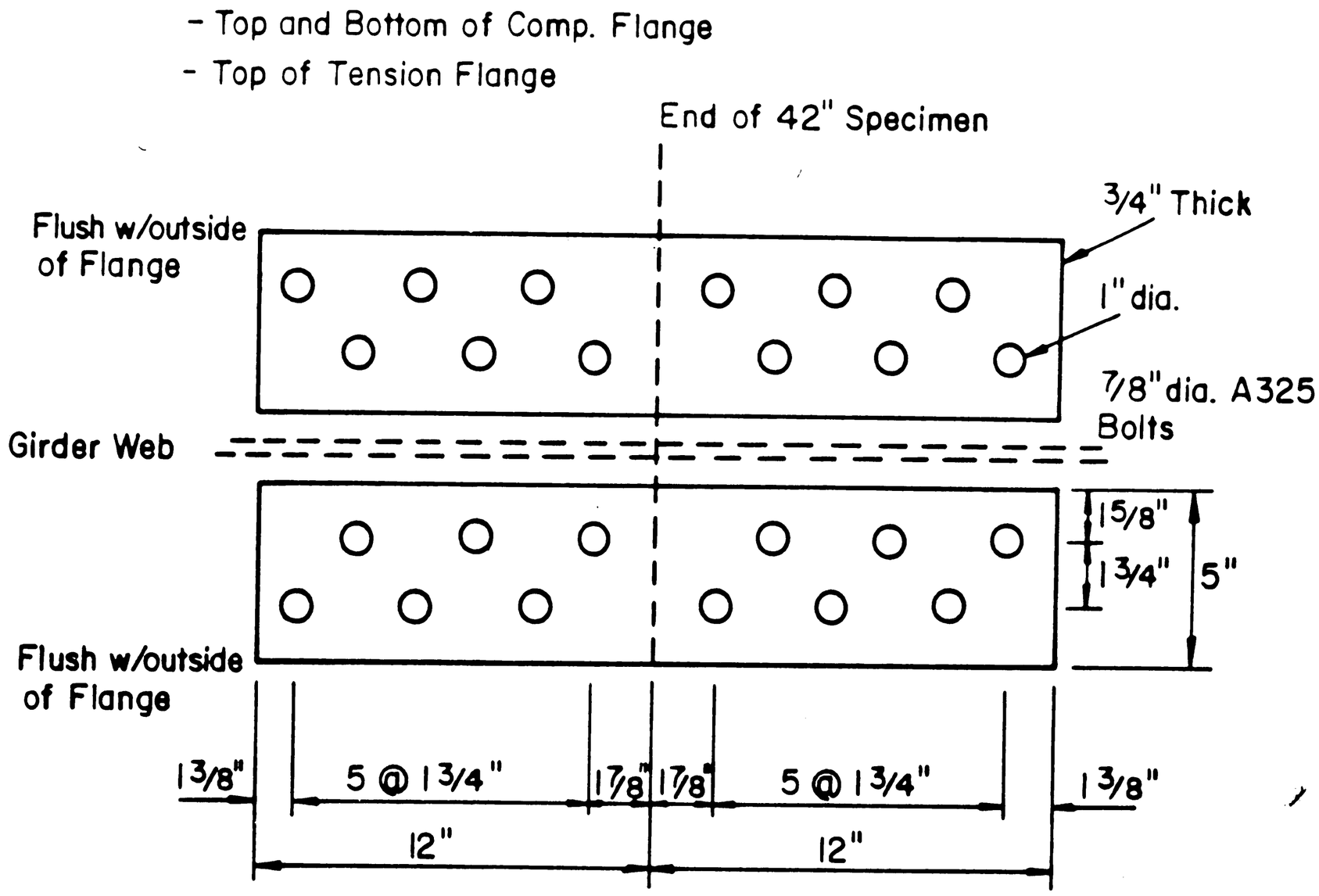

Figure 12: Splice Plates for Compression and Tension Flanges

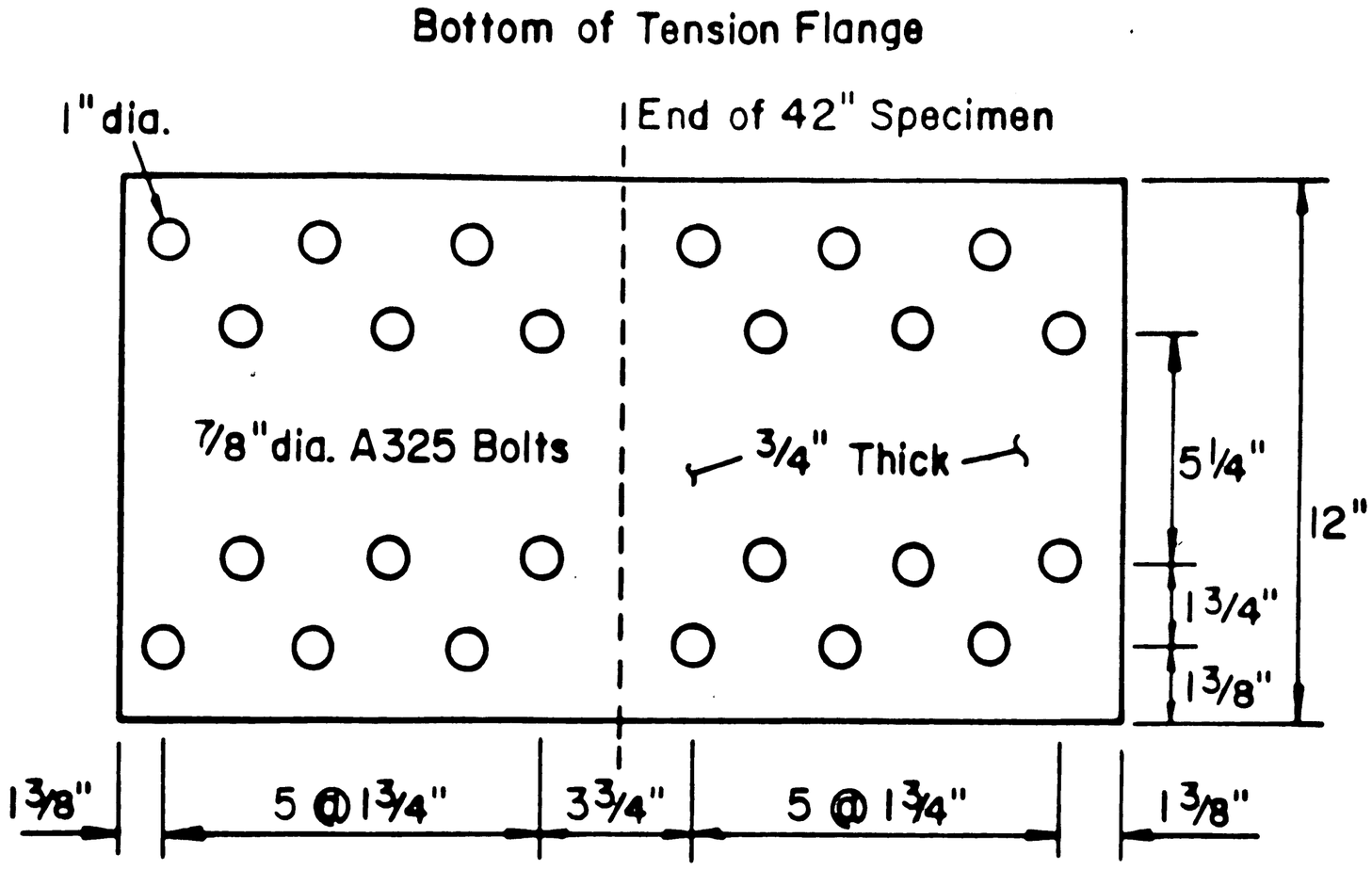

Figure 13: Splice Plate for the Bottom of the Tension Flange

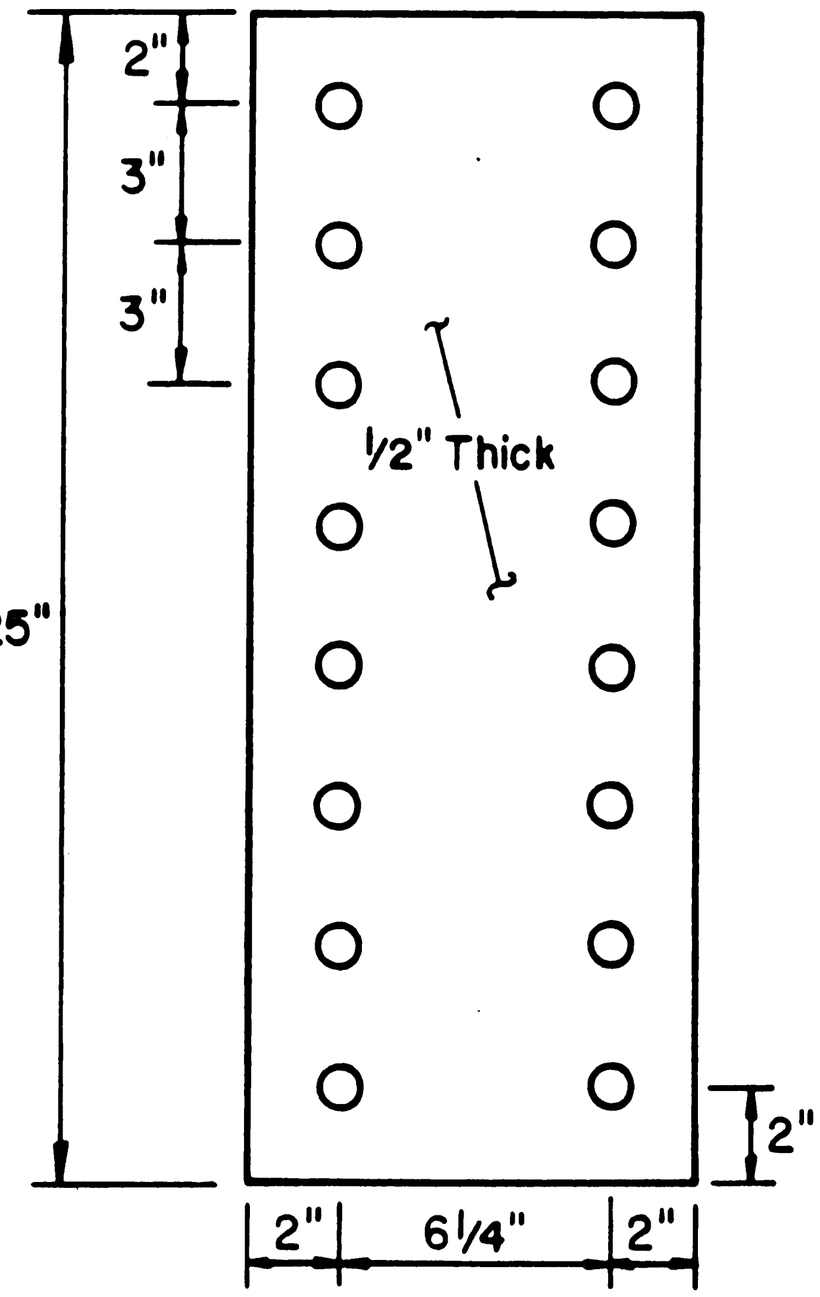

Figure 14: Web Splice Plate

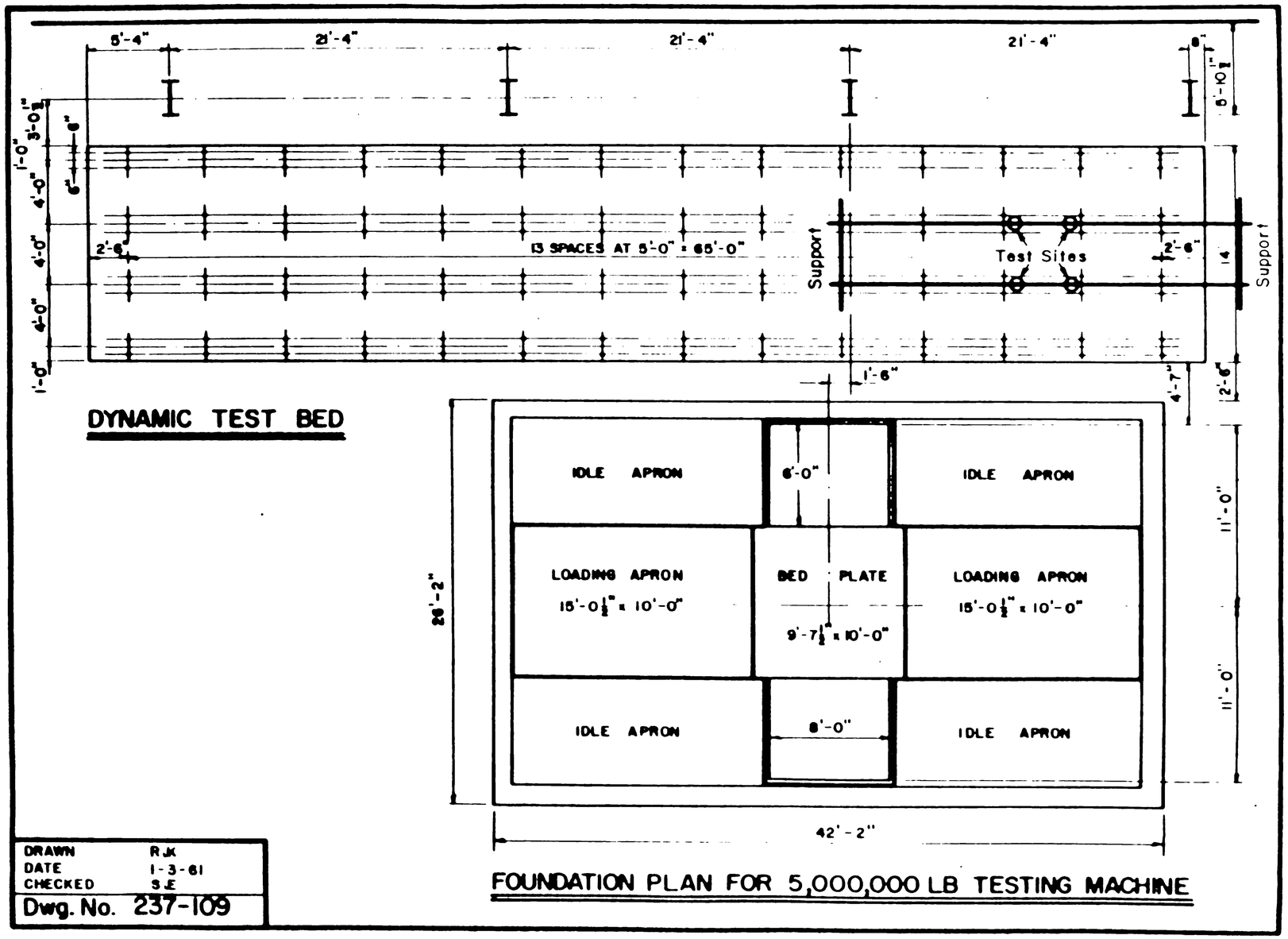

Figure 15: Laboratory Dynamic Test Bed Layout

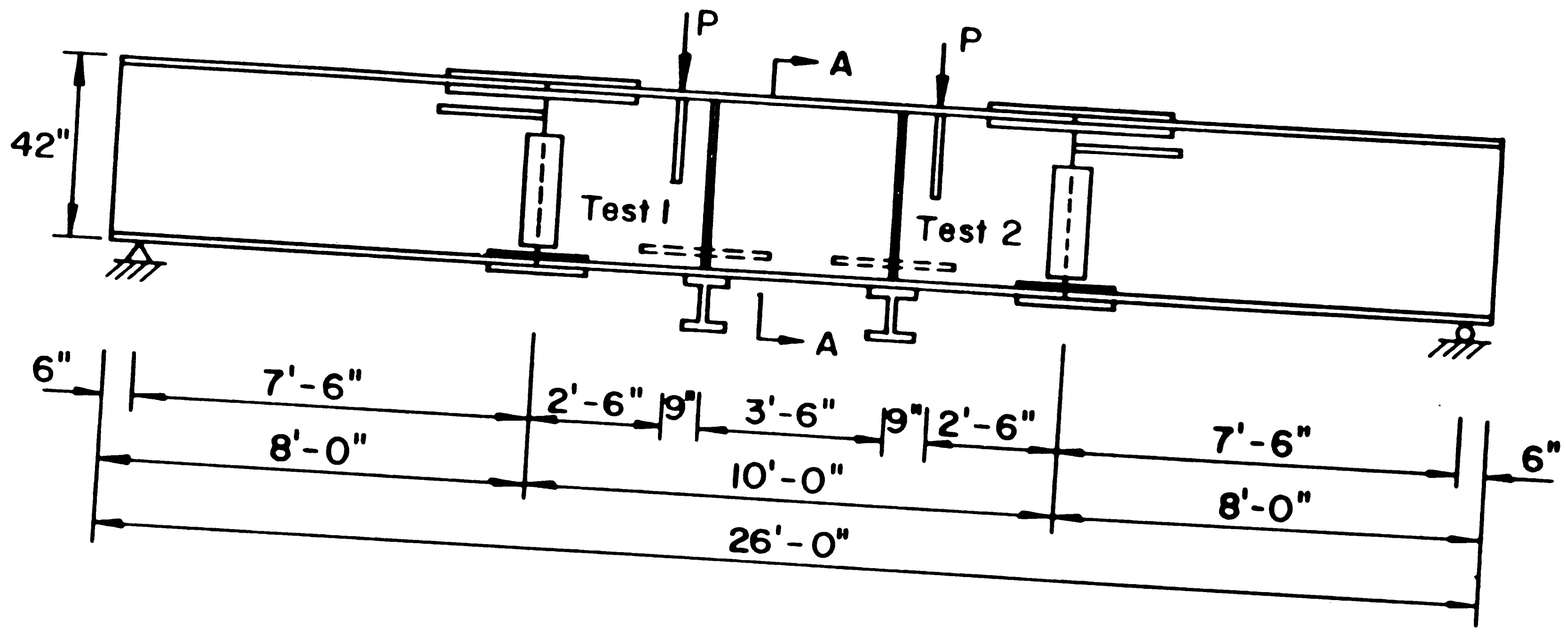

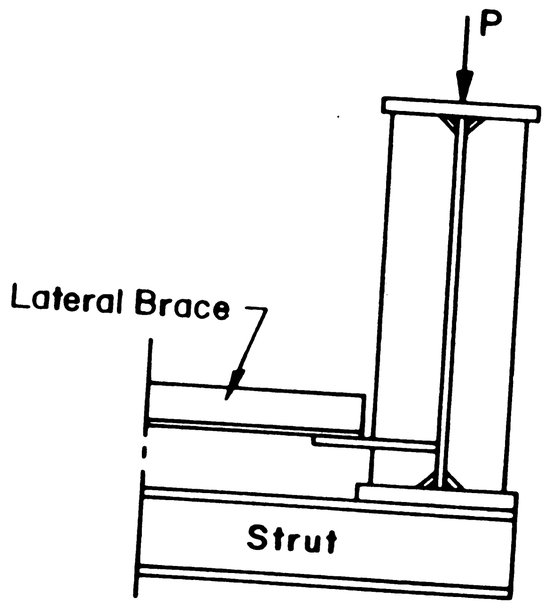

Section A-A

Figure 16: Continuous Test Girder

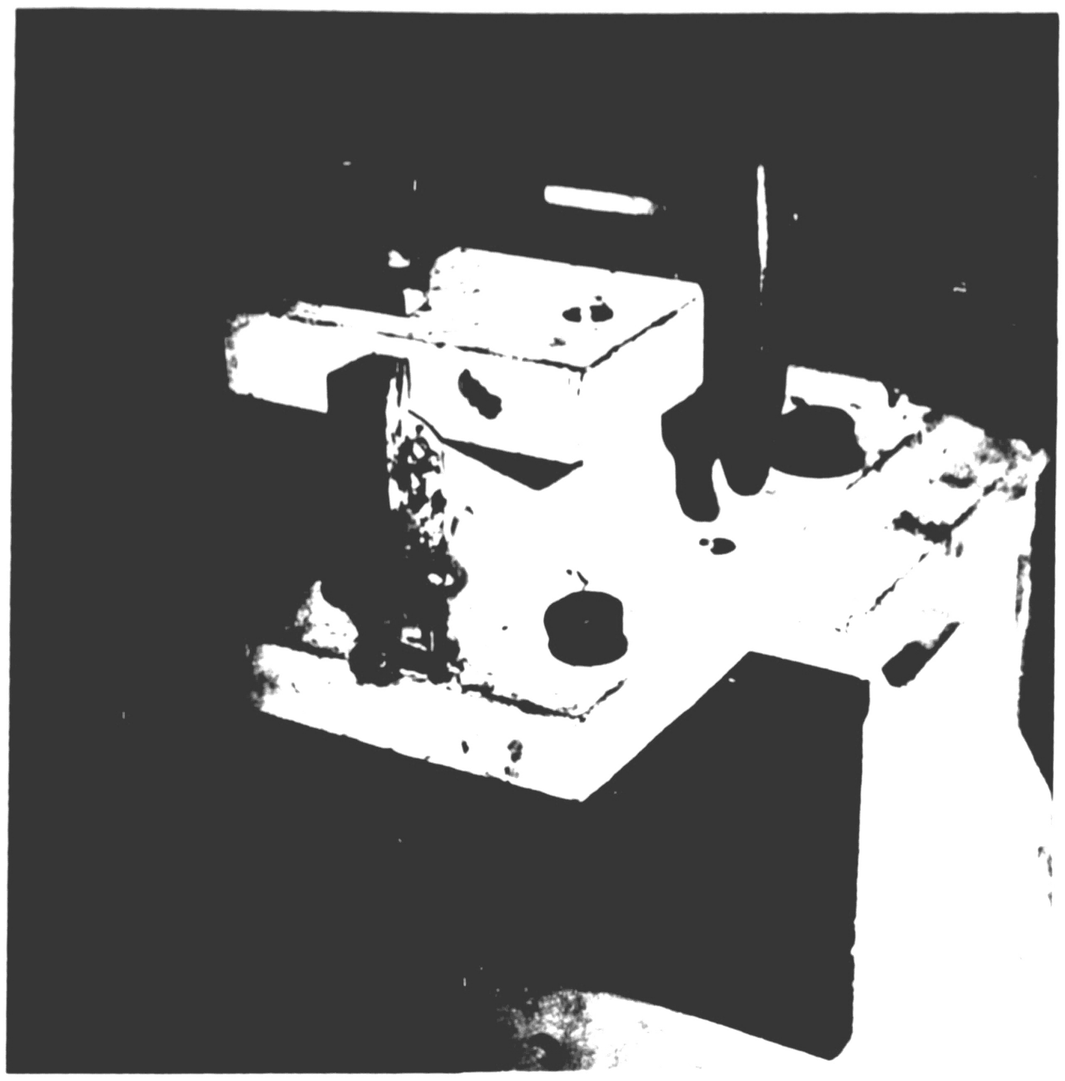

Figure 17: Pinned Support

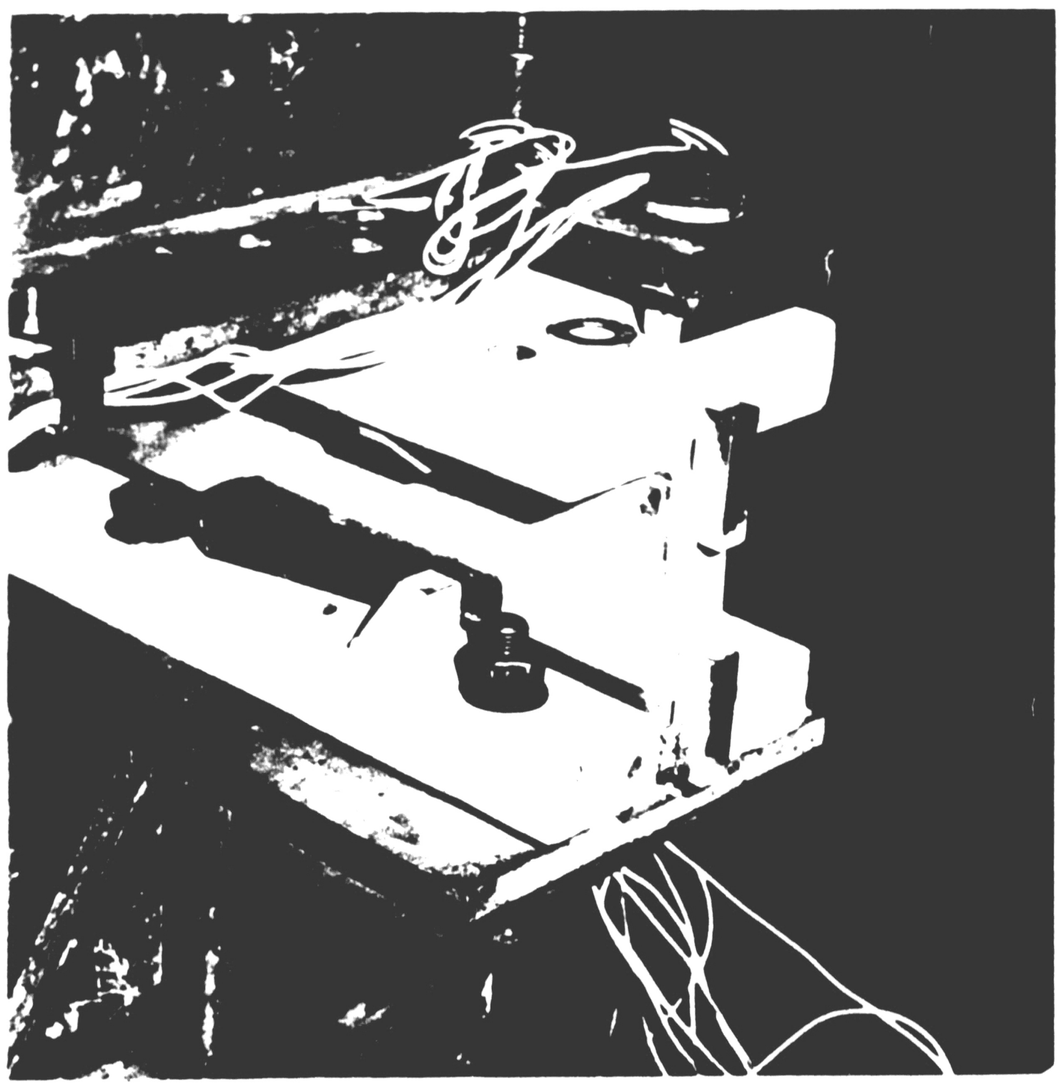

Figure 18: Roller Support

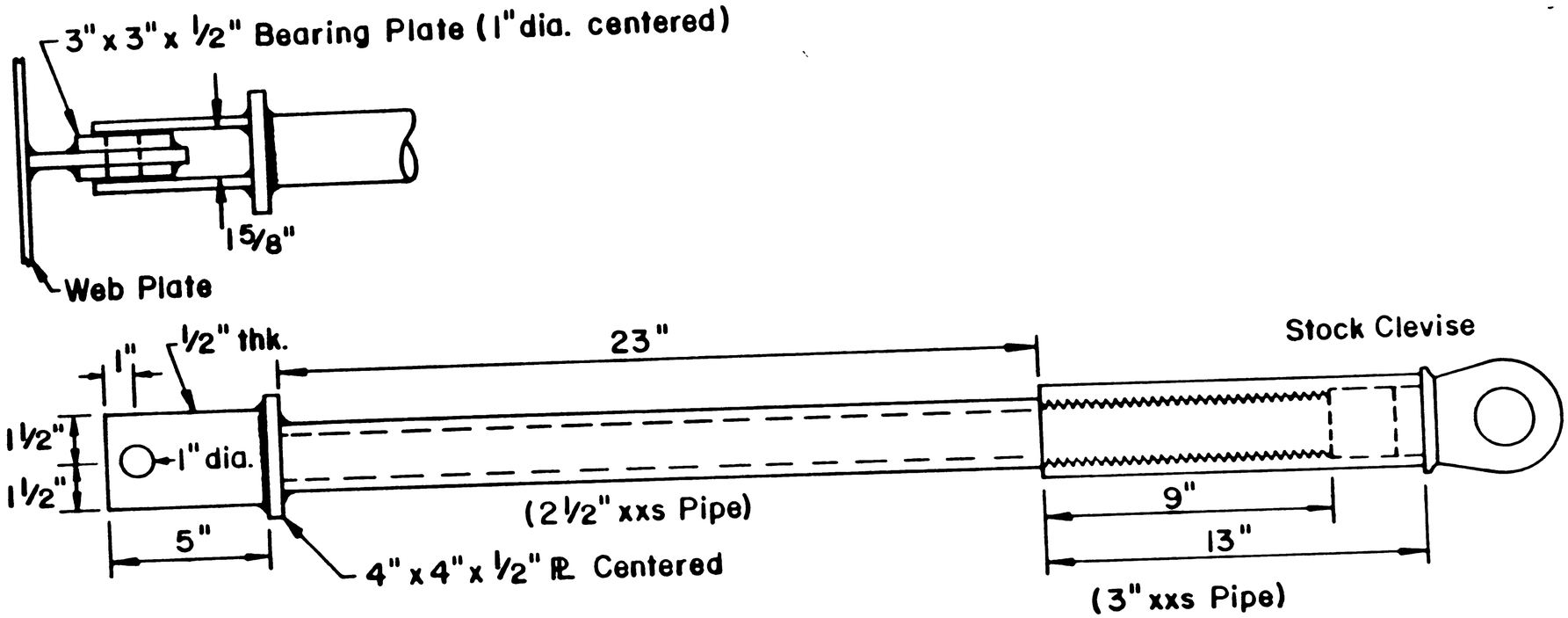

Stiffener	Build-Up	Clearance to Rod Grips
⅜"	½" PL (2)	⅛" To Each Side
½"	½" PL (2)	1/16" To Each Side

All Stiffener Related and Attachment-To-Rod Welds to be ¼" Fillet.

Figure 19: Lateral Displacement-Inducing Rod

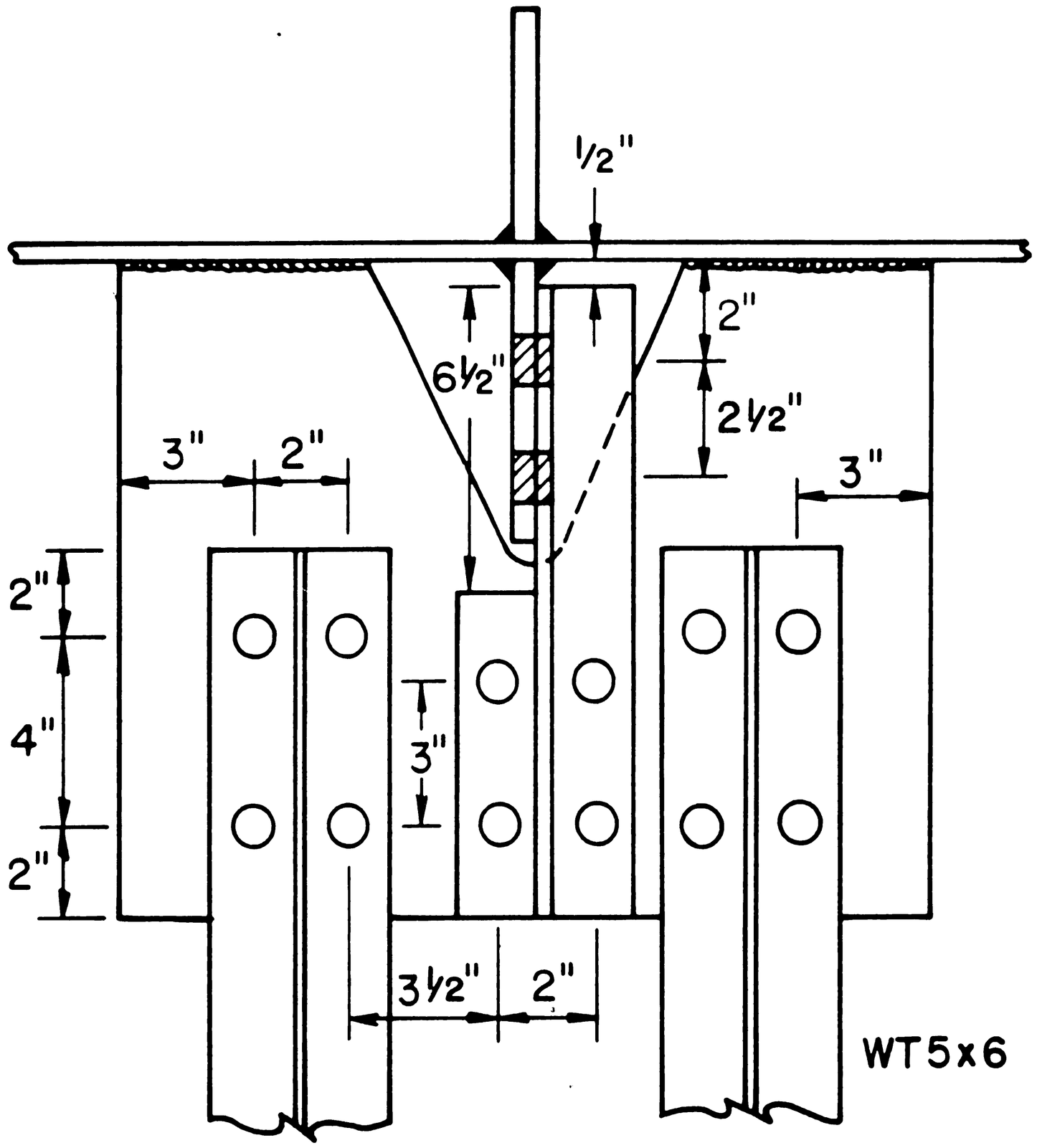

Figure 20: Gusset Plate Bolt Pattern

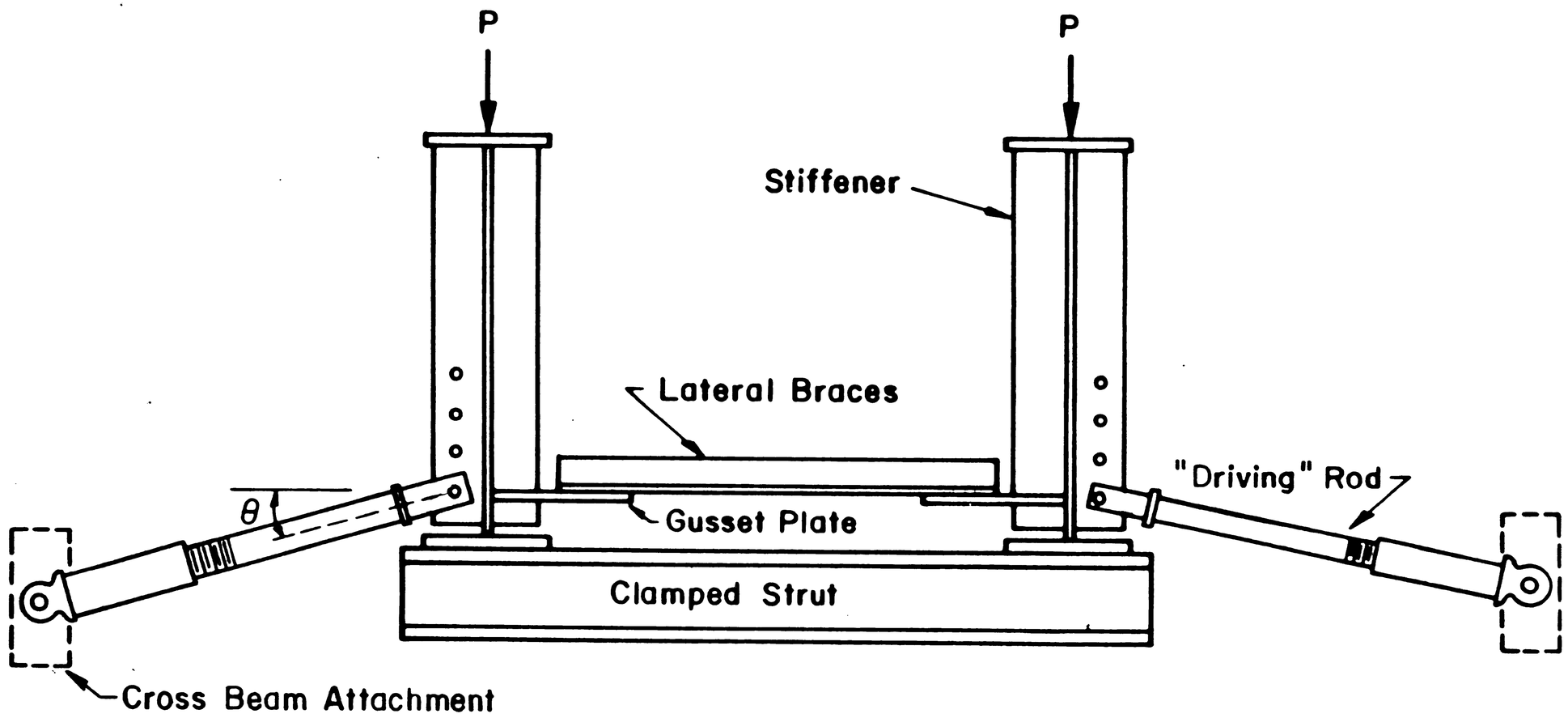

Figure 21: System of Loading and Restraint

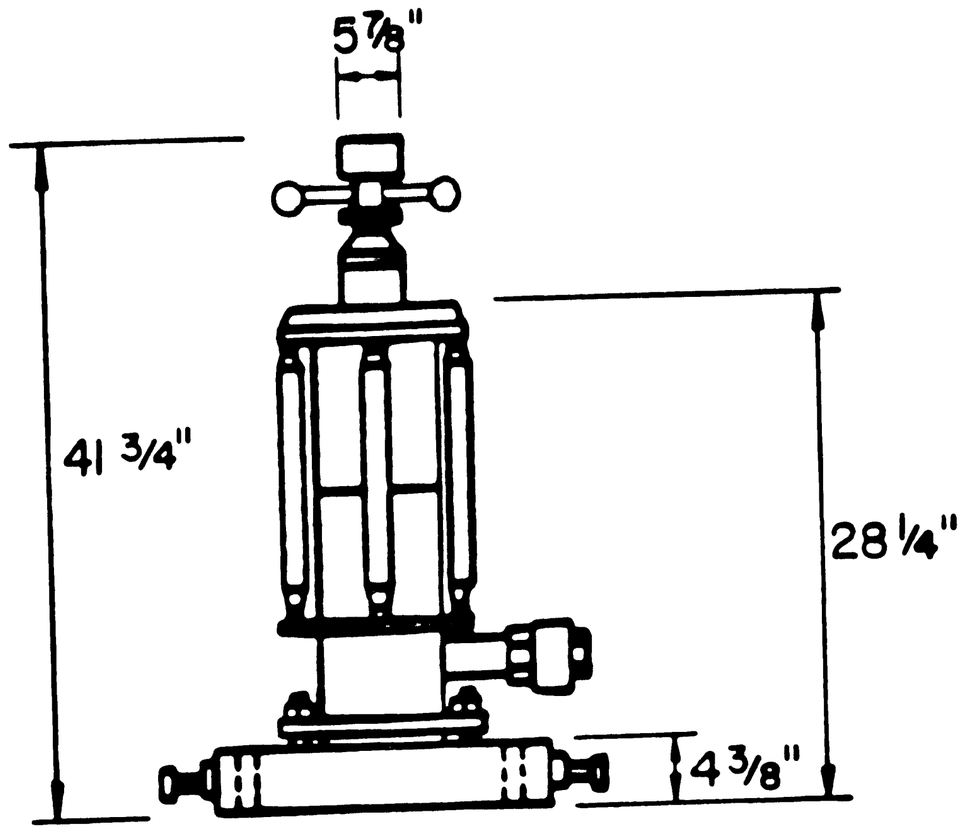

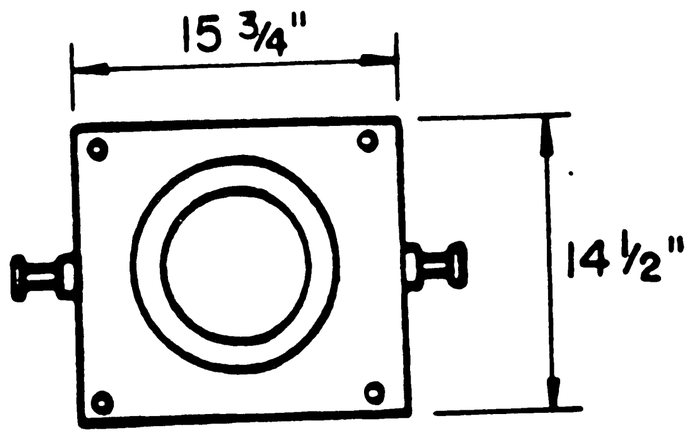

Figure 22: Amsler Hydraulic Jack

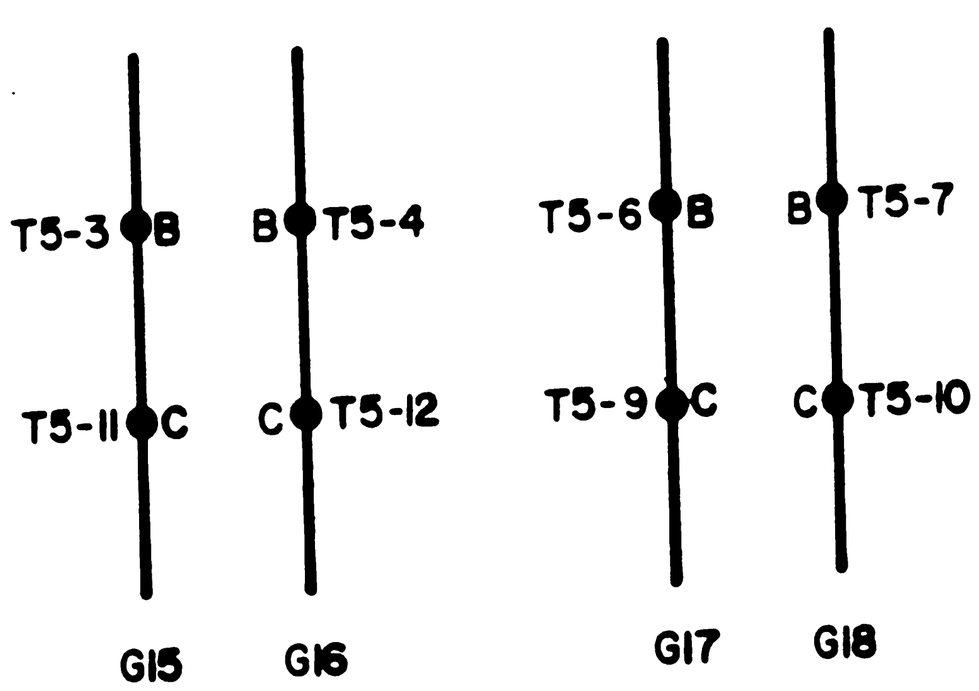

Figure 23: Arrangement of Girder Pairs

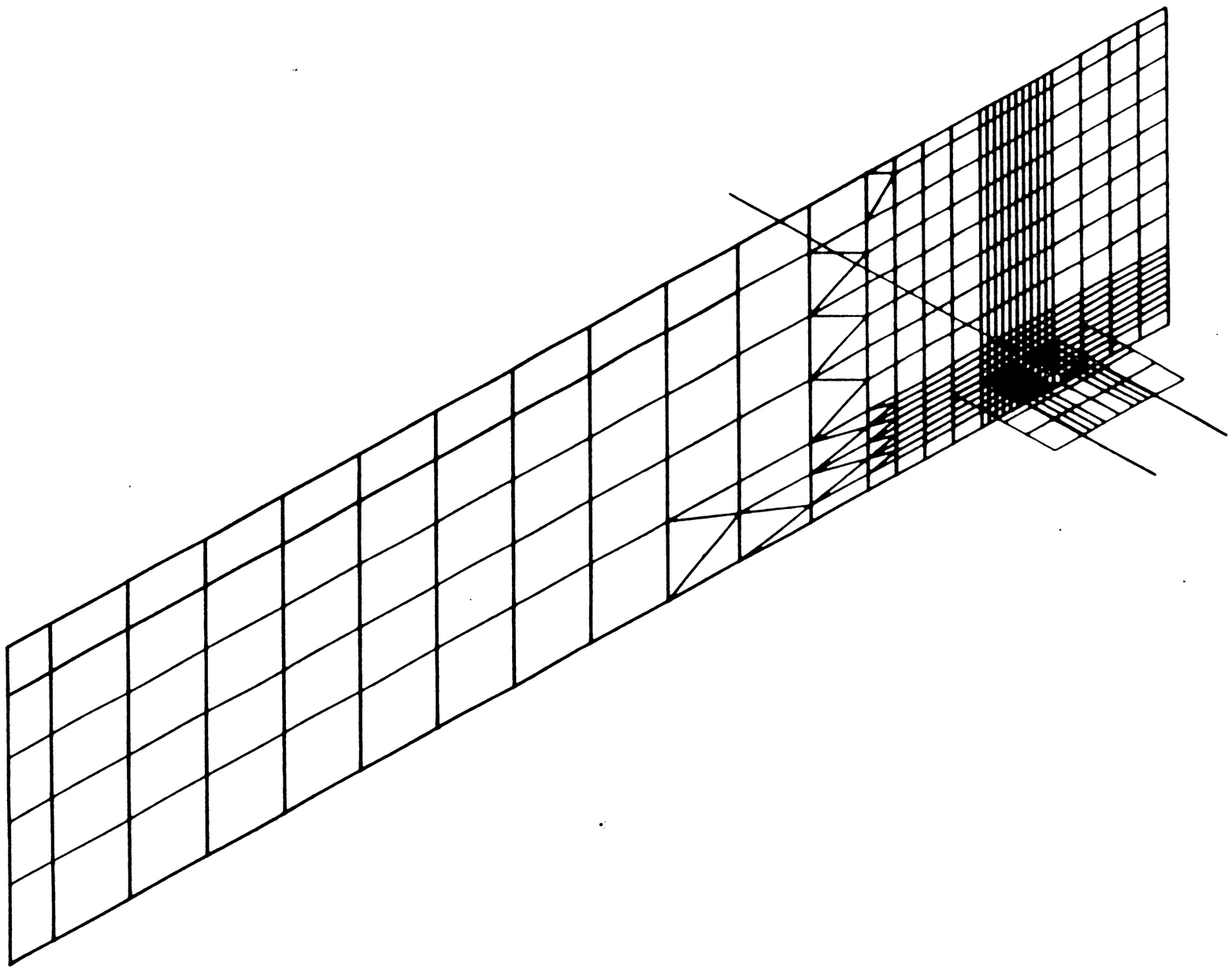

Figure 24: Finite Element Model

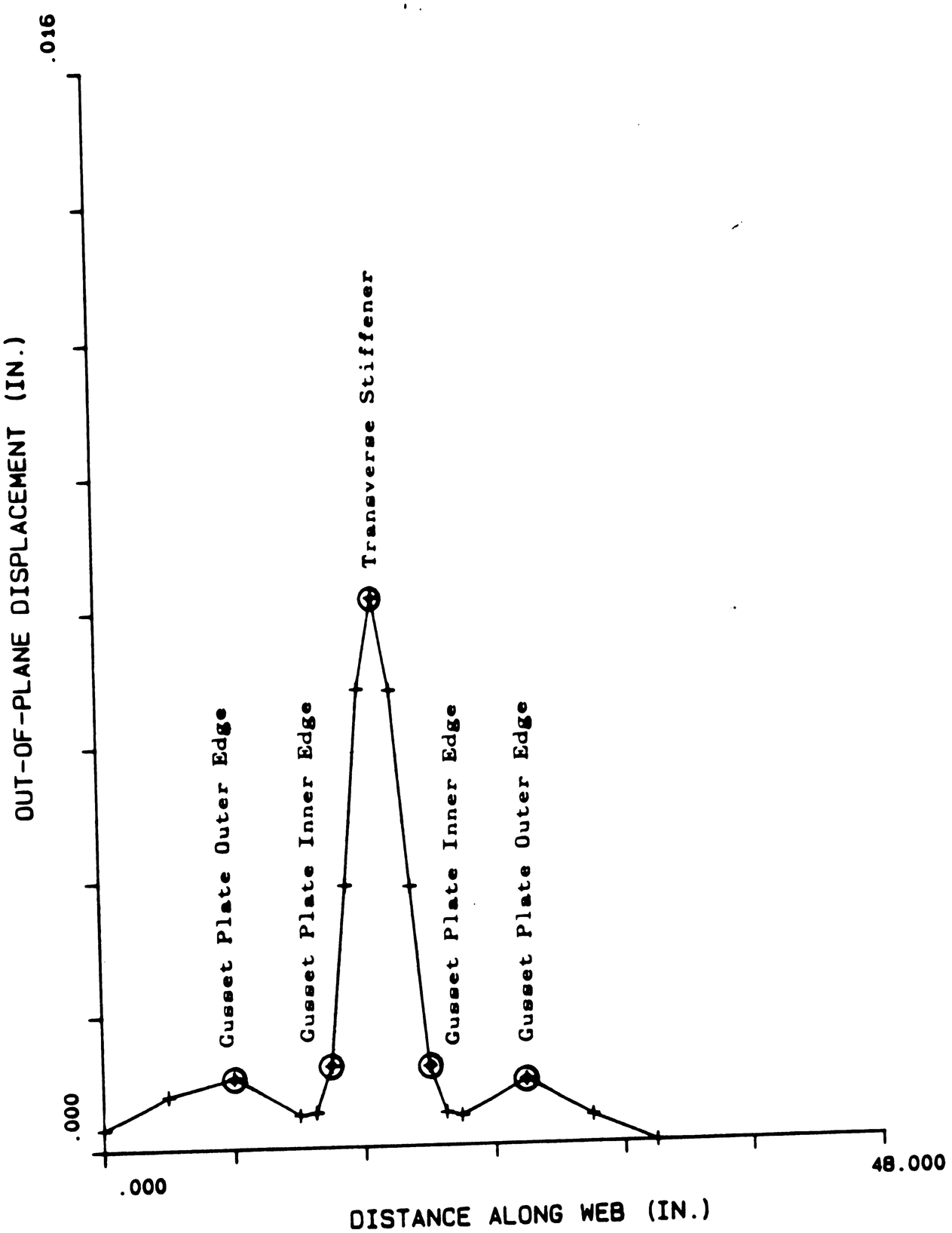

Figure 25: Lateral Displacements Along Detail C; Θ = -20°, 3.0 in. Gap

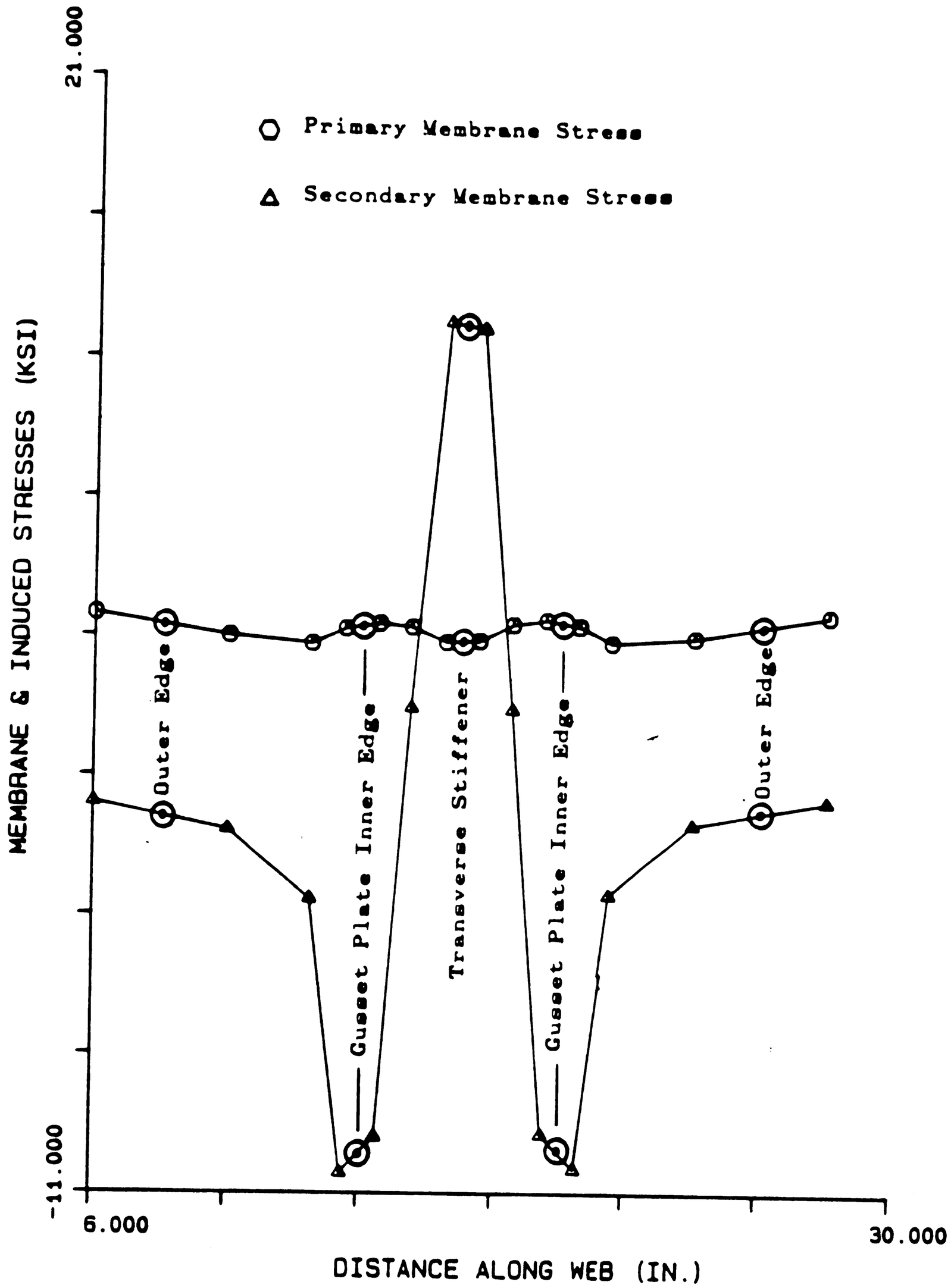

Figure 26: Stress Distributions Along Detail C; Θ = -20°, 3.0 in. Gap

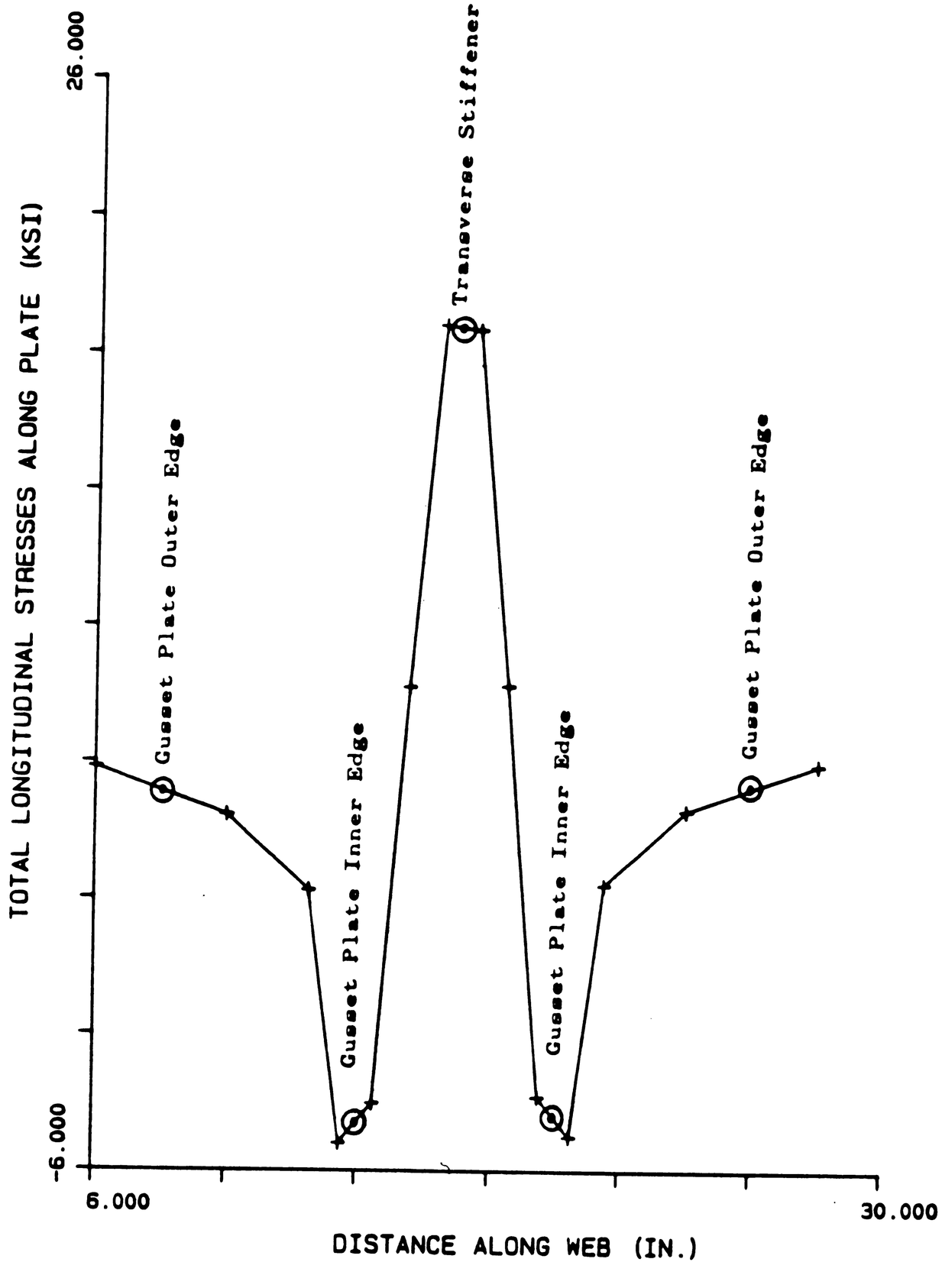

Figure 27: Combined Stress Distribution, Detail C; Θ = -20°, 3.0 in. Gap

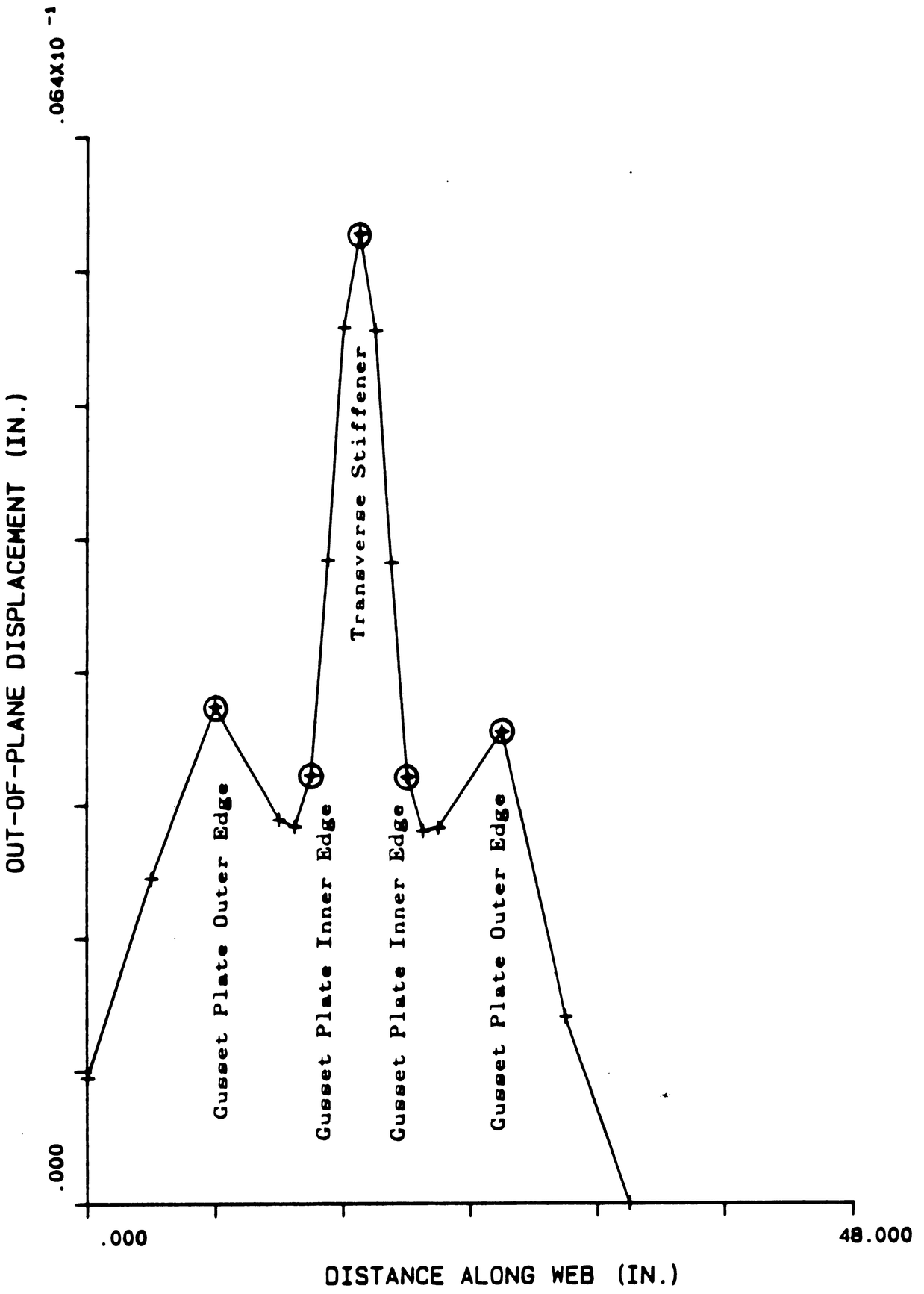

Figure 28: Lateral Displacement Along Detail B; Θ = -20°, 3.0 in. Gap

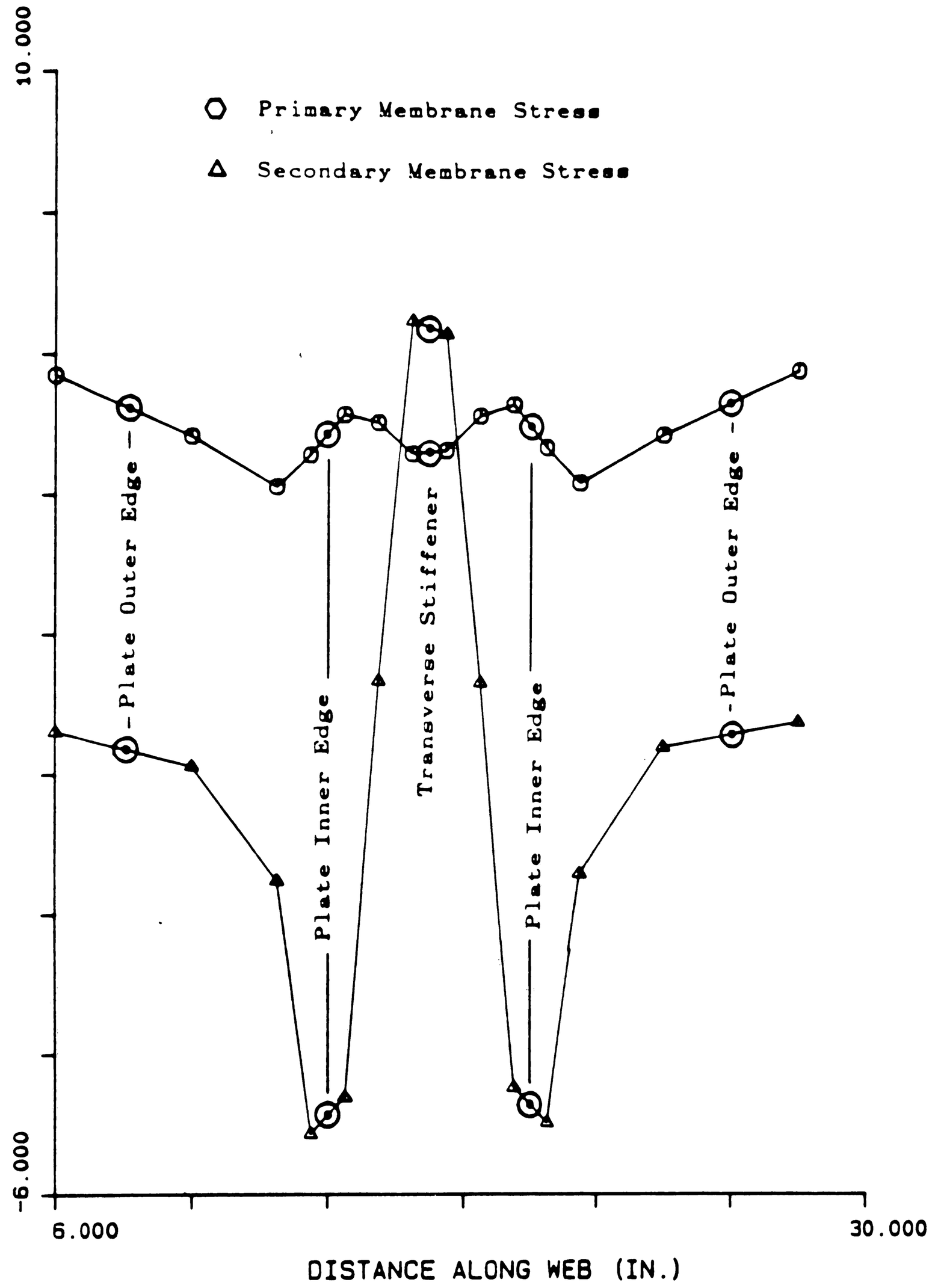

Figure 29: Stress Distribution Along Detail B; Θ = -20°, 3.0 in. Gap

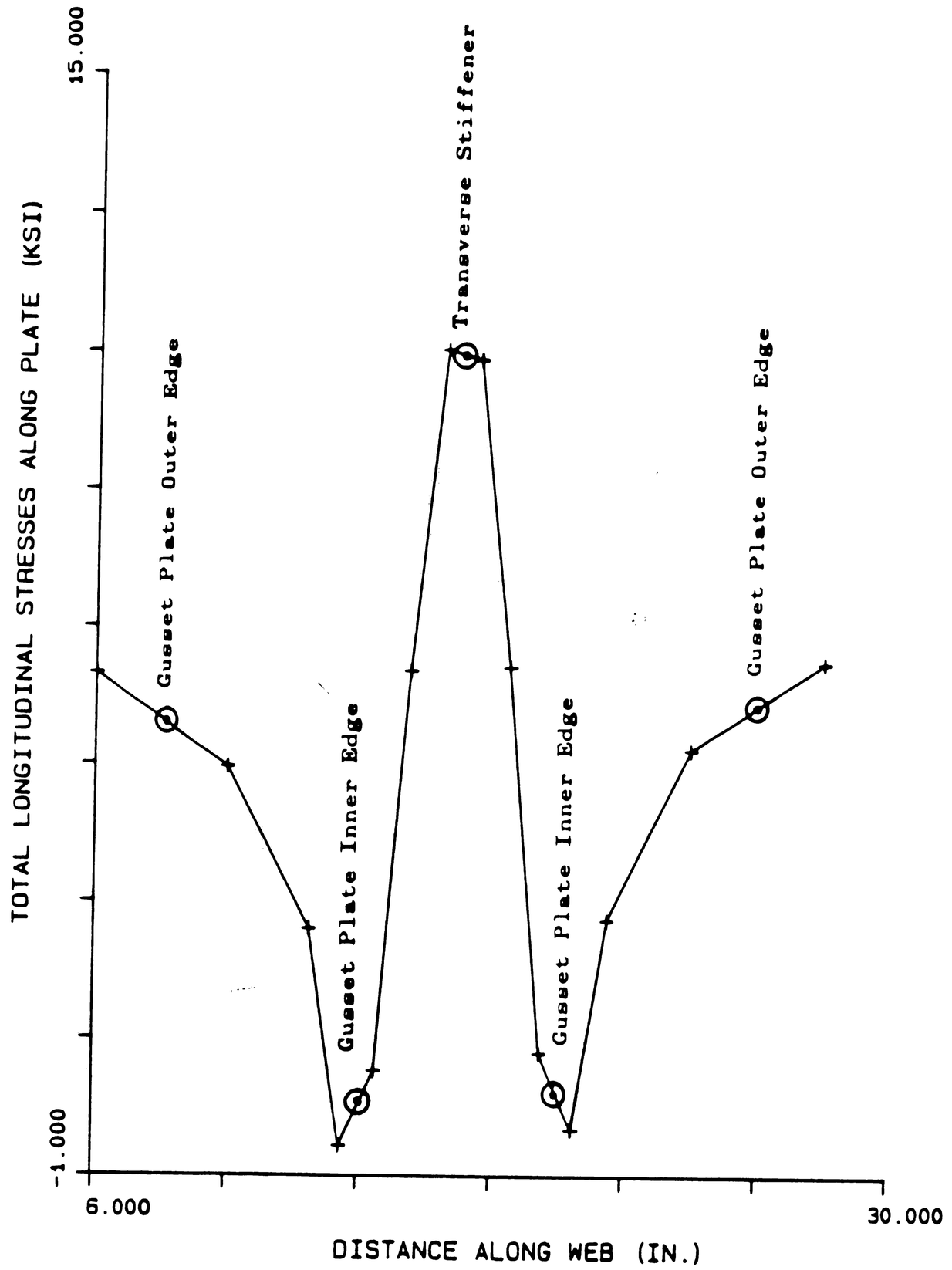

Figure 30: Combined Stress Distribution, Detail B; Θ = -20°, 3.0 in. Gap

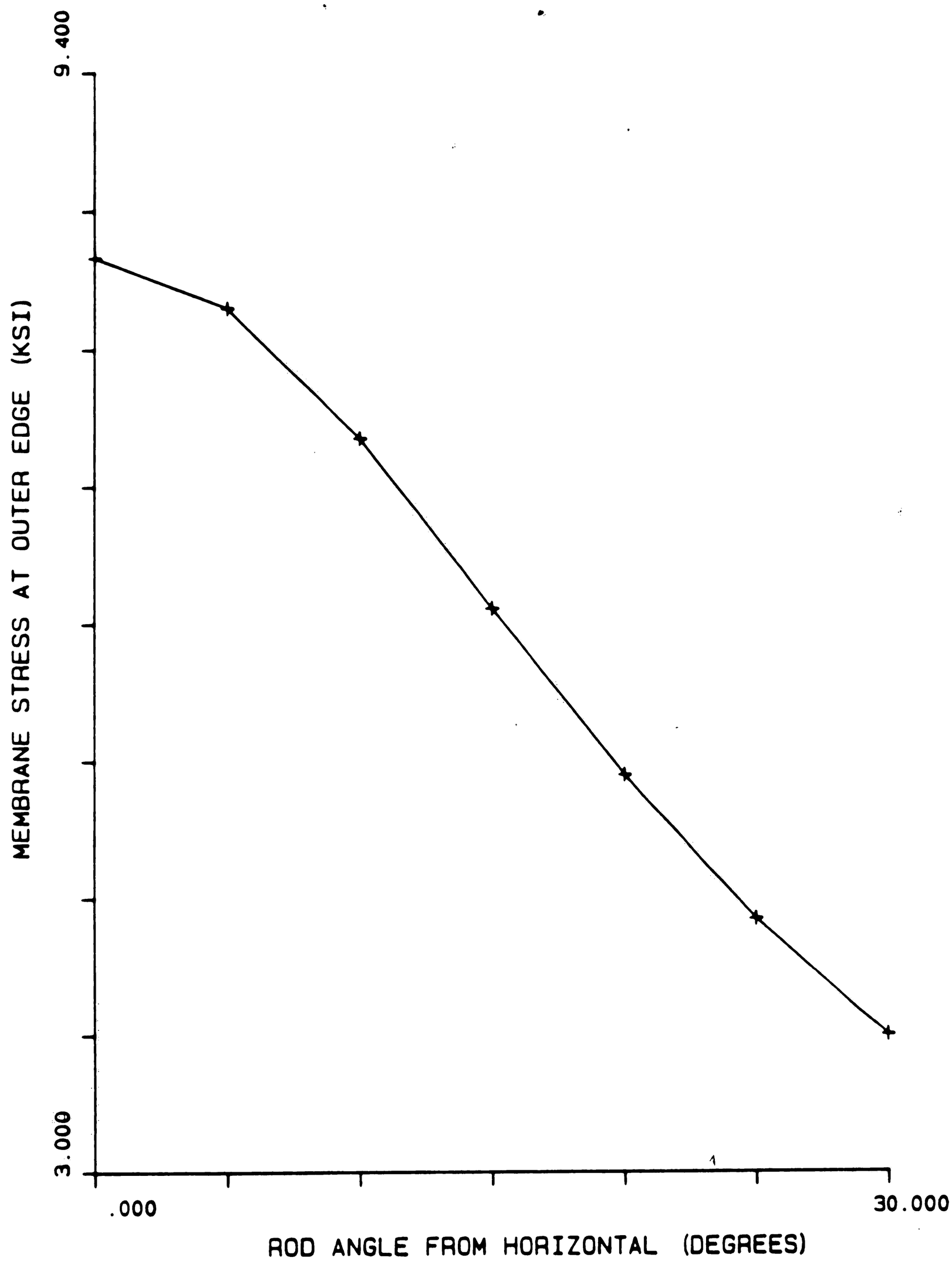

Figure 31: Primary Stress/Rod Angle Relation For Detail C; 3.0 in. Gap

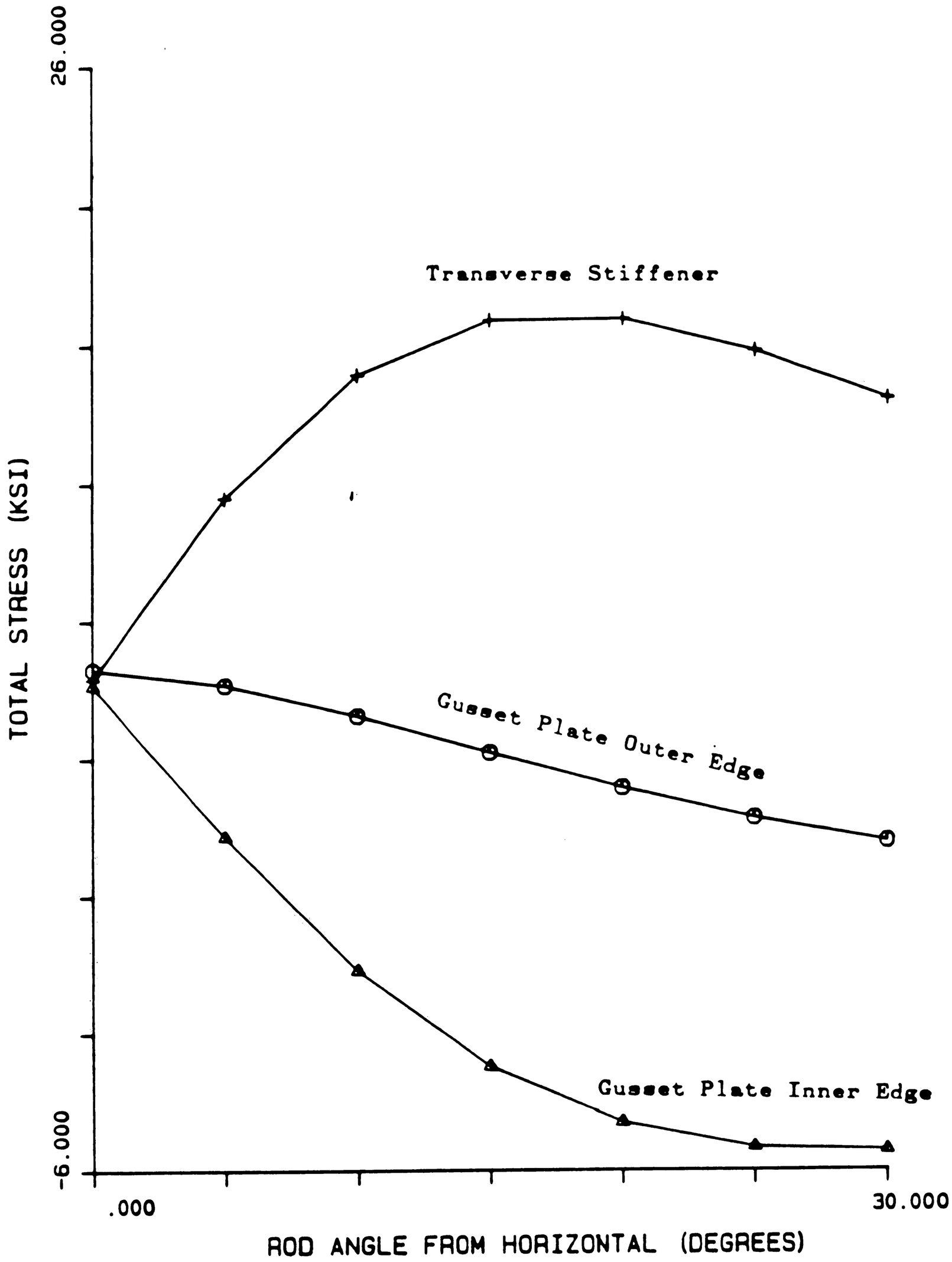

Figure 32: Total Stress/Rod Angle Relation For Detail C; 3.0 in. Gap

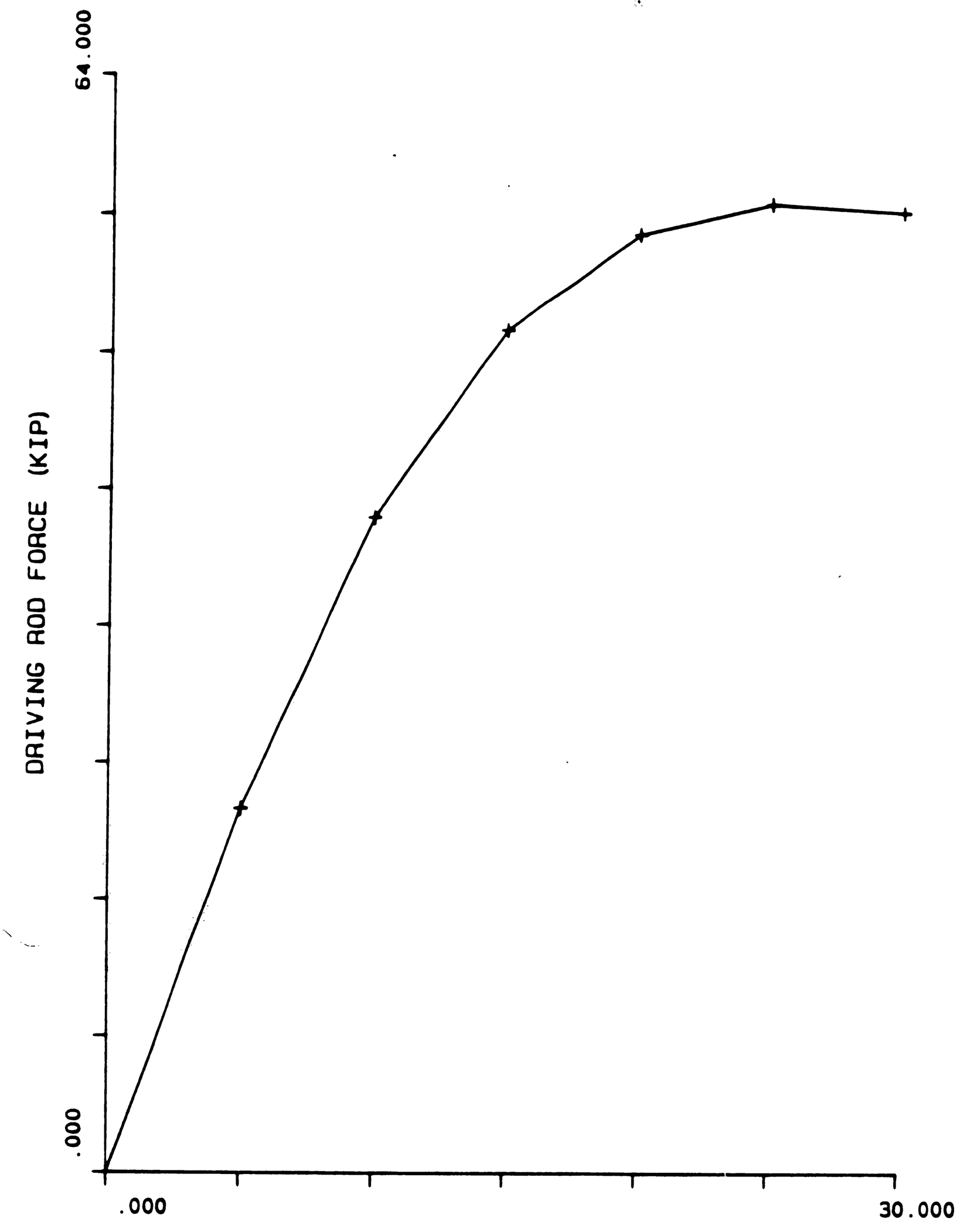

Figure 33: Rod Force/Rod Angle Relation For Detail C; 3.0 in. Gap

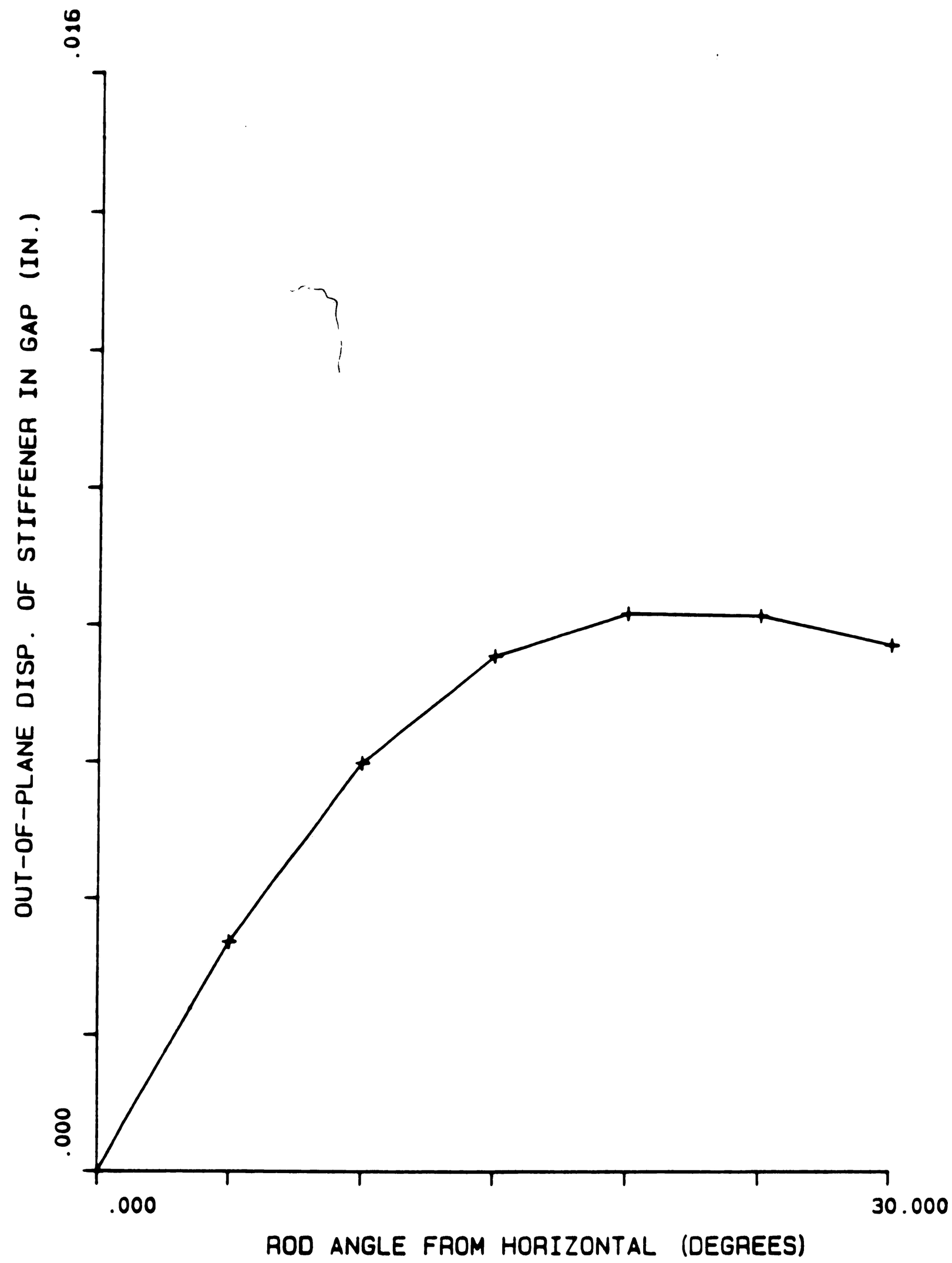

Figure 34: Lateral Disp./Rod Angle Relation For Detail C; 3.0 in. Gap

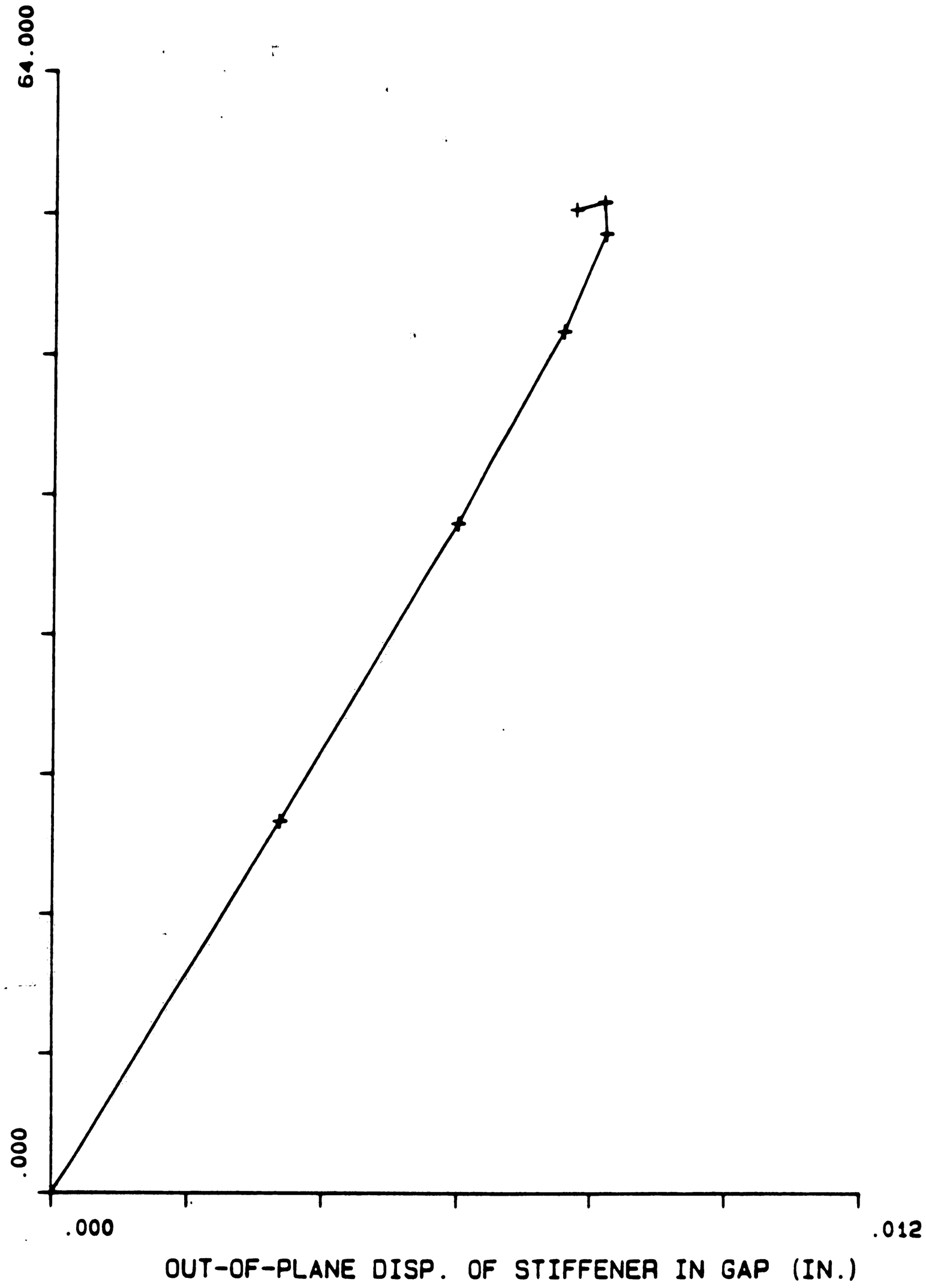

Figure 35: Rod Force/Lateral Disp. Relation For Detail C; 3.0 in. Gap

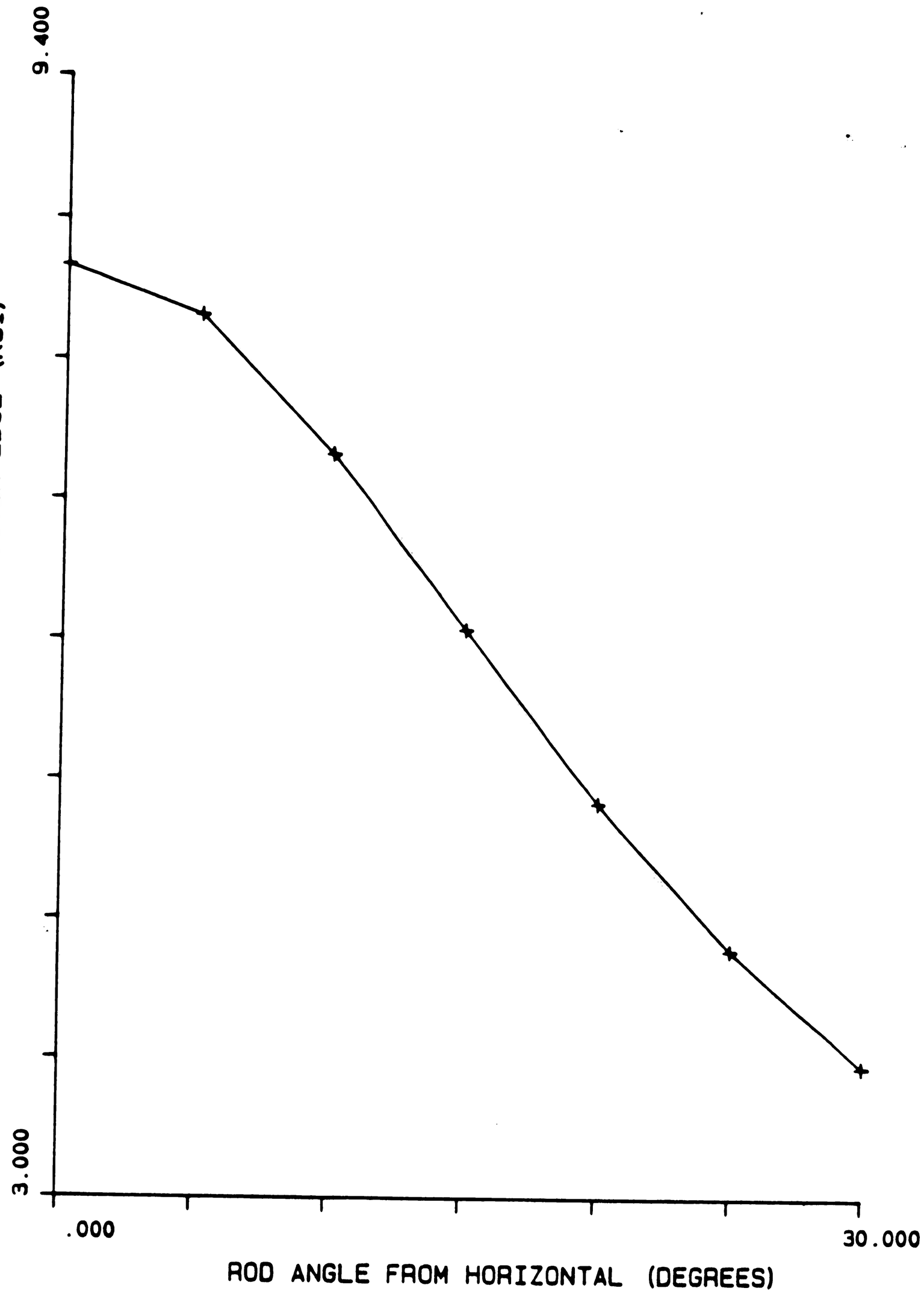

Figure 36: Primary Stress/Rod Angle Relation For Detail B; 3.0 in. Gap

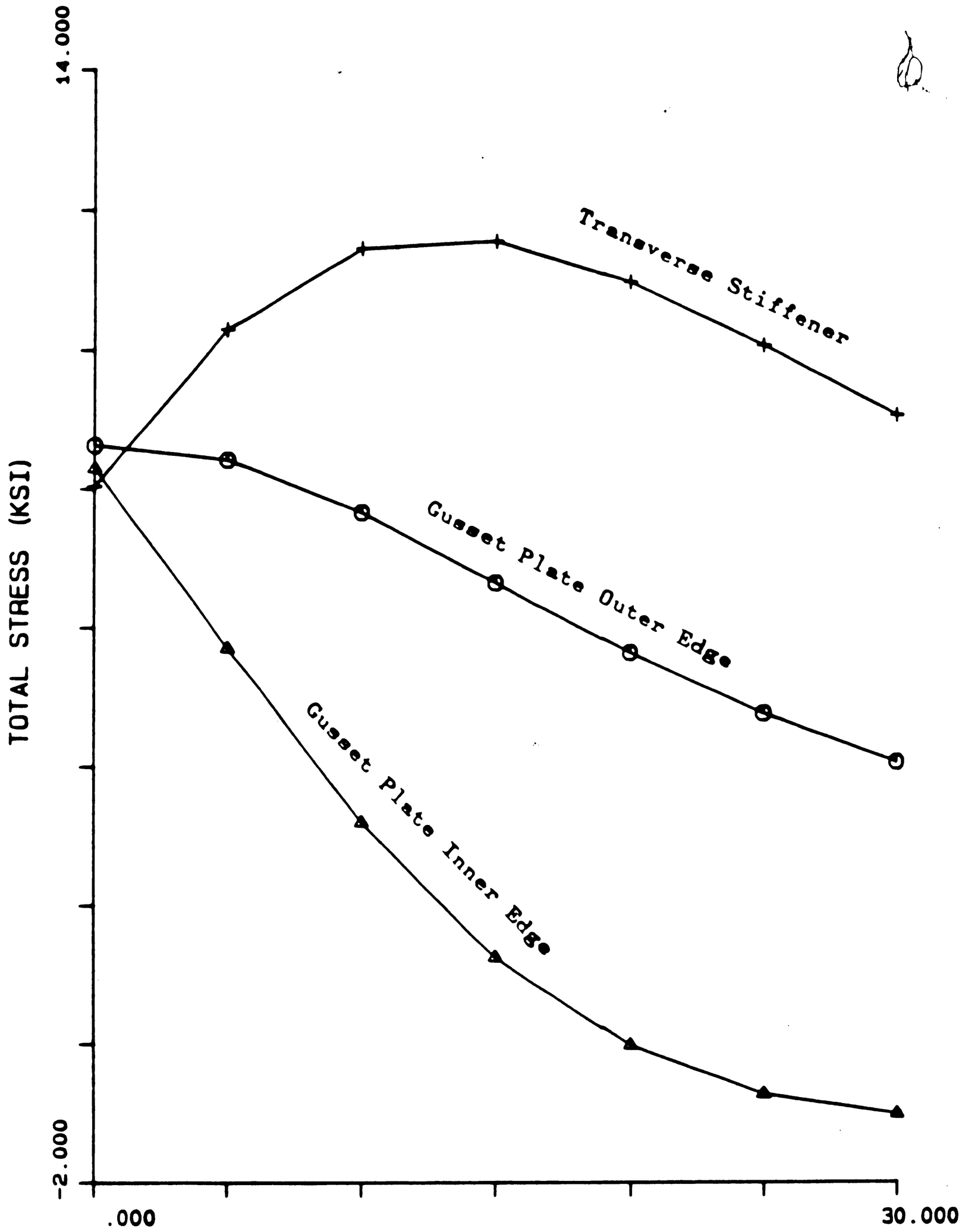

Figure 37: Total Stress/Rod Angle Relation For Detail B; 3.0 in. Gap

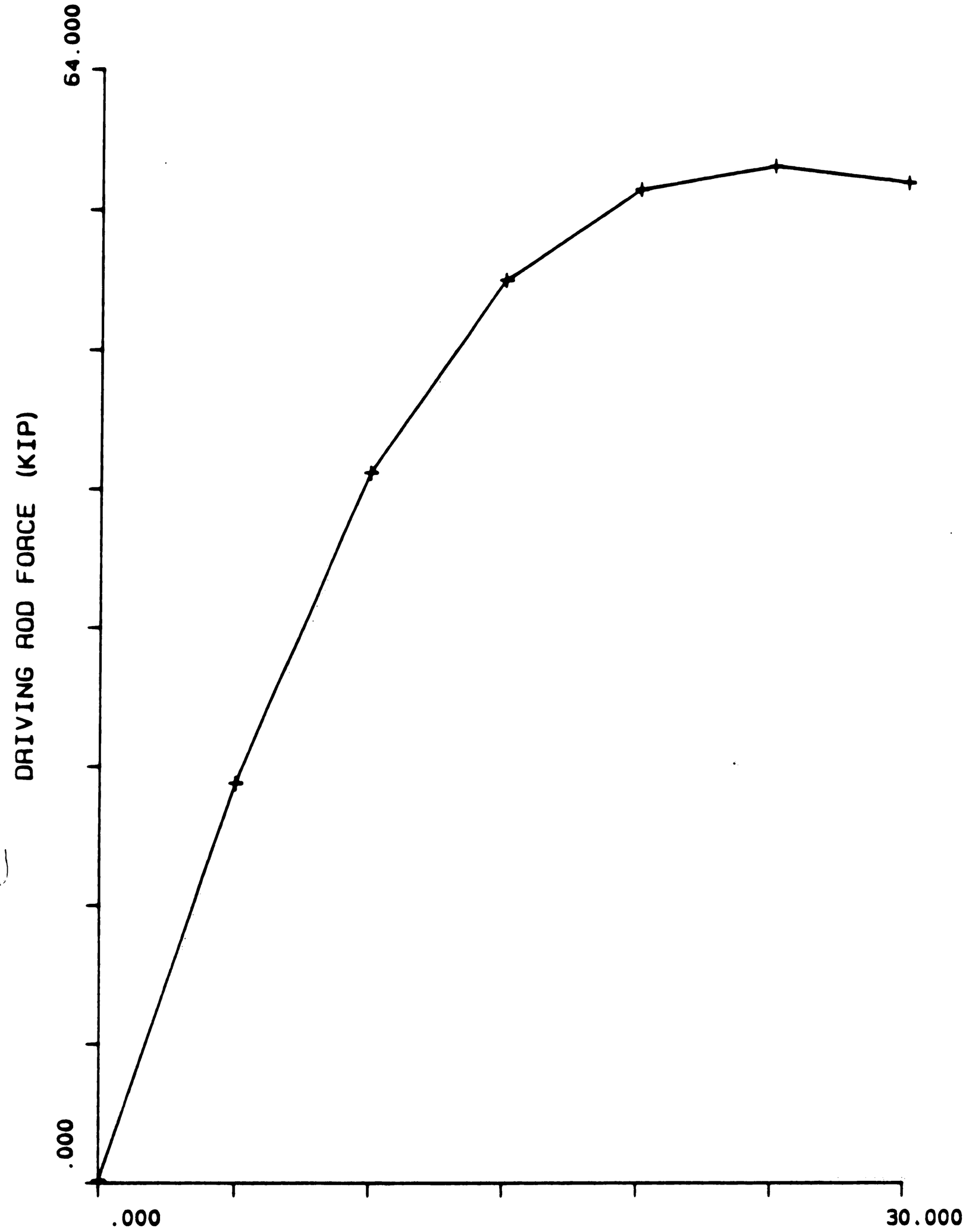

Figure 38: Rod Force/Rod Angle Relation For Detail B; 3.0 in. Gap

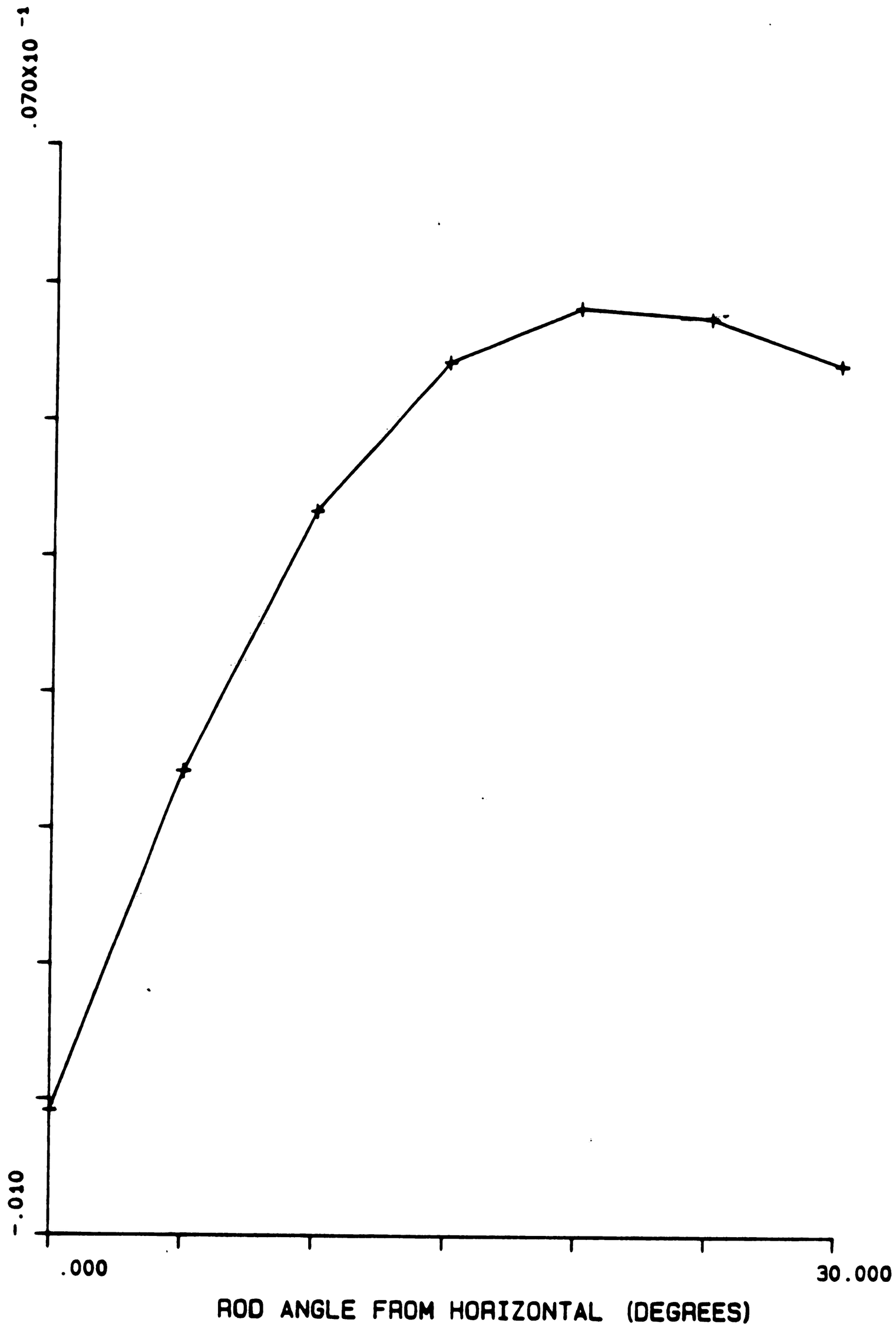

Figure 39: Lateral Disp./Rod Angle Relation For Detail B; 3.0 in. Gap

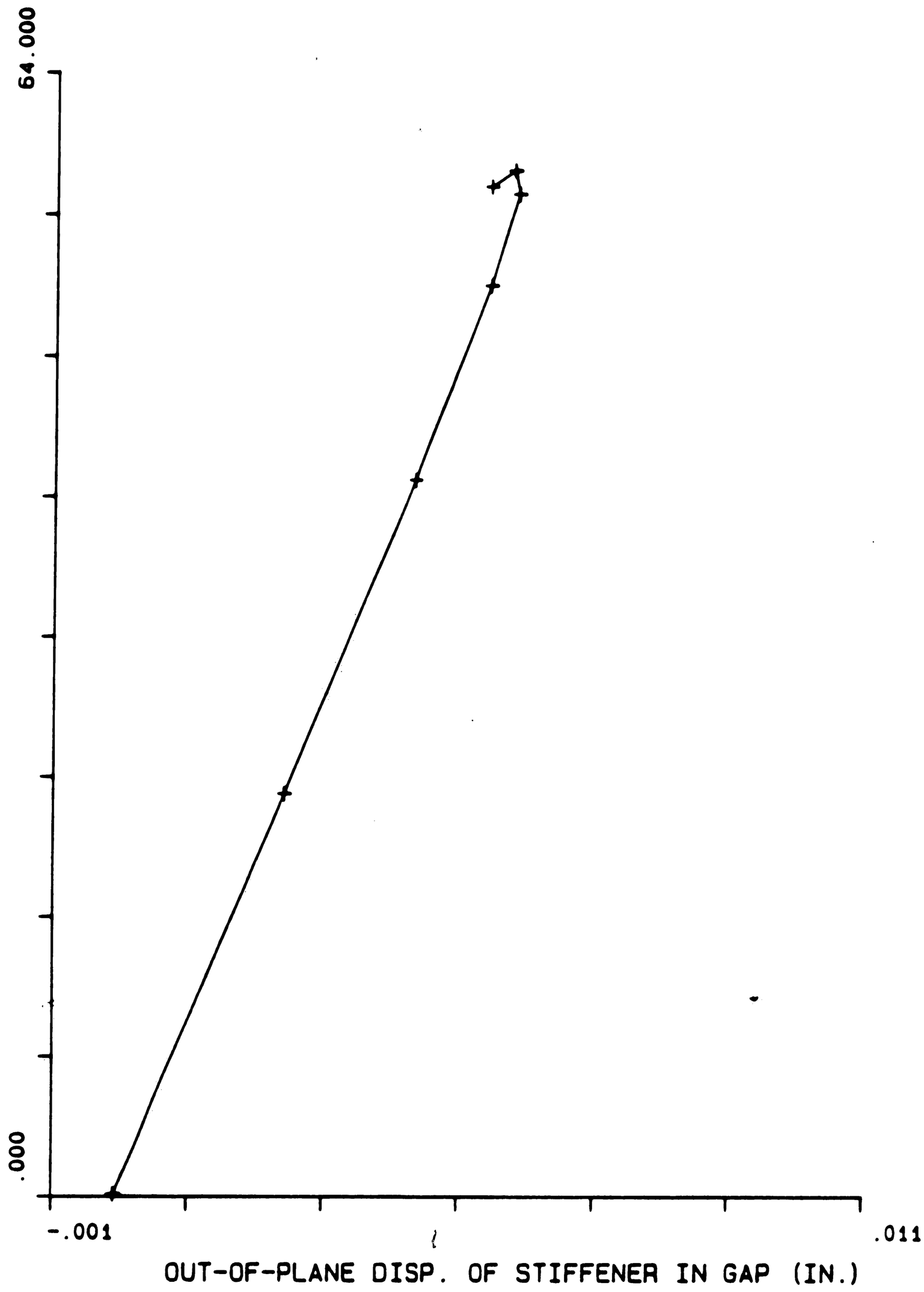

Figure 40: Rod Force/Lateral Disp. Relation For Detail B; 3.0 in. Gap

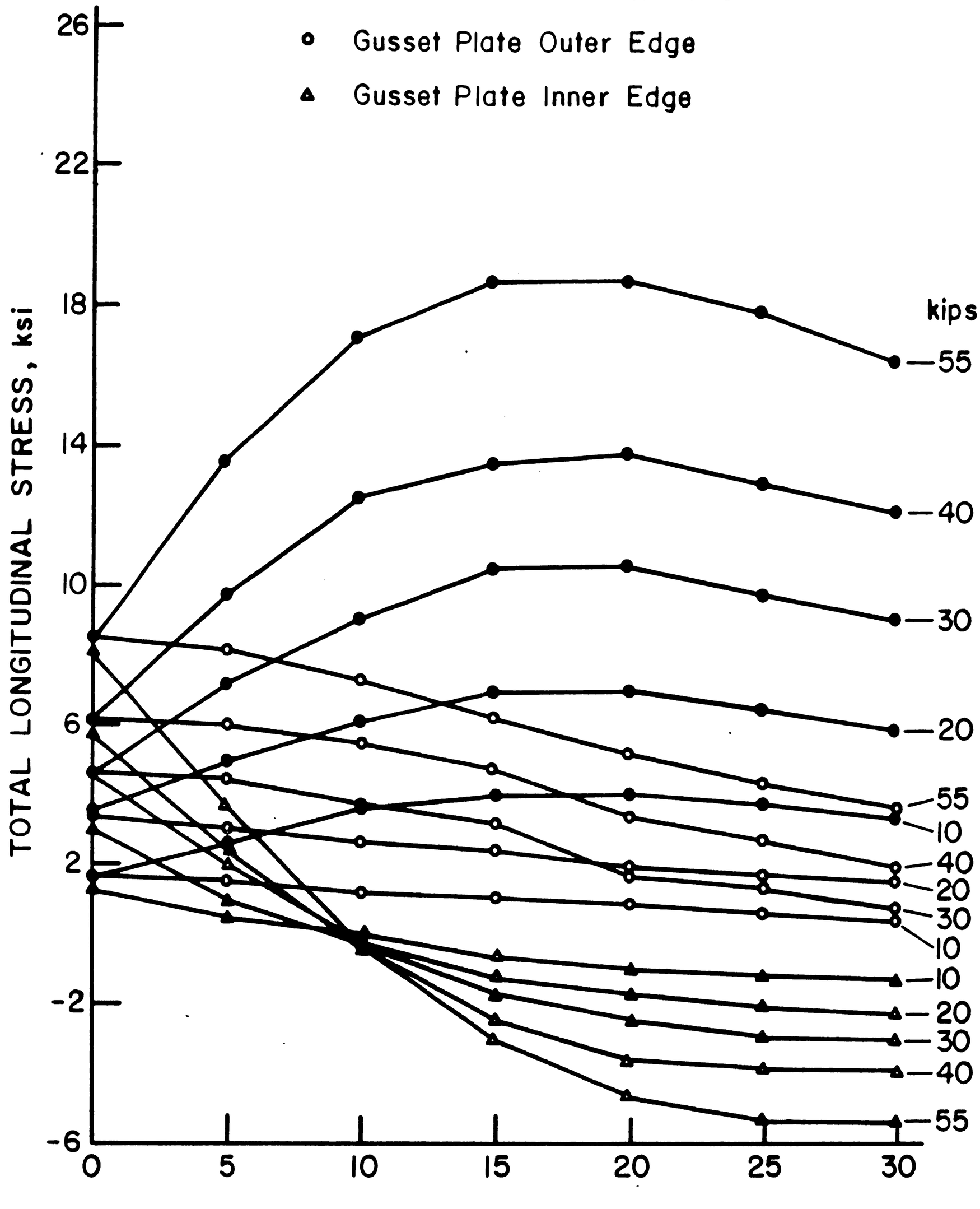

Figure 41: Test Curves For Detail C With 3.0 in. Web Gaps

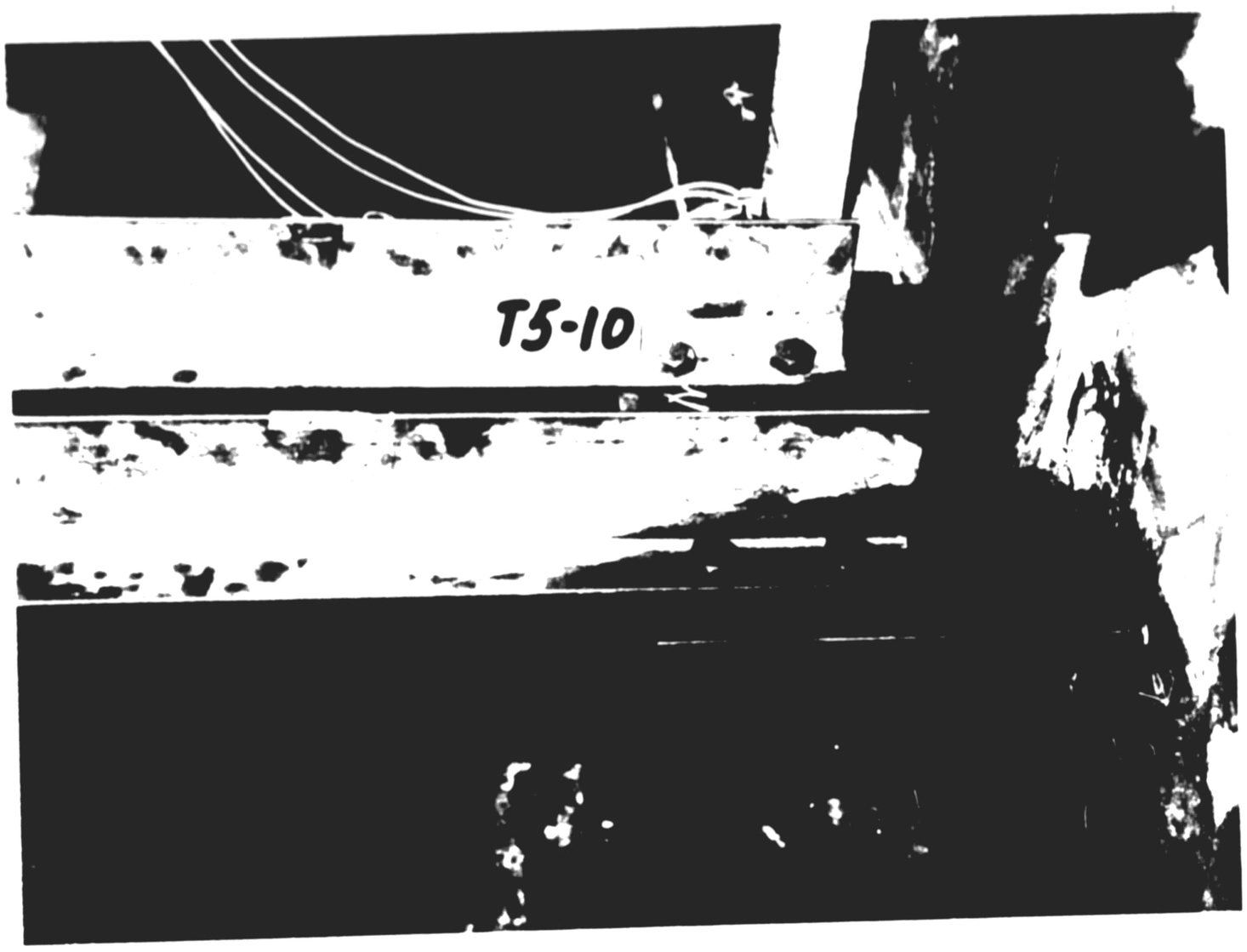

Figure 42: Detail C Gusset Plate and Laterals

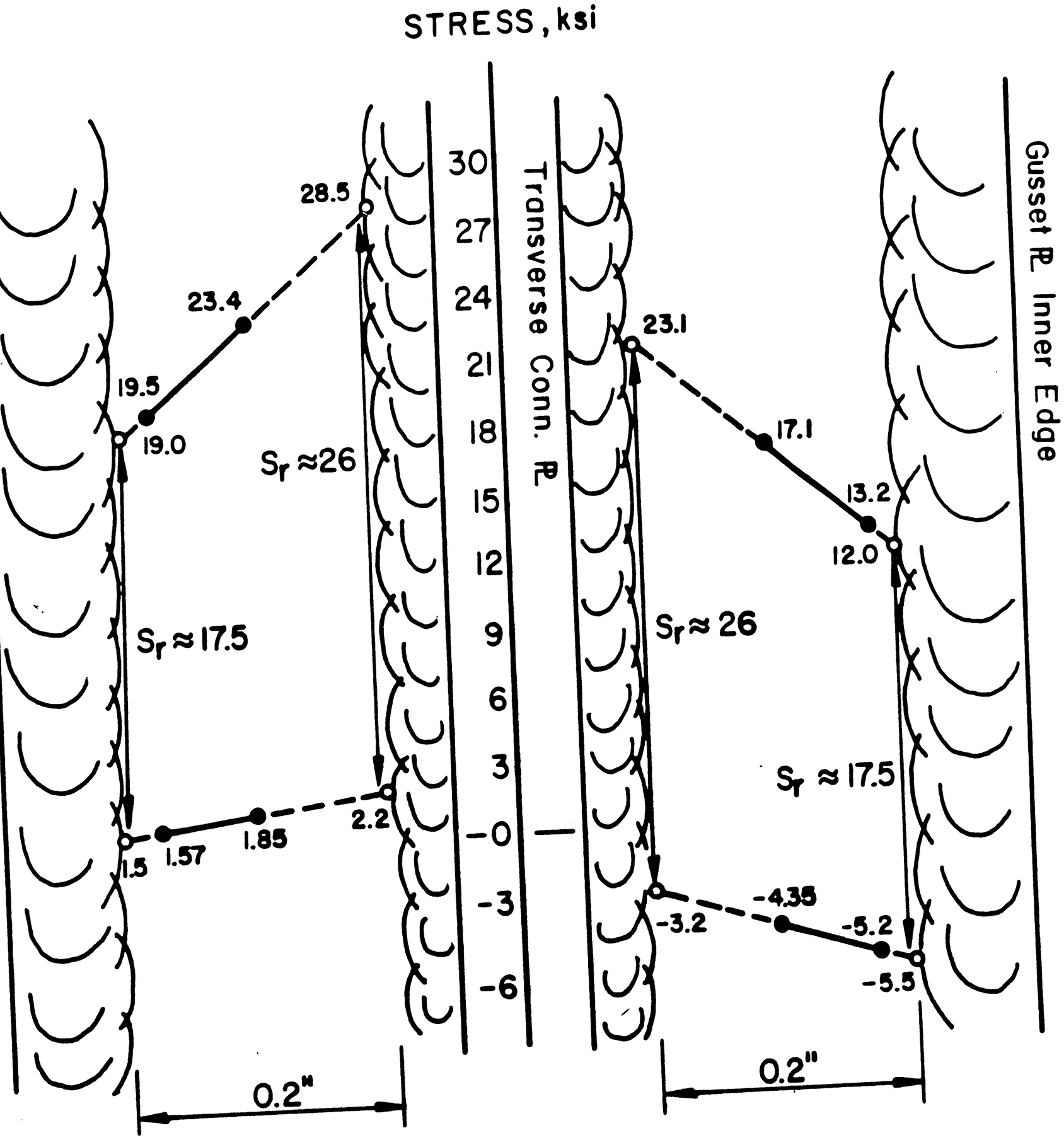

Figure 43: Typical Stress Gradients for Detail T5-10

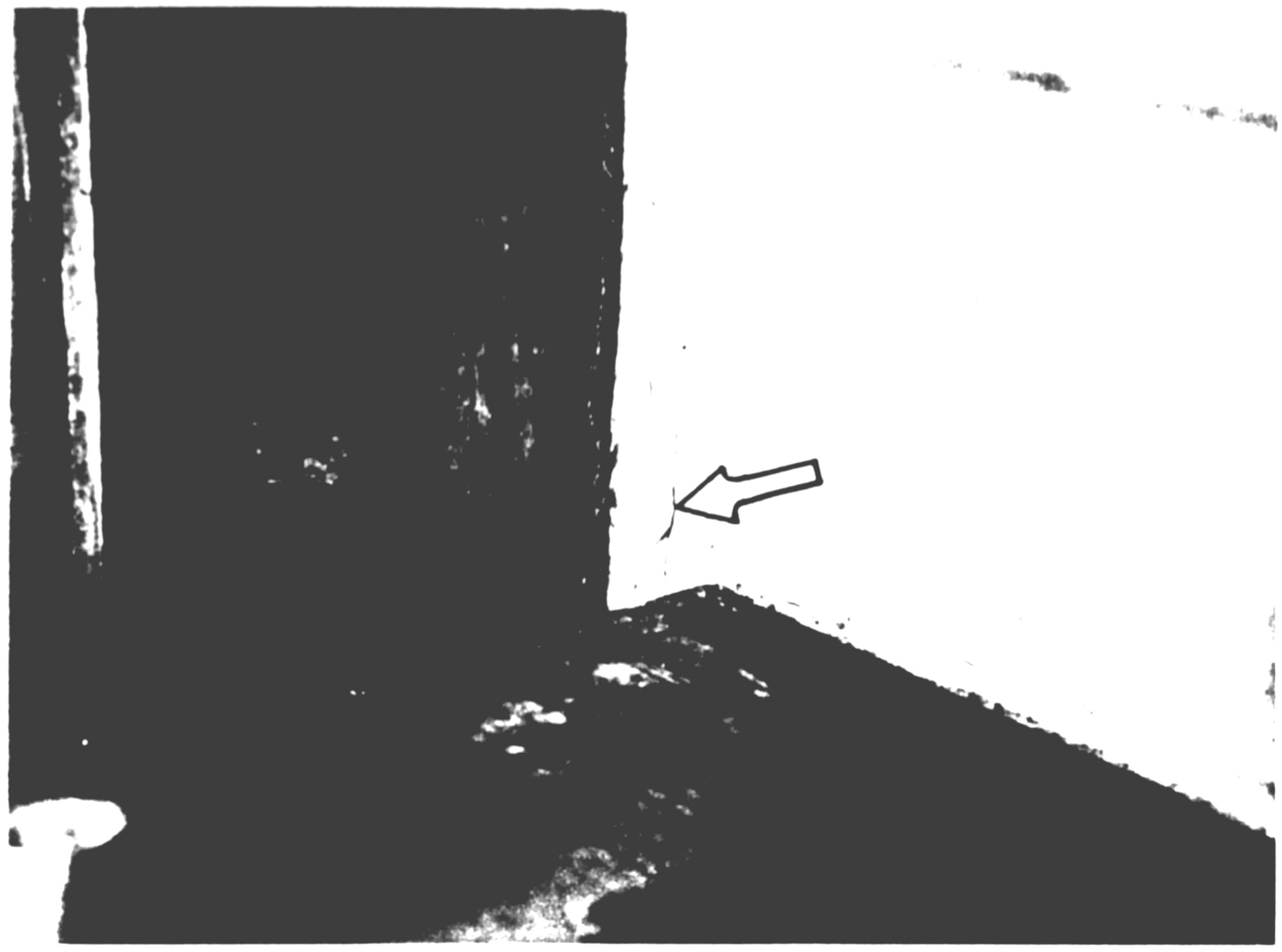

Figure 44: Cracking At Vertical Weld Toe in Horizontal Web Gap

Figure 45: Initial Retrofit of Vertical Fatigue Cracks

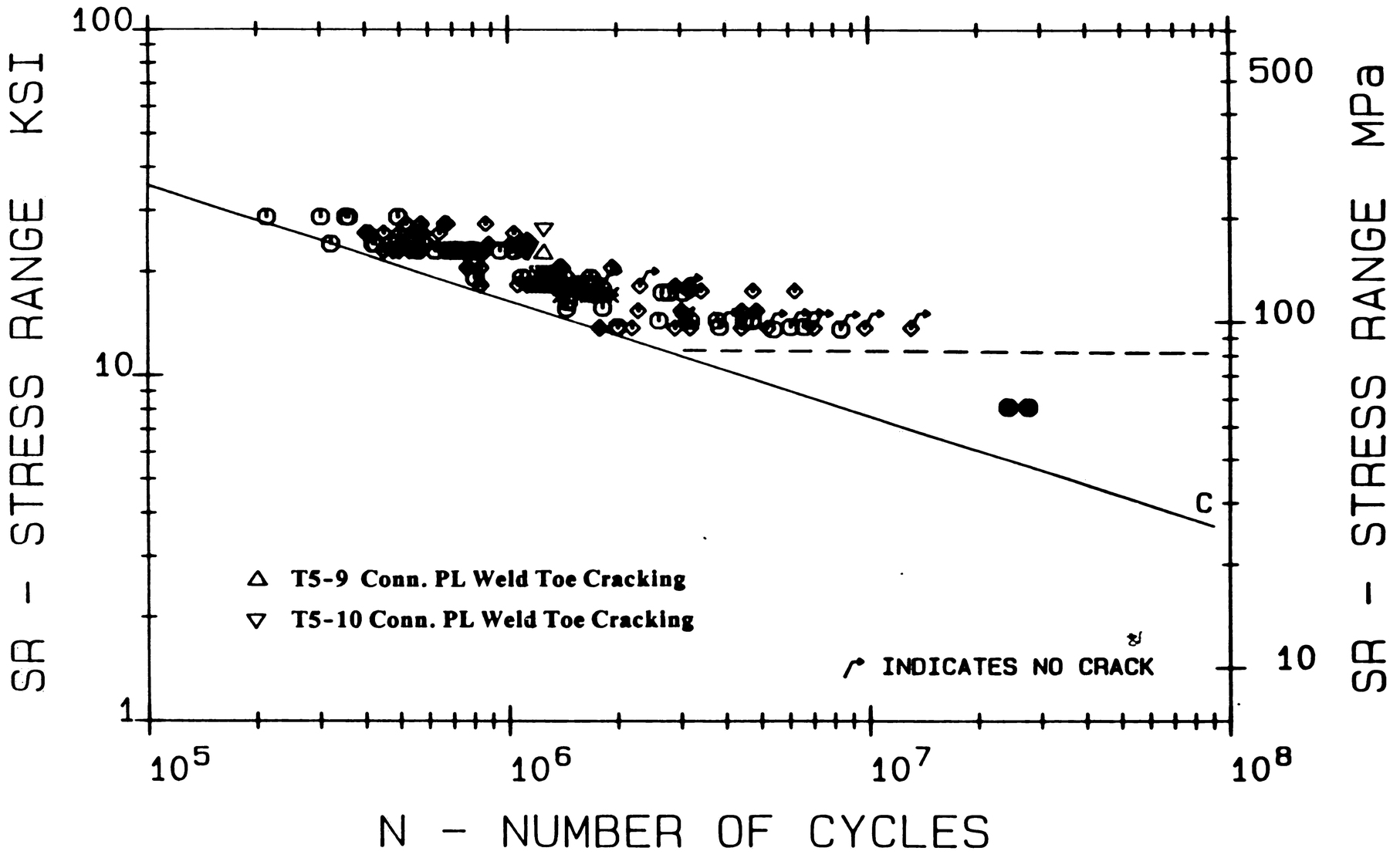

Figure 46: Comparison to AASHTO Category C Curve and Test Data

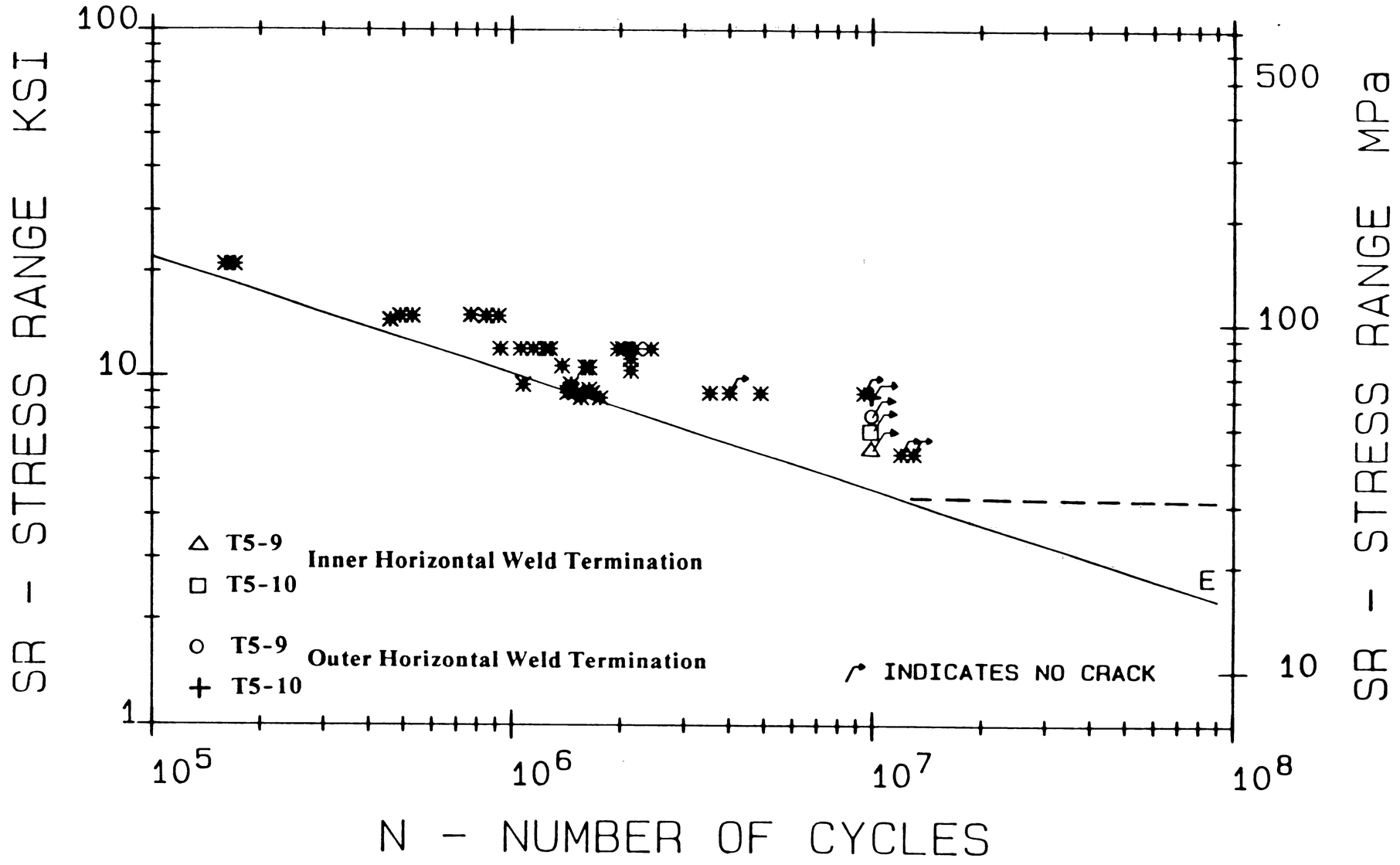

Figure 47: Comparison to AASHTO Category E Curve and Test Data

Figure 48: Detail B Gusset Plate and Laterals

Figure 49: Detail T5-6 Attachment and Web Gap

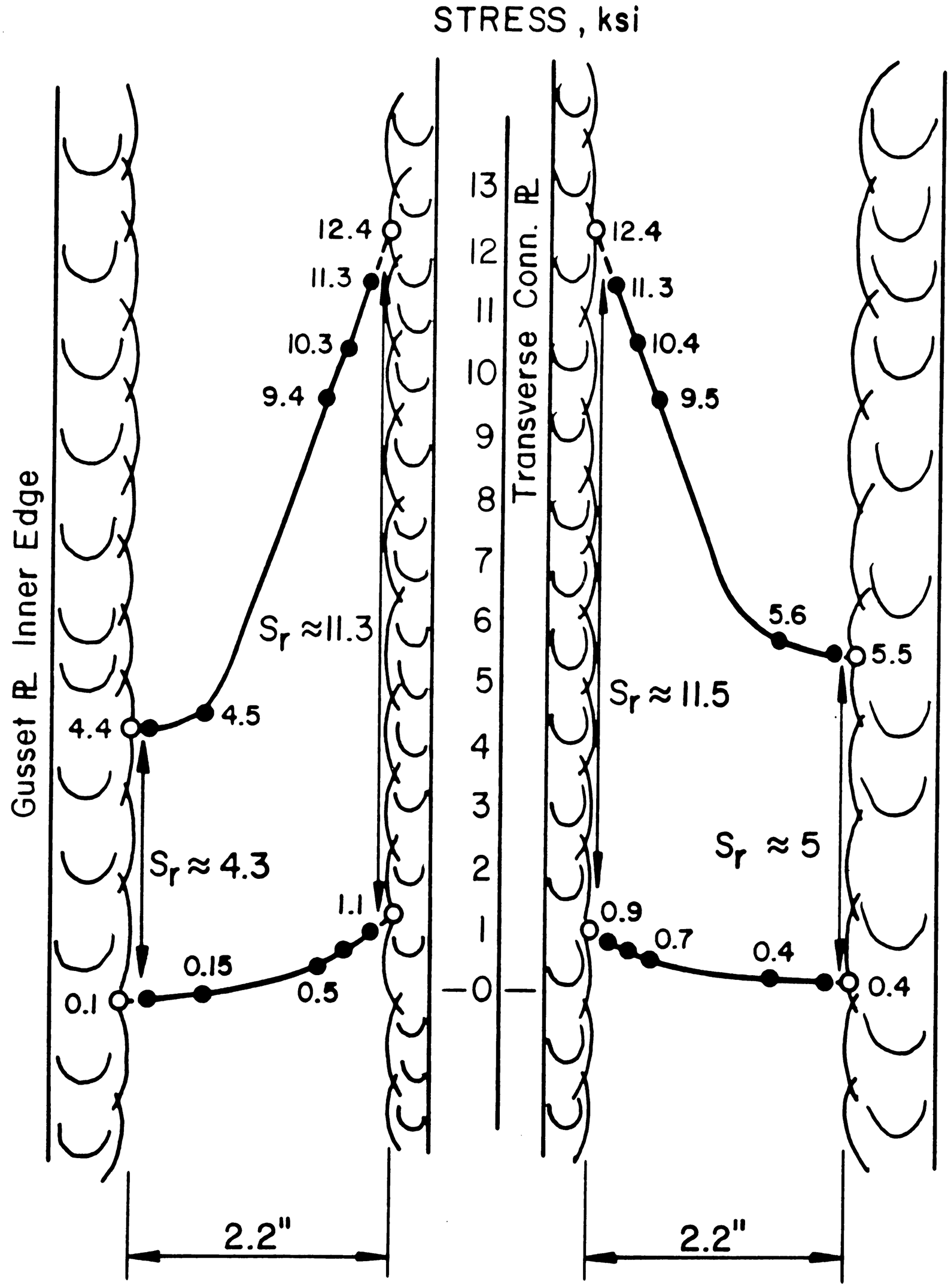

Figure 50: Typical Stress Gradients for Detail T5-7

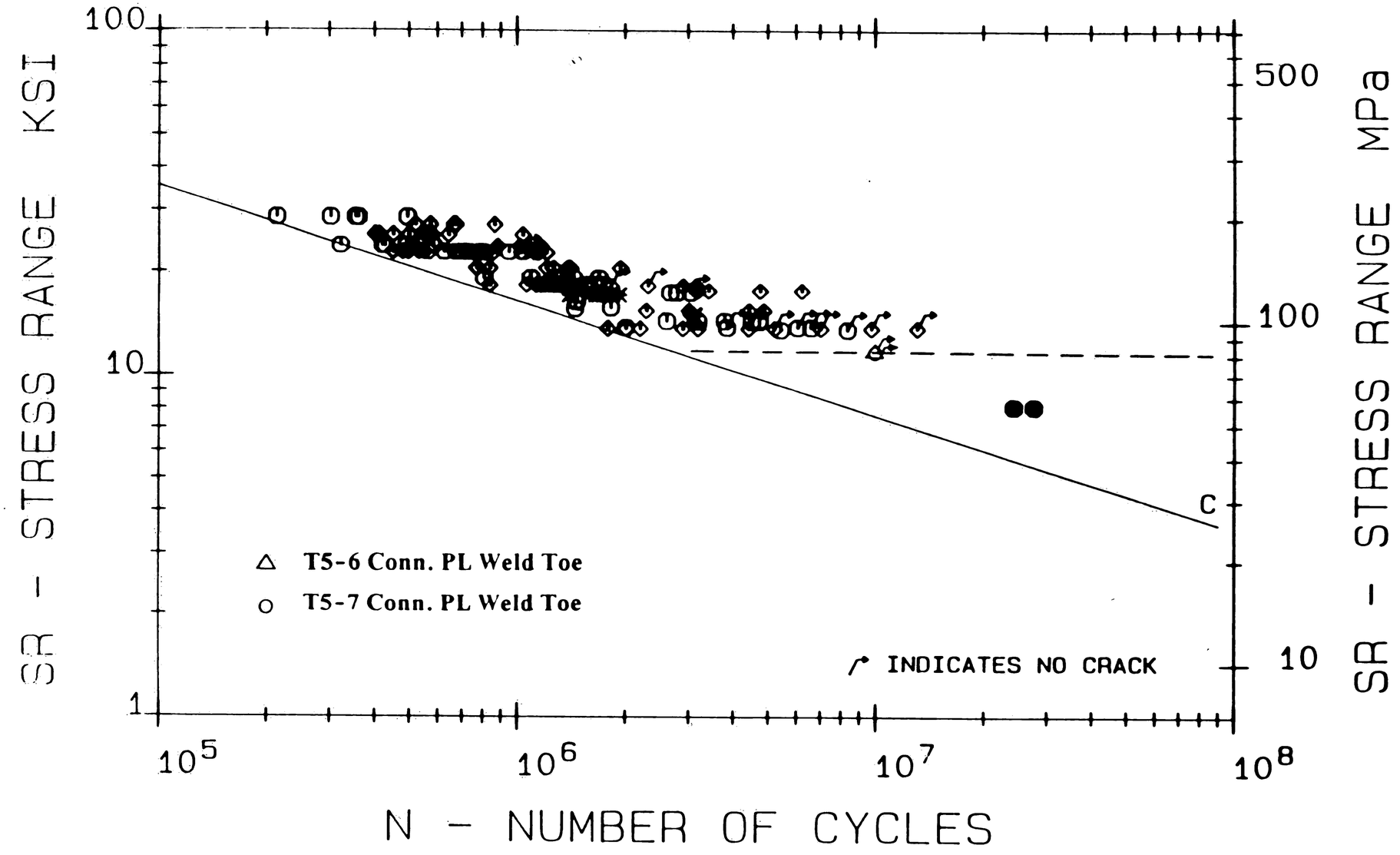

Figure 51: Comparison to AASHTO Category C Curve and Test Data

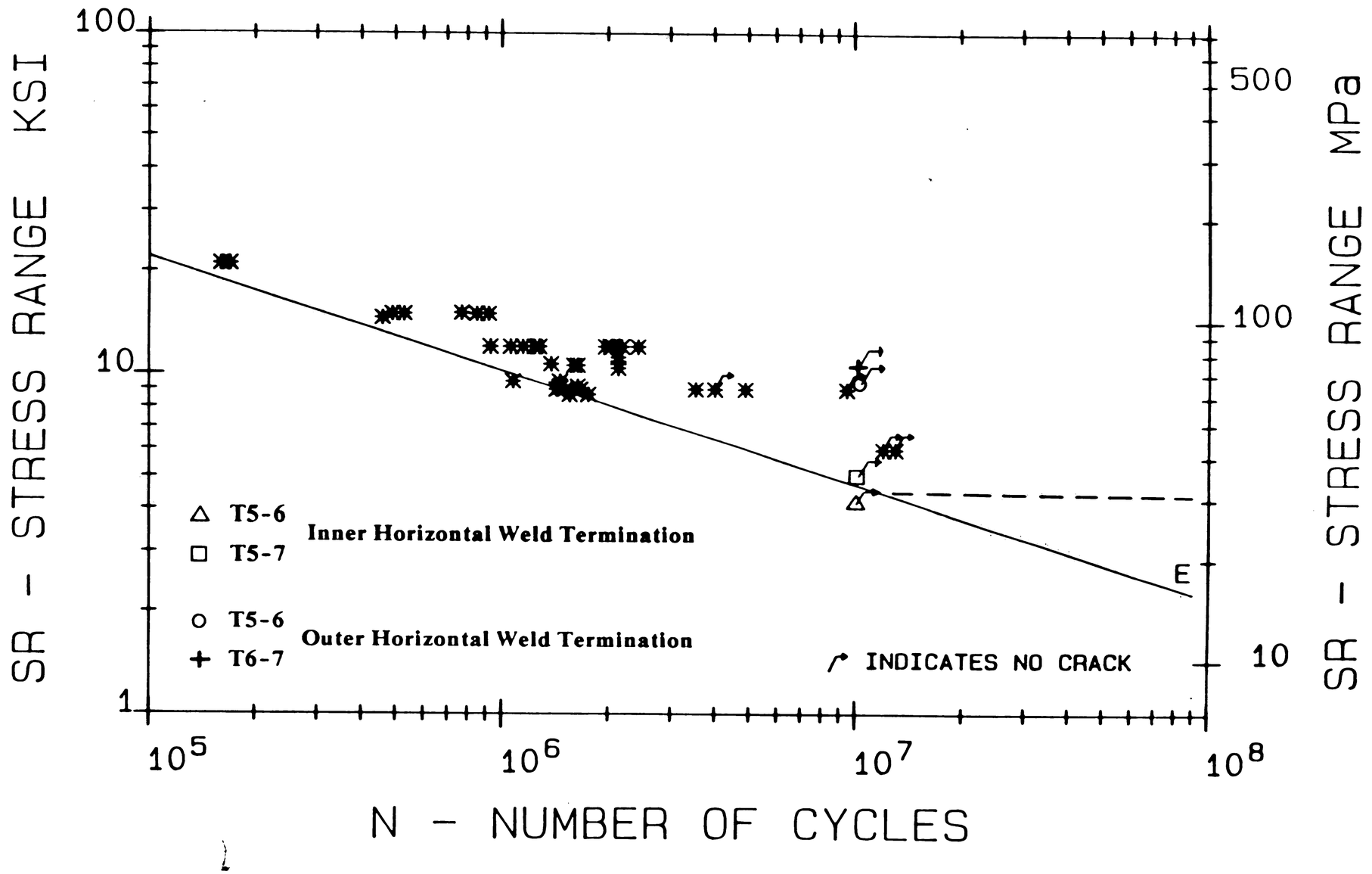

Figure 52: Comparison to AASHTO Category E Curve and Test Data

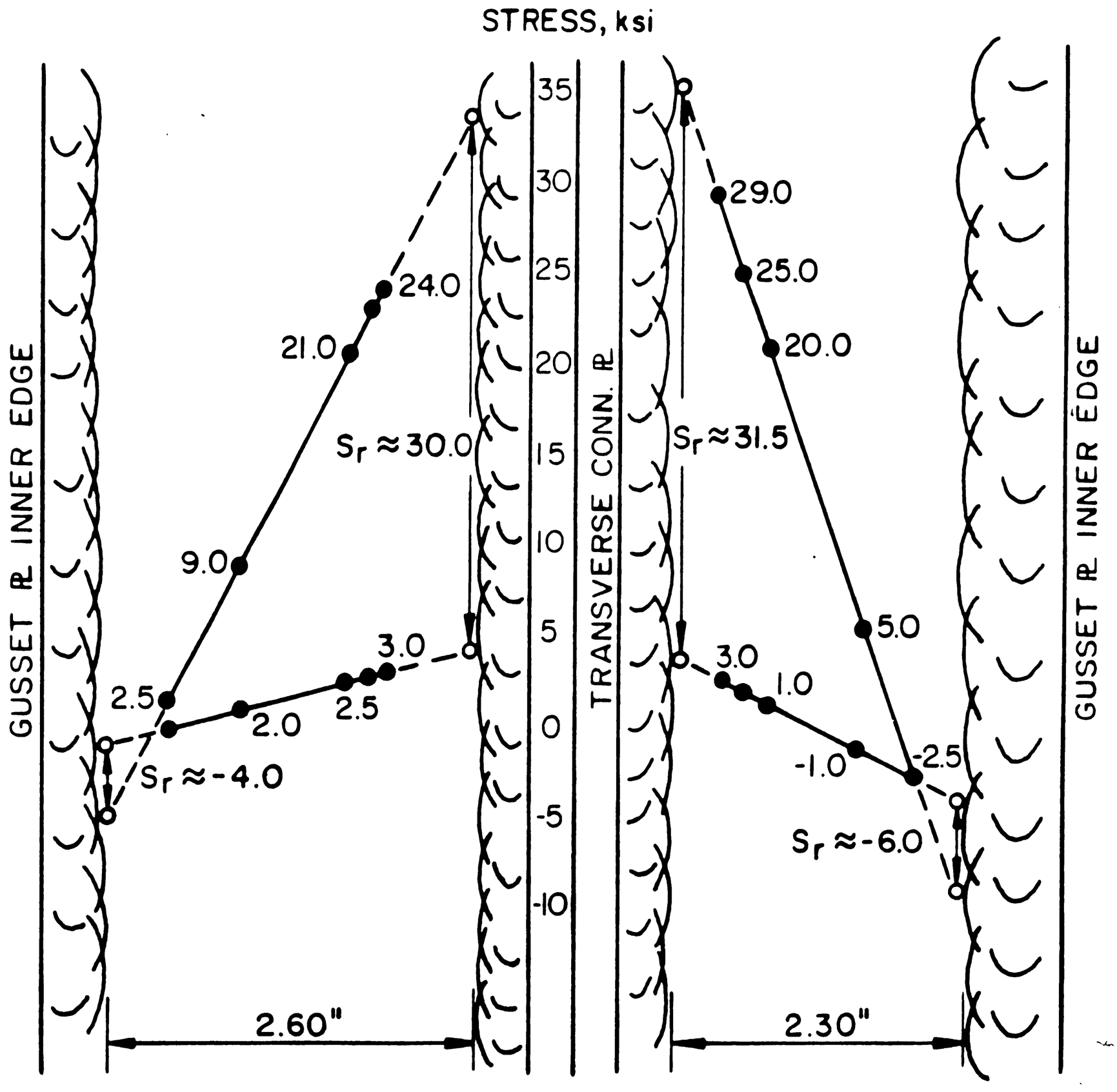

Figure 53: Typical Stress Gradients for Detail T5-12

Figure 54: Cracking at Weld Toe Within the Horizontal Web Gap

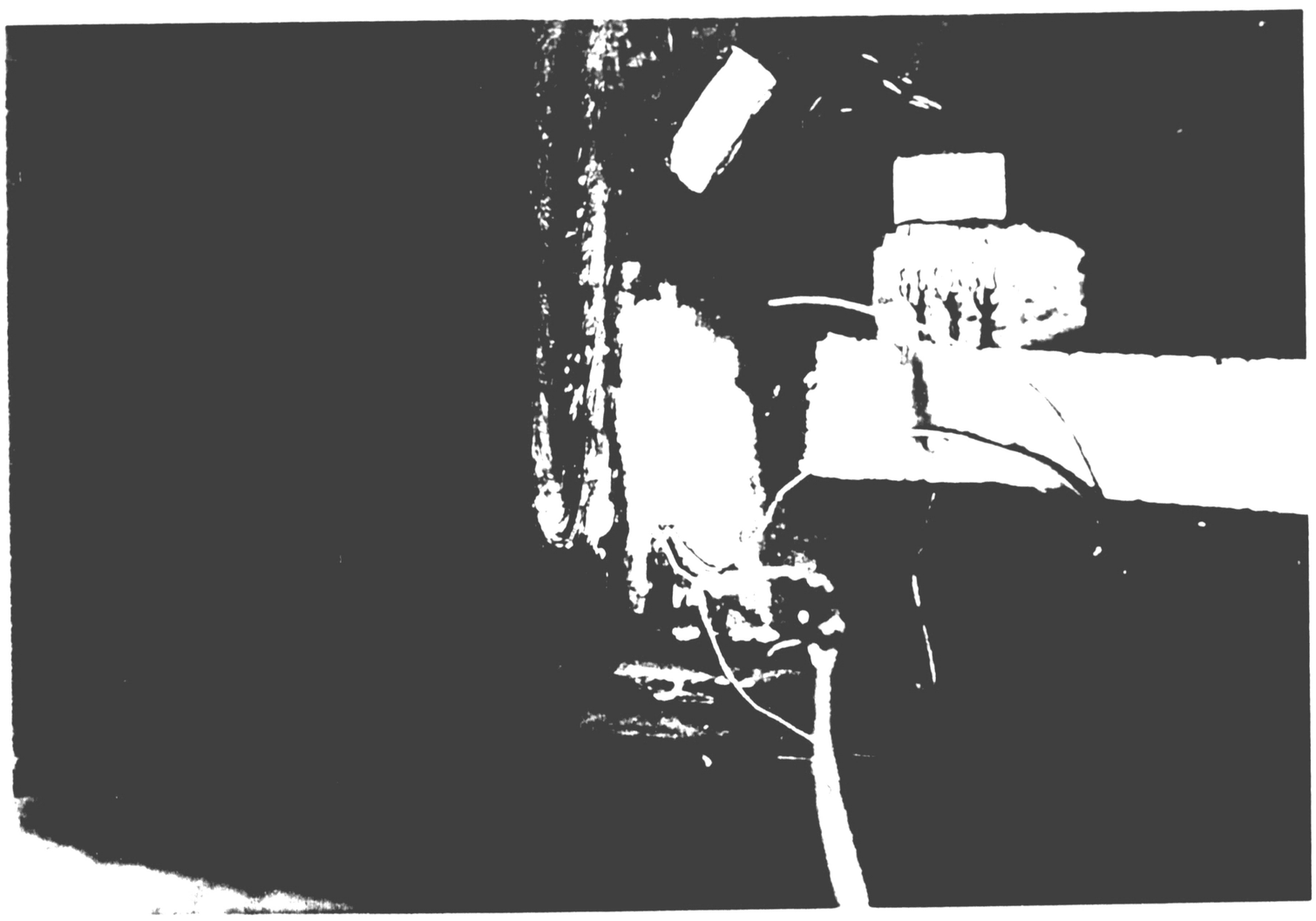

Figure 55: Cracking Within Transverse Gap at Longtidudinal Weld

Figure 56: Overall Crack Length on Outer Surface

Figure 57: Retrofit for Vertical Fatigue Cracks

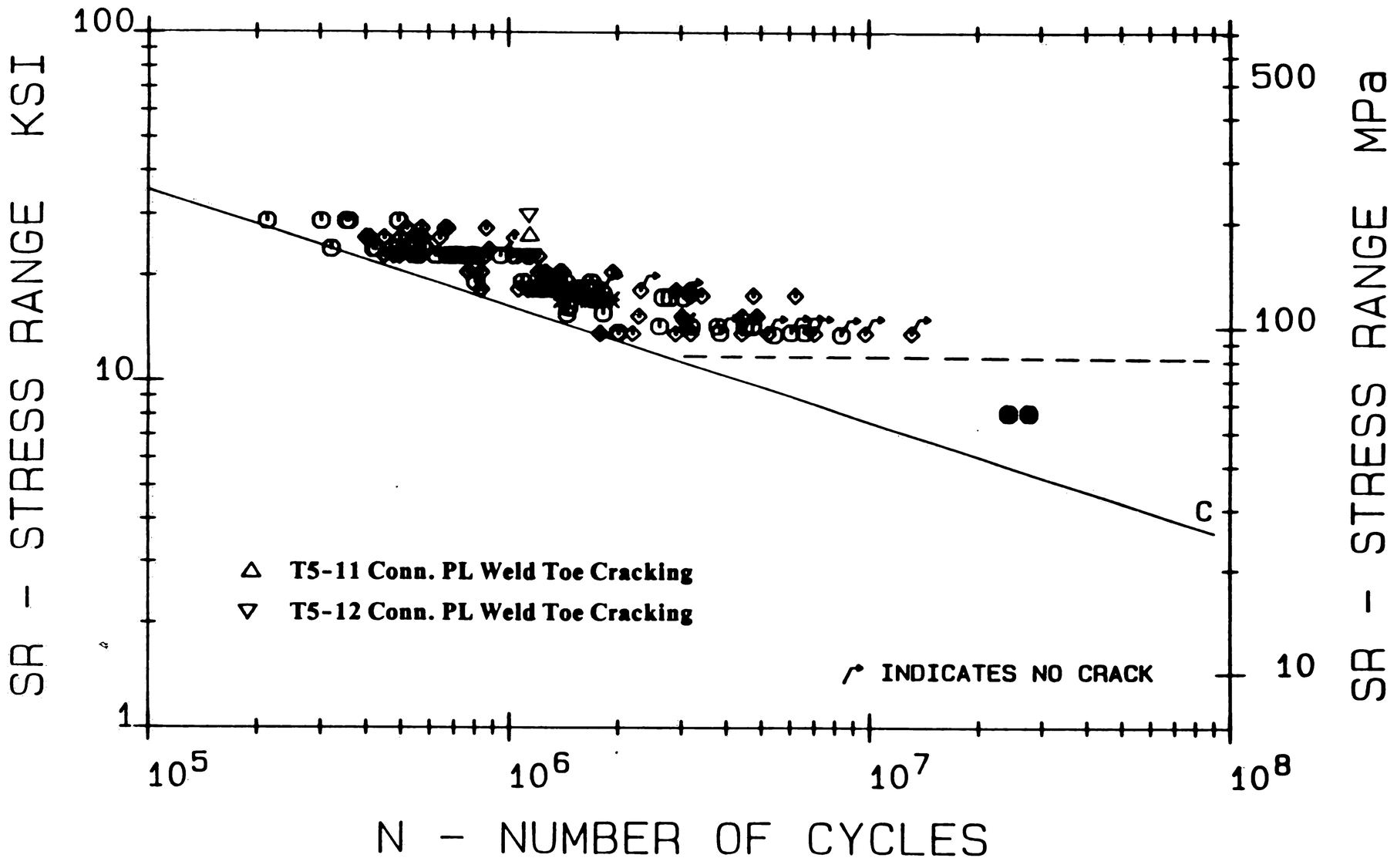

Figure 58: Comparison to AASHTO Category C Curve and Test Data

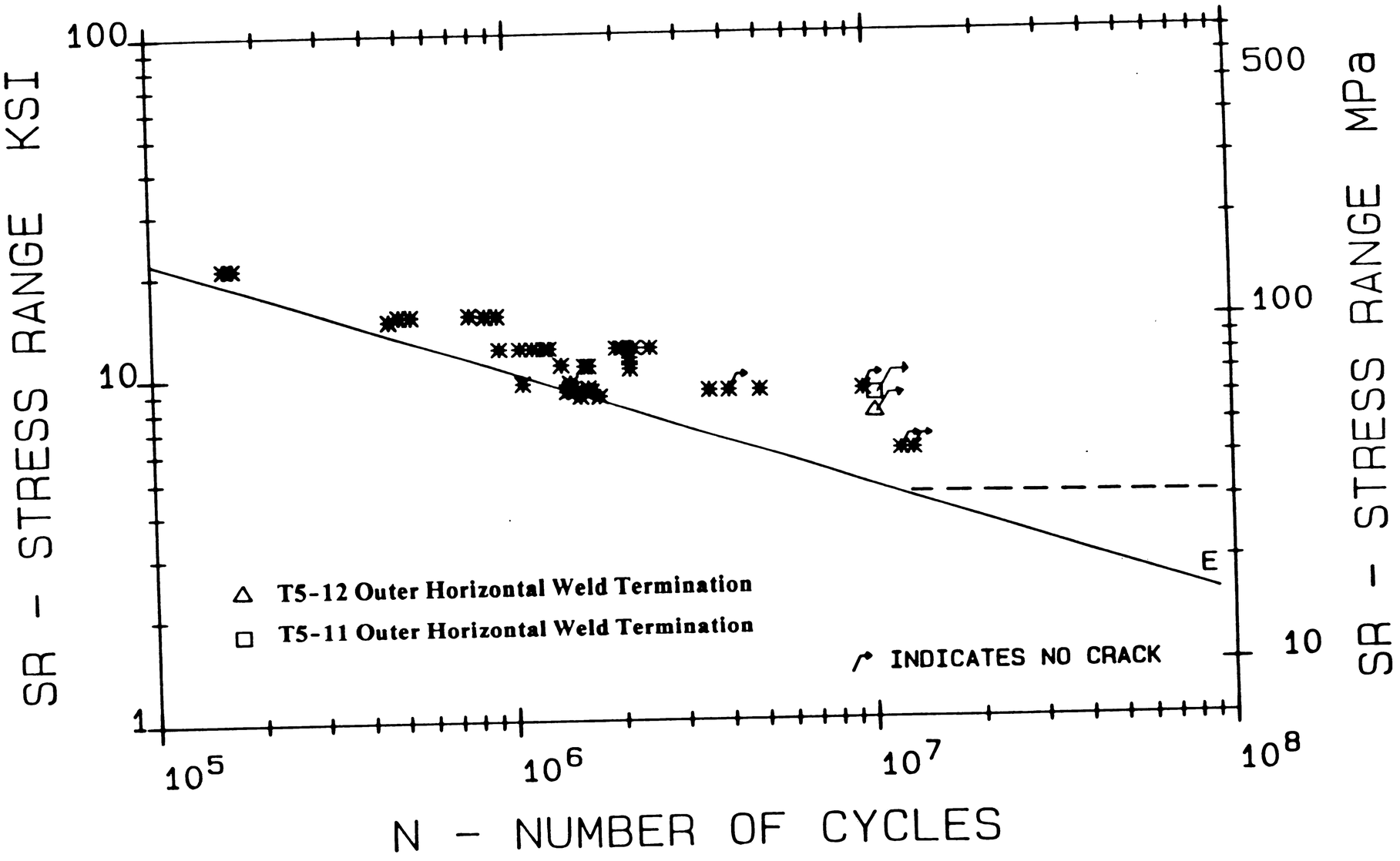

Figure 59: Comparison to AASHTO Category E Curve and Test Data

Figure 60: Detail T5-4 Attachment and Web Gap

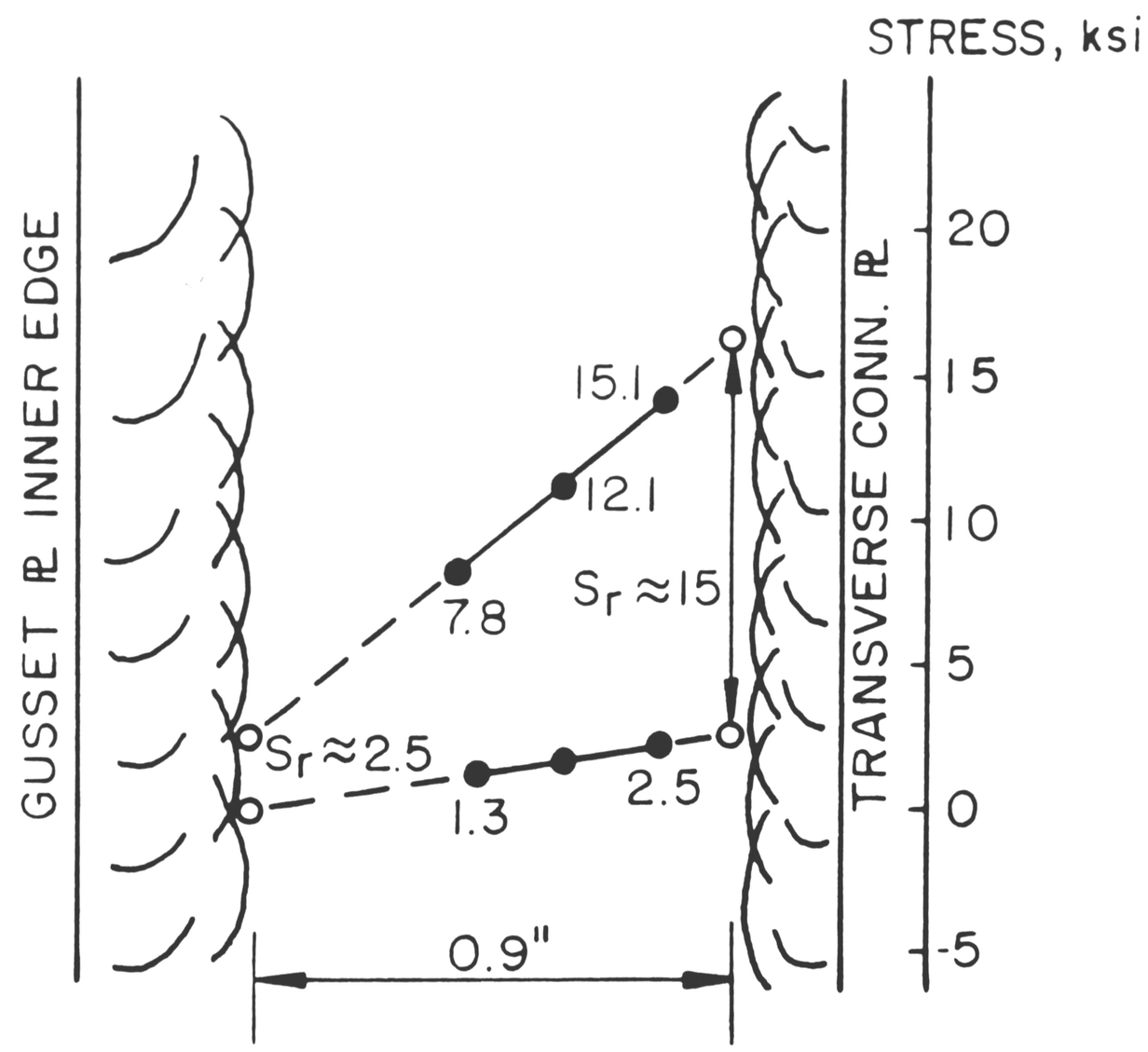

Figure 61: Typical Stress Gradients for Detail T5-4

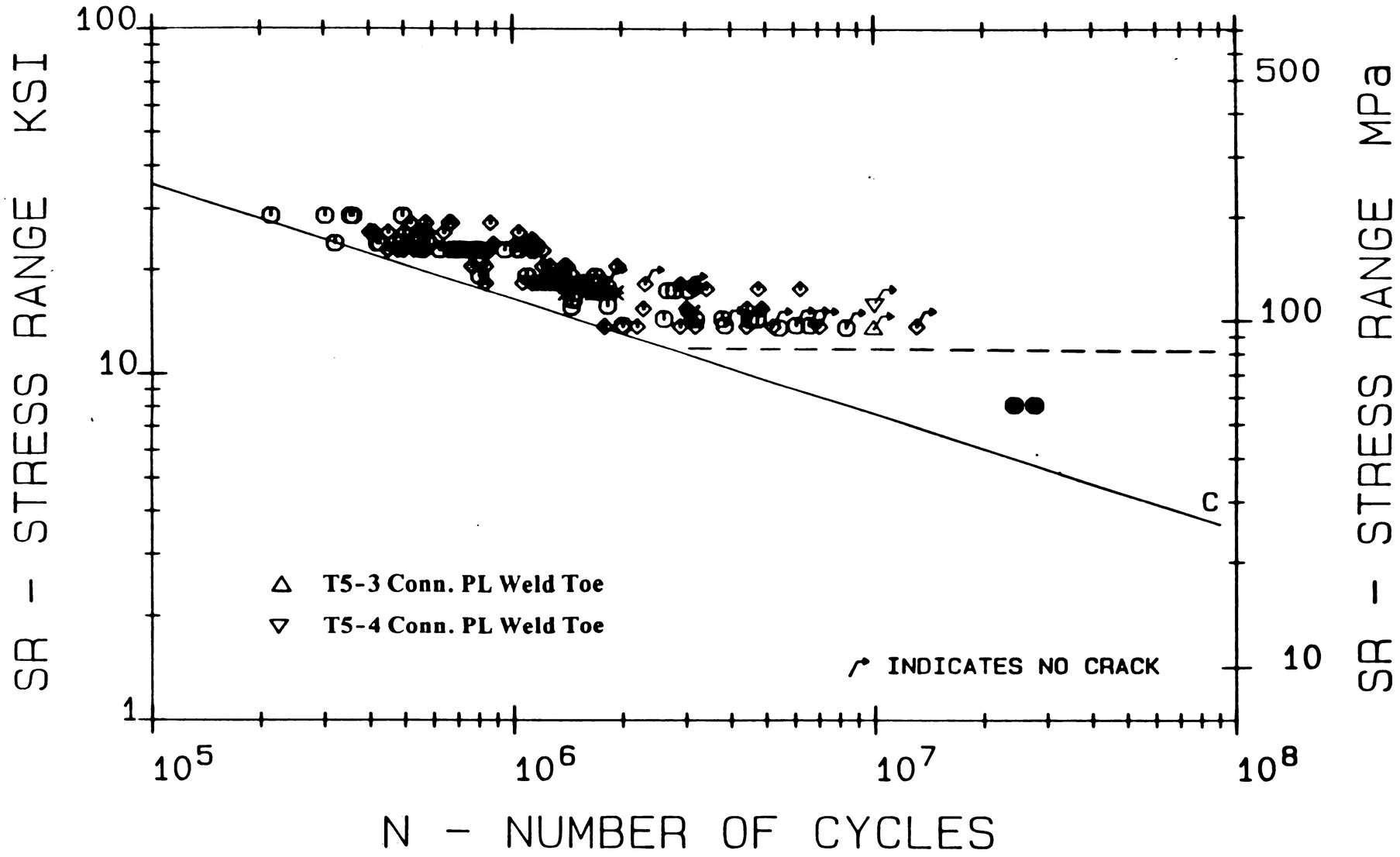

Figure 62: Comparison to AASHTO Category C Curve and Test Data

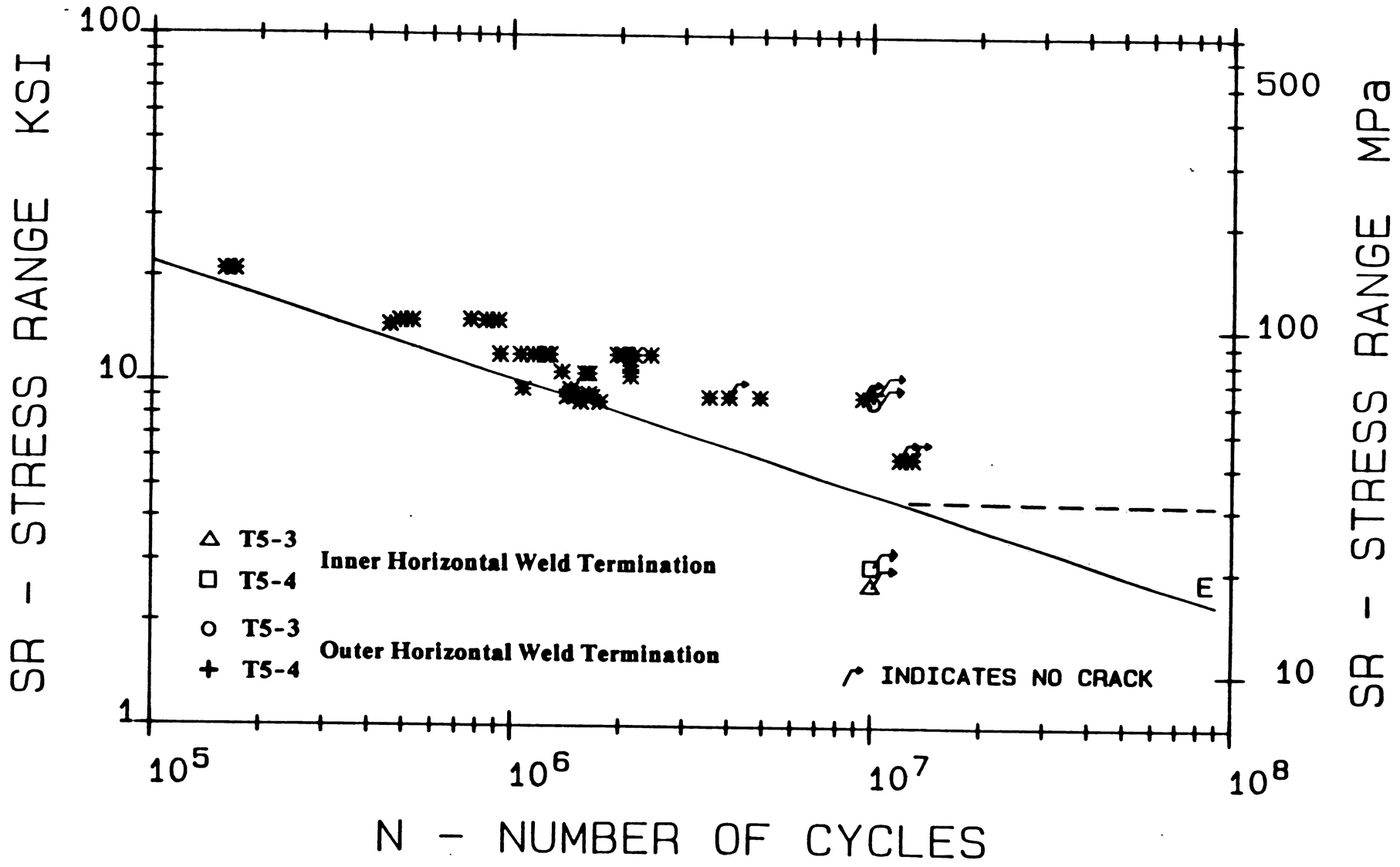

Figure 63: Comparison to AASHTO Category E Curve and Test Data

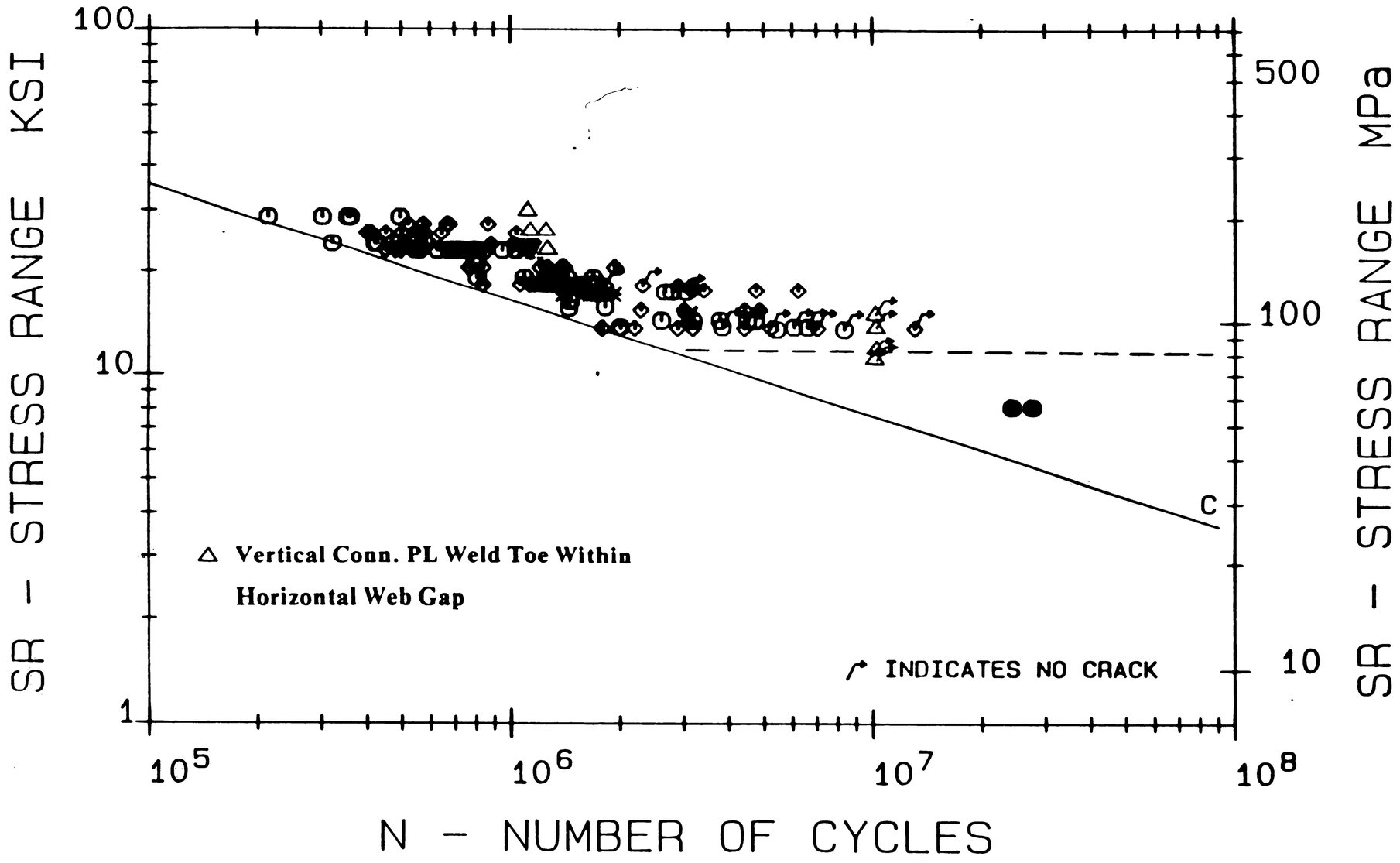

Figure 64: Comparison of Results With AASHTO Category C Test Data

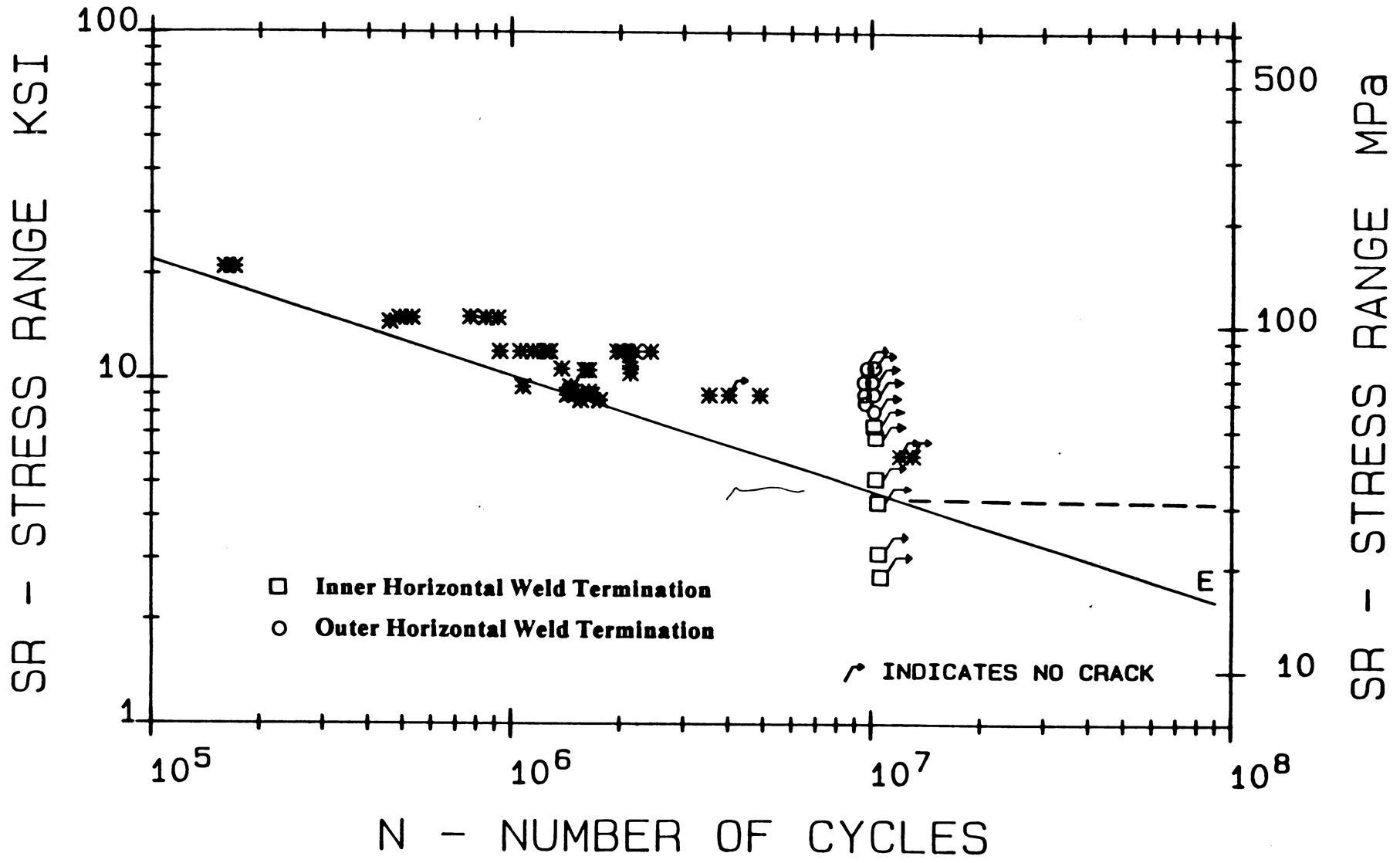

Figure 65: Comparison of Results With AASHTO Category E Test Data

References

[1] Fisher, J.W., **Bridge Fatigue Guide - Design and Details**, American Institute of Steel Construction, 1977.

[2] Wagner, D.C., Fisher, J.W., Yen, B.T., **Review of Field Measurements For Distortion-Induced Fatigue Cracking in Steel Bridges**, NCHRP Research Record, Transportation Research Board, National Research Council, Washington, D.C., 1987.

[3] Fisher, J.W., Hausammann, H., Sullivan, M.D., and Pense, A.W., **Detection And Repair of Fatigue Damage in Welded Highway Bridges**, NCHRP Report No. 206, Transportation Research Board, National Research Council, Washington, D.C., 1979.

[4] AASHTO, **Standard Specifications For Highway Bridges**, 13th Edition, American Association of State Highway and Transportation Officials, Washington, D.C., 1983.

[5] Fisher, J.W., Pense, A.W., et al., **Final Report on Cracking of I-79 Bridges 2680 and 2682**, Fritz Engineering Laboratory Report 501-1(85), Lehigh University, May 1985.

[6] Fisher, J.W., Menzemer, C.A., et al., **Distortion-Induced Stresses in a Floorbeam-Girder Bridge: Canoe Creek**, Fritz Engineering Laboratory Report 500-2(86), Lehigh University, April 1986.

[7] **Specification for the Design, Fabrication, and Erection of Structural Steel for Buildings**, American Institute of Steel Construction, Chicago, 1978.

[8] Bathe, K.J., Wilson, E.L., Peterson, F.E., **SAP IV : A Structural Analysis Program for Static and Dynamic Response of Linear Systems**, EERC Report No. 73-11, June 1973.

[9] Mertz, D.R., **Displacement-Induced Fatigue Cracking in Welded Steel Bridges**, PhD. Dissertation, Submitted to Lehigh University, Bethlehem, April 1984.

[10] Frank, K.H., **The Fatigue Strength of Fillet Welded Connections**, PhD. Dissertation, Submitted to Lehigh University, Bethlehem, October 1971.

Vita

The author was born in Camden, New Jersey, on June 13, 1963. He is the youngest son of Charles R. and Catherine I. Wagner.

The author received his early education at Haddon Township High School where he graduated in June of 1981. He enrolled in Lehigh University in August of 1981 to pursue an education in structural engineering through the Department of Civil Engineering. He was inducted into *Phi Eta Sigma* Freshman Honor Society in Fall of 1982. The author was then inducted into *Chi Epsilon* Civil Engineering Honor Society, and *Tau Beta Pi* Engineering Honor Society in the Spring of 1984. During his senior year, the author was the recipient of an award from The James F. Lincoln Arc-Welding Foundation for *"Advances in the Design of Welded Structures."* He is a member of Delta Tau Delta Fraternity and is listed in *Who's Who in Fraternity Leaders.* The author passed the *Engineer-In-Training* test in April of 1985, and is a member of the *American Society of Civil Engineers.* In June of 1985, he was awarded the Bachelor of Science Degree with Highest Honors in Civil Engineering.

The author was then employed for a summer term with the Electric Boat Division of General Dynamics Corp. in Groton, Connecticut. He was involved with the structural analysis of Trident deck components.

The author once again entered Lehigh University in August of 1985. He worked as a Research Assistant in the Fatigue & Fracture Division of Fritz Engineering Laboratory. During this time, he also completed the academic requirements for the Master of Science Degree in Civil Engineering. The author was involved with research in *"Distortion-Induced Fatigue Cracking in Steel*

Bridges" with Dr. John W. Fisher. It is this research that formed the basis for the author's publications and thesis work.